

ANALYSIS AND SIMULATION OF EXIT TIME PROBLEMS

by

Qunhui Han

A dissertation submitted to the Faculty of the University of Delaware in partial fulfillment of the requirements for the degree of Doctor of Philosophy in Applied Mathematics

Fall 2013

© 2013 Qunhui Han
All Rights Reserved

ANALYSIS AND SIMULATION OF EXIT TIME PROBLEMS

by

Qunhui Han

Approved: _____
John Pelesko, Ph.D.
Chair of the Department of Mathematical Sciences

Approved: _____
George H. Watson, Ph.D.
Dean of the College of Arts and Sciences

Approved: _____
James G. Richards, Ph.D.
Vice Provost for Graduate and Professional Education

I certify that I have read this dissertation and that in my opinion it meets the academic and professional standard required by the University as a dissertation for the degree of Doctor of Philosophy.

Signed: _____

Pak-Wing Fok, Ph.D.
Professor in charge of dissertation

I certify that I have read this dissertation and that in my opinion it meets the academic and professional standard required by the University as a dissertation for the degree of Doctor of Philosophy.

Signed: _____

Louis F. Rossi, Ph.D.
Member of dissertation committee

I certify that I have read this dissertation and that in my opinion it meets the academic and professional standard required by the University as a dissertation for the degree of Doctor of Philosophy.

Signed: _____

Rakesh, Ph.D.
Member of dissertation committee

I certify that I have read this dissertation and that in my opinion it meets the academic and professional standard required by the University as a dissertation for the degree of Doctor of Philosophy.

Signed: _____

Adam J. Fleischhacker, Ph.D.
Member of dissertation committee

ACKNOWLEDGEMENTS

First of all, I would like to thank my parents, twin sister, and my boyfriend, Mingjiang Zhan, for giving me love, strength, encouragement to be able to obtain Ph.D degree. Especially, my father, I would never pursue higher education in U.S without his enlightenment.

I am deeply grateful to my advisor, Dr. Pak-Wing Fok, for his instructive guidance, useful advice, and support throughout my research. I really appreciate his patience and help over these years. Thanks as well to my committee, Dr. Rossi, Dr. Rakesh, and Dr. Fleischhacker for their insightful comments and suggestions to my work. In addition, I would like to thank all the professors who taught me a lot of beautiful and powerful mathematics, as well as all the staff for providing a kind and convenient environment.

I would like to thank everyone that has helped me during my doctoral study, especially my officemates Jiahua Tang, and David Rowan.

Finally, I would like to thank the University of Delaware for the financial support of my research.

TABLE OF CONTENTS

LIST OF TABLES	vii
LIST OF FIGURES	viii
ABSTRACT	xii
 Chapter	
1 INTRODUCTION	1
1.1 Motivation	1
1.2 Broadwell Processes	2
1.3 Clinical Trials	5
1.4 Dissertation Outline	8
2 FORWARD AND BACKWARD EQUATIONS FOR A STOCHASTIC PROCESS	10
2.1 Forward and Backward Kolmogorov Equation	10
2.2 Derivation of Backward Equation for Broadwell Process	14
3 MONTE-CARLO SIMULATION FOR THE BROADWELL PROCESS	19
3.1 Monte-Carlo Simulation Using Rejection-Acceptance	19
3.2 Generation of Noisy Distributions from a Finite Number of Exit Times	21
4 RECONSTRUCTION OF THE FLIP RATE IN A BROADWELL PROCESS USING PROJECTION METHODS	26
4.1 Two-state Broadwell Model and The Statement of Inverse Problem	27
4.2 Solution to the Forward Problems	29
4.3 Projection Method to Solve Inverse Problem	35
4.4 Results and Discussion	36
4.4.1 Flip Rate Reconstruction	36

4.4.2	Instability of Projection Method	39
4.4.3	Sensitivity of Reconstruction to Advection Speed	40
4.5	Conclusions	44
5	RECONSTRUCTION OF BROADWELL PROCESS USING LAYER STRIPPING METHOD	46
5.1	Two-state Broadwell Model and Statement of Inverse Problem	46
5.2	Solution to The Forward Problem	48
5.2.1	Propagation of Singularities	48
5.2.2	Numerical Method for The Forward Problems	53
5.3	Relationship between $F(x)$ and w_1, w_2 along $t = \frac{L}{2v} \pm \frac{x}{v}$	54
5.4	Layer Stripping Algorithm to Solve Inverse Problem	55
5.4.1	First Order Layer Stripping Algorithm	56
5.4.2	Second Order Layer Stripping Algorithm	58
5.5	Results and Discussion	59
5.6	Conclusion	65
5.7	Future Work	67
6	FIRST PASSAGE TIMES IN CLINICAL TRIALS	68
6.1	Stochastic Model of A Clinical Drug Trial	68
6.2	Calculation of Mean Exit Time	71
6.2.1	The 2-site Case	71
6.2.2	The 3-site Case	77
6.2.3	The m -site Case	82
6.3	Approximation Using Laplace's Method	84
6.4	Monte-Carlo Simulation	87
6.5	Results and Discussion	88
6.6	Conclusions and Future Work	94
	BIBLIOGRAPHY	97
	Appendix	
	DERIVATION OF EQUATIONS	105

LIST OF TABLES

4.1	Local condition numbers κ_s and κ_t for $F^*(x)$ corresponding to the objective functions (4.25) and (4.24) respectively. M denotes the number of basis functions used in (4.23).	40
6.1	Compare $t(\mathbf{n}^*; h)$ and $t_{sim}(\mathbf{n}^*; h)$ for different number of sites	91
6.2	Global and local search results for different number of sites.	93

LIST OF FIGURES

1.1	Random walk on one dimensional integer lattice	1
2.1	Diagram for forward equation	11
2.2	Diagram for backward equation	12
3.1	Simulated exit times of a Broadwell process starting from $x = 0$. (a) $F(y) = 10y^3 + 5e^y + 1$, $v = 1/2$ and (b) $F(y) = 1 + y^2$, $v = 1$. Insets show Laplace-transformed data. Solid line: solution to equations (4.5), (4.6). Diamonds: Laplace transform of histogram data. The number of realizations was $N = 40,000$ in each case. . .	24
3.2	Simulated exit time distributions of a Broadwell process with flip rate $F(y) = 0.5 + 0.2 \cos(16y) + 0.1 \sin(64y)$, constant velocity $v = 1$, and $L = 1$. (a) The flip rate function $F(y)$. (b) Exit time distribution w_1 starting from $x = -0.5$ with velocity $+v$, generated by $F(y)$ in (a). (c) Exit time distribution w_2 starting from $x = 0.5$ with velocity $-v$, generated by flip rate $F(y)$ in (a). The number of exit times to generate each distribution is $N = 10^5$	25
4.1	(a) Propagation of discontinuities of equations (2.37) - (2.42) in the $x-t$ plane. The solution $w_1(x, t)$ is formally infinite on $x = L/2 - vt$ while $w_2(x, t)$ is infinite on $x = -L/2 + vt$. These singularities give rise to discontinuities in W_1 and W_2 that can be seen in (b,c). (b) Numerical computation of cumulative probability densities (cdfs) $W_1(x_0 = -L/4, t)$, $W_2(x_0 = -L/4, t)$ and auxiliary functions $Z_1(x_0 = -L/4, t)$, $Z_2(x_0 = -L/4, t)$ computed through (4.10) and Algorithm 4 using using 101 Chebyshev grid points and 51 eigenfunctions $\mathbf{u}_1, \mathbf{u}_2, \dots, \mathbf{u}_{51}$. (c) Numerical computation of cdfs $W_1(x_0 = L/3, t)$ and $W_2(x_0 = L/3, t)$ (solid) along with results from Monte Carlo simulations (diamond). Inset shows Laplace-transformed probability densities $\tilde{w}_1(x_0 = L/3, s)$ and $\tilde{w}_2(x_0 = L/3, s)$. Common parameters in (b,c) are $v = 1$, $F(y) = 1 + y$ and $L = 1$	31

4.2	Reconstructed approximations to flip rate functions $F^*(x)$ from noisy exit time data. (a,b) $F^*(x) = 1 - 0.7x - 0.3x^2 + 6x^3$, $M = 4$; (c,d) $F^*(x) = x^2e^{-x}/10 + 1/10$, $M = 5$; (e,f) $F^*(x) = 1 + x + 3x^2$, $M = 3$. The t -method was used in the left panels and the s -method was used in the right panels. $N = \infty$ corresponds to perfect, noiseless data, which is generated by solving the forward problems (4.1)-(4.4) and (4.5)-(4.7).	38
4.3	Error in reconstructed flip rate as a function of particle velocity. Each point is an average over 10 sets of $2N = 20,000$ exit times. Target flip rate $F^*(x) = \frac{9}{4}x^2 - \frac{3}{4}x + \frac{9}{16}$, corresponding to target coefficients $\mathbf{a}^* = [0.75, -0.375, 0.375, 0]$. Initial guesses are (a) $\mathbf{a} = [1, 1, 1, 1]$, (b) $\mathbf{a} = [0.76, -0.385, 0.365, 0.01]$. The same exit times were used for both (a) and (b). The difference in the errors is shown in (c). . . .	41
4.4	Dependence of error in reconstructed flip rate function $F(x)$ on the number of exit times per initial particle state N when $F(x) = 1 - 0.7x - 0.3x^2 + 6x^3$ using (a) t -method and (b) s -method. For each N , the error is calculated by performing minimizations for 10 data sets and taking the average, with each set containing $2N$ exit times.	44
5.1	Simulated exit time distributions of a Broadwell process with flip rate $F(y) = 0.5 + 0.2 \cos(16y) + 0.1 \sin(64y)$, constant velocity $v = 1$, and $L = 1$. (a) The flip rate function $F(y)$. (b) Exit time distribution w_1 starting from $x = -0.5$ with velocity $+v$, generated by $F(y)$ in (a). (c) Exit time distribution w_2 starting from $x = 0.5$ with velocity $-v$, generated by flip rate $F(y)$ in (a). The number of exit times to generate each distribution is $M = 10^5$	48
5.2	(a) Singularity structure of (5.7) and (5.12) – (5.14). (b) Singularity structure of (5.21) - (5.24)	50
5.3	Finite difference stencils for forward problem (5.13) – (5.7). a_1 is known on the diagonal $t = x/v + L/(2v)$, b_1 is known on the left boundary $x = -L/2$	54
5.4	Layer stripping algorithm. Dashed circles are values of $W_1(x, [\frac{x}{v} + \frac{L}{2v}]^+) \equiv U_1(x)$. Solid circles are values of $W_2(x, [\frac{L}{2v} - \frac{x}{v}]^+) \equiv U_2(x)$. $W_1^{(j,i)}$ and $W_2^{(j,i)}$ are updated along solid and dashed arrows respectively.	57

5.5	Reconstruction of flip rate functions $F(x)$: (a) $F(x) = 0.5 \sin(8x) + 1$, (b) $F(x) = \sin(5x) \cos(8x) + \cos(0.3x) \exp(0.5x) + x^2 \sin(-0.6x^3) + 0.5$, (c) $F(x) = 2.5x + 1.55$ for $-0.5 \leq x \leq -0.3$, $F(x) = -x + 0.5$ for $-0.3 < x < 0.2$, $F(x) = 0.25x + 0.25$ for $0.2 \leq x \leq 0.5$, and (d) $F(x) = 0.5 + 0.2 \cos(16x) + 0.1 \sin(64x)$, $N = 100$, $M = 200,000$	61
5.6	Reconstruction of flip rate functions $F(x)$: (a) $F(x) = 0.5 \sin(8x) + 1$, (b) $F(x) = \sin(5x) \cos(8x) + \cos(0.3x) \exp(0.5x) + x^2 \sin(-0.6x^3) + 0.5$, (c) $F(x) = 2.5x + 1.55$ for $-0.5 \leq x \leq -0.3$, $F(x) = -x + 0.5$ for $-0.3 < x < 0.2$, $F(x) = 0.25x + 0.25$ for $0.2 \leq x \leq 0.5$, (d) $F(x) = 0.5 + 0.2 \cos(16x) + 0.1 \sin(64x)$, $N = 100$, $M = 1,000,000$	62
5.7	Dependence of error in flip rate function $F(x)$ reconstruction on the number of subintervals N . (a) The probability density function $W_2(L/2, t) \equiv W_{2,\text{data}}(t) =$ $-0.1403t^6 - 0.7352t^5 + 2.9494t^4 - 3.1707t^3 + 1.1536t^2 + 0.1476t + 0.0015$ for $t \in [0, L/v]$. (b) Given $W_2(L/2, t)$, we use both first and second order layer stripping methods to reconstruct $F(x)$, $0 \leq x \leq L/2$	63
5.8	Reconstruction of flip rate functions $F(x)$ with small velocity from Monte-Carlo simulation data and artificial noisy data: (a) and (c) $F(x) =$ $0.3 \sin(5x) \cos(8x) + 0.3 \cos(0.3x) \exp(0.5x) + 0.3x^2 \sin(-0.6x^3) + 0.15$, (b) and (d) $F(x) = 0.5 + 0.2 \cos(16x) + 0.1 \sin(64x)$, $N = 200$, $v = 0.1$. (a) and (b) are reconstructed from simulated noisy data with $M = 1,000,000$. (c) and (d) are reconstructed from artificial noisy data.	64
6.1	Patient recruitment in a drug trial. m sites are allocated n_1, n_2, \dots, n_m drug doses which must be tested. Patients arrive at each site at a rate λ_j , consume the drugs and are recruited into patient horizon is reached.	69
6.2	Interpretation of $\lambda t(n_1, n_2; h)$ in equation (6.12) by summing terms in the regions R_1, R_2 and R_3	72
6.3	Interpretation of equations (6.4) - (6.6). (a) shows the number of drugs consumed. (b) extends the grids to infinity in i and j direction with ghost nodes, and shows the number of patients arrive.	73

- 6.4 Comparison of simulated and analytical mean recruiting time. The total number of drugs $n = 1200$, the number of patients $h = n$, $\Lambda = [2, 4]$, the number of exit times used to generate the mean recruiting time is $K = 10^3$. (a, b) both show simulated and analytical mean recruiting time (equation (6.16)), but (b) zooms in (a), and shows the simulated and analytical mean recruiting time in the neighborhood of the predicted optimal drug inventory $\mathbf{n}^* = [n_1^*, n_2^*]$. 78
- 6.5 Contour plots for t_{sim}, t and surface plot for $t_{sim} - t$. (a, b, c) $n = 800$, $\Lambda = [3, 4, 7]$, $R = 100$, $\mathbf{n}^* = [172, 229, 399]$, $\mathbf{n}_{sim}^* = [168, 224, 408]$. (d, e, f) $n = 900$, $\Lambda = [8, 6, 4]$, $R = 100$, $\mathbf{n}^* = [400, 300, 200]$, $\mathbf{n}_{sim}^* = [404, 298, 198]$. (g, h, i) $n = 1100$, $\Lambda = [4, 4.1, 4.2]$, $R = 100$, $\mathbf{n}^* = [358, 367, 375]$, $\mathbf{n}_{sim}^* = [356, 364, 380]$. 94

ABSTRACT

A random walk process can be described as a walker's path which consists of a sequence of random steps associated with a time parameter. The exit time is defined to be the time taken for the random walker to first reach a specified point (or set of points). Exit times are very useful in many stochastic problems, because they are easy to measure compared with the probability of a random walker being at a particular position.

This dissertation is concerned with two exit time problems: reconstructing the flip rate of a persistent random walk from its exit time distribution and calculating the mean exit time of a high-dimensional random walk on a lattice.

The first problem is actually an inverse stochastic problem, where the underlying physics of the random walker is modeled by a one-dimensional Broadwell process. The Broadwell process can be described as a random walk, where the particle transitions, with a given flip rate, between two states having the same speed but opposite directions. The time taken for the particle to first reach either endpoint of a finite interval is recorded as the exit time. The goal is to infer the flip rate function of the Broadwell process from its exit time distribution. We provide a detailed description and analysis of two algorithms used for reconstructing the flip rate function of the Broadwell process. The first algorithm studied is the projection method, which reduces the dimensionality of the problem by representing the flip rate function as a linear combination of Legendre polynomials. The other algorithm is the layer stripping method, where we utilize a finite difference method and the causality of propagation to reconstruct the flip rate function. To verify the analytical solutions, we develop a Monte Carlo algorithm to simulate the Broadwell process, and acquire the exit time distributions, which are used to reconstruct the flip rate.

The second problem arises from clinical trials. In clinical trials, new drugs enjoy significant profitability during the patent protection period. Any clinical trial delays would increase the cost. Thus, how to accurately estimate the patient recruiting time and efficiently plan drug inventory so that the recruiting time is minimized is vital to clinical trials. We model the patient recruitment process by a particle undergoing a high-dimensional, integer-valued random walk. The patient recruiting time becomes the exit time of the random walk. We derive analytic approximations for the optimal drug distribution and associated mean recruiting time for multiple testing centers. We also develop a Monte Carlo algorithm to simulate the clinical trial recruiting process, then calculate the mean exit time and the optimal drug distribution from simulations to test the accuracy of analytical approximations.

Chapter 1

INTRODUCTION

1.1 Motivation

A random walk process can be described as a walker's trajectory which is composed of a series of successive random steps associated with a time parameter. It is used as a fundamental model for many stochastic phenomena, such as queueing-based computer networks in computer science [1, 2], fluctuating stock price in finance [3, 4] and the search paths of foraging animals in ecology [5, 6]. Random walks have many properties, such as exit times, dispersal distribution, and recurrence rates. Among these properties, in particular, we are interested in the exit time [7], which is defined to be the time taken for the random walker to first reach a specified value (or set of values). For example, Figure 1.1 shows a discrete-time random walk on a one dimensional integer lattice. Let $X(t) \in \mathbb{Z}$ be the position of a random walk at time $t \in \mathbb{Z}$. A particle starts the random walk from $X(0) = 0$ at $t = 0$, and moves one step to the right ($X(1) = 1$) or left ($X(1) = -1$) at time $t = 1$ with probability p or q respectively, where $0 \leq p, q \leq 1$, $p + q = 1$. If the exit time τ is defined as the time it takes for the particle to reach N for the first time, then $\tau = \inf\{t \in \mathbb{Z} : X(t) = N\}$.

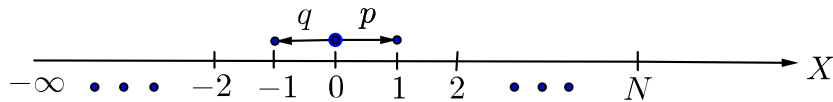


Figure 1.1: Random walk on one dimensional integer lattice

Exit times are very useful in studying random walk problems, because they are easy to measure compared with the probability of a random walker being at a particular position. Exit times are studied in biology, supply chain management, finance, and chemical physics. For example, in the mammalian central nervous system, the integrate-and-fire neuron model [8, 9, 10] is a classic model for neural behavior analysis. The voltage (or membrane potential) between the interior and exterior of a neuron’s membrane fluctuates as a result of the noisy synaptic inputs from other neurons. Once the voltage reaches a limit, a spike (or action potential) is generated and the potential resets to zero. The interspike times, which are experimentally measured [11], define the exit times of the fluctuating voltage. The biophysicist may want to infer the intrinsic current-voltage relationship of the neuron by studying the exit time distribution. For another example, in the stock market, reaching the break-even point (gains equal losses) is the first major step towards profitability. Because the stock price fluctuates from time to time, investors trading with stock options may want to make stock investment decisions based on the mean exit time when the stock price reaches break-even point, or exceeds a specified price for the first time [12, 7]. One common feature in these phenomena is that fluctuations in the quantity of interest are stochastic and the systems generate data in the form of exit times. In this dissertation, we focus on studying two exit problems arising from biophysics and clinical trial supply chain management.

1.2 Broadwell Processes

Of all the stochastic processes, Brownian motion is the most classic model and governed by the stochastic differential equation $dX = \sqrt{2D}dW$, where D is the diffusion coefficient and W is the Wiener process. However, in this dissertation, we will define any stochastic process governed by $dX = cdt + \sqrt{2D}dW$, where c is the drift coefficient, as a “Brownian-like” random walk or a general stochastic process. There are many cases where the researchers would like to infer the parameters of a random walk from the first exit time [13, 14, 15]. Problems of this type are essentially stochastic

inverse problems. One application of stochastic inverse problems arises in the reconstruction of bond potentials from rupture time distributions [16, 17, 18]. Because many macromolecules can be stretched under mechanical force, applying controlled mechanical forces on single molecules plays an important role in understanding their structures and functions. In force spectroscopy experiments, an increasing force is applied across a macromolecular bond until it ruptures. Because of thermal fluctuations, the rupture force is a random variable; thus the goal is to infer properties of the bond potential from the *distribution* of rupture forces [19]. Stochastic inverse problems also commonly arise in diffuse optical tomography [20, 21]. In all these applications, the exit time distribution of a “Brownian-like” motion leaving a finite interval is measured, and one wishes to reconstruct the drift and/or diffusion function.

While “Brownian-like” motion is a canonical stochastic model, the inverse problem associated with “Brownian-like” motion is ill-posed [22, 13] and motivates the study of stochastic exit time problems based on other types of random walk. Ill-posedness is a trademark of many inverse problems. A problem is *well-posed* if a solution exists, is unique and depends continuously on the data. Otherwise the problem is *ill-posed*. At present, issues of existence and uniqueness of spatially dependent parameters for random walks are generally not well established, although some important results for “Brownian-like” motions can be found in [22]. This triggers our interest to study stochastic problems of other types of random walk.

We generalize the study of “Brownian-like” inverse problems to Broadwell processes which was first introduced by Broadwell [23, 24, 25, 26] in 1964. A one dimensional Broadwell process can be described as the random walk of a particle that randomly transits between two states, where the two states are associated with the same speed but have opposite directions. The particle changes its traveling direction with a spatially dependent flip rate. The time it takes for the particle to first reach either endpoint of the interval is recorded as the exit time. Broadwell phenomena are ubiquitous in a wide range of areas, such as bacteria chemotaxis [27], microtubule growth [28], diffuse optical tomography [20], charge transport in DNA [29], and interactions

of individuals in fish schools [30].

The Broadwell process is governed by the telegrapher’s equation [31, 32] and has the desirable property that it interpolates between a ballistic and diffusive motion [28, 29]: the time between transitions decreases as the flip rate increases, but increases as the flip rate decreases. The Broadwell model opens the analysis of the inverse problem for these two types of limiting processes; studying the inverse Broadwell problem may therefore provide insights into the important, fully diffusive problem. We specialize to the constant speed Broadwell process, assuming that transition probabilities are spatially dependent. From the distribution of exit times out of a finite interval, our goal is to find the transition probability (“flip-rate”) function.

Many well-established optimization theories and numerical methods have been used to address the inverse problems, such as the minimization of a Tikhonov regularized objective function. However, it might be time consuming to optimize an objective function due to the large number of iterations. Geophysicists have developed the layer stripping algorithm (or downward continuation algorithm) [33, 34, 35] as an alternative to solving an optimization problem. The layer stripping algorithm, which arises from one-dimensional inverse scattering (impulse-response) problem in reflection seismology [36], speech synthesis [37] and transmission-line models [38], is established on the method of characteristics [39], the finite difference method, and causal boundary data. Another classical inversion method commonly used for inverse scattering problems is formulated in the form of an integral equation and non-causal boundary data. Boundary data is causal if it is generated by solving an initial boundary value problem; otherwise, the boundary data is non-causal. There are various integral equation based methods proposed by Krein [40], Gopinath and Sondhi [41, 42], Gelfand and Levitan [43, 44], and Marchenko *et al* [45], for solving this inverse problem. These integral equations, which are associated with special structured kernels, such as Toeplitz [46] and Hankel [47], are formulated by considering particular impulse-response pairs of scattering data measured at the boundary of the medium. The difference between the

layer stripping algorithm and the method of integral equations is that the layer stripping algorithm utilizes the differential structure and the causality of propagation to reconstruct the medium layer by layer, while the integral equation utilizes the causality, symmetry and losslessness properties of the medium for reconstruction.

Accurately simulating the exit times of a Brownian motion can be quite involved although reliable methods do exist: see [48, 49, 50, 51] for example. Nevertheless, one important advantage of studying the Broadwell model is the ease with which it can be simulated. Accurate simulations are critical for comparisons between reconstructed flip-rate functions and the underlying target functions that produced the exit data. When generating the exit time distribution from our simulations, the only error (besides round-off) stems from using a finite number of realizations.

1.3 Clinical Trials

Clinical trials are a series of tests at certain stages of drug development to generate safety and efficacy data before pharmaceutical companies can commercialize their new drugs. On average, for an oncology drug, it usually takes 7 years to complete clinical trials [52]. For other drugs, it takes a similar amount of time to complete the trials. It is obvious that the trial duration occupies a significant fraction of the 20 years of patent protection time in the US. The pharmaceutical companies can only make a large profit during the patent protection time. Hence, it is very important for the drug manufacturers to avoid clinical trial delays and accelerate clinical trials to guarantee profitability.

In addition, clinical trials are often very expensive. Recently, there has been a trend of conducting clinical trials in developing countries in Eastern Europe, Latin America and Asia [53]. The clinical trial globalization requires an internationally flexible drug supply chain, which increases the associated cost [54]. It is expensive to adopt the traditional practice of keeping a large supply of drugs in testing centers. Pharmaceutical companies need to optimize drug inventories to save cost [55, 56].

As the time and cost problems are interwoven in clinical trials, one question arises: how can the drug inventory be efficiently planned so that the recruiting time is minimized while the drug is distributed in numerous locations globally? In clinical trials, sufficient patient recruitment is crucial. However, less than one third of publicly funded trials successfully recruit the planned number of patients on time [57, 58]. Also, the investigators often underestimate the time to recruit the target number of patients. Estimating the patient recruiting time accurately is critical to the success of the trial.

Currently, there are five main models to estimate the recruiting time: the unconditional model, the conditional model, the Poisson model, the Bayesian model, and the Markov model. The unconditional model was developed by Carter [59], which assumes that all the testing centers start recruiting at the same time, and estimates the recruiting time by dividing the target patient sample size by expected total patient arrival rate, which is the sum of all individual arrival rates at each center. The expected individual arrival rate is estimated from historical data at each testing center, and assumed to be a fixed constant during the whole trial. However, this model fails to consider a scenario such as varying total arrival rate, and different starting times for the recruitment process. The conditional model (Carter [59] and Moussa [60]) addresses the limitation of the unconditional model by allowing different testing centers to have different total arrival rates, allowing varying number of testing centers, or letting the recruitment process start at different times, depending on the needs of the clinical trial. The Poisson model with time-constant rate is discussed in Carter and Anisimov's papers [61, 62, 59, 63]. Carter discussed the model theoretically [63] and its implementation [59]. Anisimov proposed [61, 62] that the recruitment rate is Gamma distributed in his Poisson model. Based on the Poisson-gamma model, Anisimov used statistical techniques to estimate the parameters of the model, predicted the remaining recruitment time, and established confidence intervals on the number of centers required to recruit in a certain time. Williford [64] and Gajewski [65] proposed a Bayesian method, which starts with a prior distribution for arrival rates, then obtains the posterior predictive distribution by calculating the weighted average of data from

the prior distribution and the actual data in the trial. As more and more actual data is collected, the weight on prior distribution decreases and the weight on the actual data increases. Five Monte-Carlo simulation Markov models are developed by Abbas [66] to simulate the recruitment process. Each model considers two states: a contacted state and an arrived state. The contacted state is the state that the volunteer patient contacts the testing center, or is contacted by a recruiter, and the patient may or may not agree to participate in the trial. The arrived state is the state that the contacted patient agrees to participate in the trial. The five models are: the simplest model (SM), the continuous time with constant probability model (SM1), the continuous time with probability distribution model (SM2), the discrete time with replacements model (SM3), and the discrete time without replacements model (SM4). SM discusses the recruitment process with fixed variables, and assumes that the recruiting time is a continuous variable, which can be calculated by summation of the continuous inter-arrival times. SM1 discusses the recruitment process with random variables, but considers the case that the contacted patients move to arrived state with constant probability. SM2 studies the same recruitment process as SM1, but the probability of contacted patients moving to the arrived state follows a uniform distribution. SM3 assumes that the recruiting time is a discrete variable, and the patients who don't move from contacted state to arrived state in the first period of time will be re-considered in the future period of time. SM4 assumes that the recruiting time is also a discrete variable, but the patients who don't move to arrived state in a certain period of time will not be considered again.

Some researchers have used multi-echelon inventory methods and discrete event simulations [67, 68, 69, 70, 71, 72] to study the clinical trial supply chain optimization problem from the perspective of cost reduction. However, the analytic solutions for clinical trial supply chain optimization with respect to time reduction have not been well studied. In this dissertation, we provide an analytic solution to the problem of finding an efficient plan for drug inventory.

In general, before the trial starts, statisticians calculate the number of patients

h needed for the trial [73, 74, 75, 76], where h is called the patient horizon. Suppose a pharmaceutical company would like to recruit h patients from m testing centers, each with n_i number of drugs respectively, $i = 1, 2, \dots, m$, and the total number of drugs $n = \sum_{i=1}^m n_i = h$. The patients arrive at each testing center with different rates and we are interested in the time taken to recruit h patients. This process can be described as a random walk on a m -dimensional lattice $[0, n_1] \times [0, n_2] \times \dots [0, n_m]$, where the walker moves one step in positive direction of i^{th} coordinate with probability p_i if center i recruits one patient. Once the walker moves h steps in total, the travel time is recorded as the exit time, which is the desired recruiting time. Problems of this type are essentially random walks on m -dimensional lattices [77, 78, 79, 80, 81, 82, 83], arising in solid state physics problems, such as the trapping of mobile defects in crystals [77, 84, 85, 86, 87] and the transient photoconductivity of amorphous semiconductors [88, 89]. In these studies, exit time properties, such as the probability for a random walker to first reach a specific point after n steps, the mean number of steps and recurrence time to return to the origin (or any other points on a m -dimensional periodic lattice) for the first time, are well studied. The mathematical tools that are used in treating these exit time problems are: Fourier and Laplace transforms, the generating function, Green's functions and basic asymptotic analysis. In this dissertation, we are interested in optimizing the drug inventory among m testing centers so that the mean exit time is minimized, and will use asymptotic methods to solve the problem.

1.4 Dissertation Outline

The work presented in this dissertation can be divided into the following chapters:

Chapter 1 herein summarizes the motivation for this work, gives the background of exit time problems in random walks and their applications in a variety of disciplines. In particular, it discusses the exit time problems arising from the Broadwell process and clinical trial supply chains.

Chapter 2 presents the backward Kolmogorov equation for the two-state Broadwell problem parameterized by a spatially dependent (but state-symmetric) flip rate and a constant speed.

Chapter 3 explains the Monte-Carlo method used to simulate a Broadwell random walker with spatially dependent velocity and flip rate.

Chapter 4 discusses the reconstruction of the flip rate function in a Broadwell process from the exit time distributions using projection methods, which involve minimizing the distance between the solution of the backward Kolmogorov equation and exit time data (derived from simulations or from the solutions of the backward Kolmogorov equation with a target flip rate function).

Chapter 5 discusses the reconstruction of the flip rate function in a Broadwell process from the exit time distributions using the layer stripping method which utilizes the finite difference method and the method of characteristics to reconstruct the flip rate function layer by layer.

Chapter 6 presents an asymptotic method to calculate the mean exit time for recruiting h patients from m testing centers, when the total number of drugs $n = h$. We also present a way to optimize the drug inventory among the centers so that the mean exit time is minimized.

Chapter 2

FORWARD AND BACKWARD EQUATIONS FOR A STOCHASTIC PROCESS

In this chapter, we first provide a brief introduction to the forward and backward equations of a stochastic process. Then we derive the backward equation for the two-state Broadwell problem parameterized by a spatially dependent flip rate and a constant speed.

2.1 Forward and Backward Kolmogorov Equation

Let $P(y, \sigma|x, \tau)$ denote the transition probability for a diffusion process, that is continuous in time and position, to transite from starting position x at time τ to current position y at time σ , $0 \leq \tau < \sigma$.

The Kolmogorov forward equation addresses the forward problem: suppose we know the probability of the particle being at the initial position x at time τ , and would like to know the probability of the particle being at position y at time σ . Thus, the Kolmogorov forward equation is a differential equation describing the dynamics of transition probability at current position and time (y, σ) , given the initial position and time (x, τ) . The “forward” refers to the fact that the PDE is integrated forward in time.

The forward Kolmogorov equation can be derived by applying the Chapman-Kolmogorov equation to $P(y, \sigma + \Delta\sigma|x, \tau)$,

$$P(y, \sigma + \Delta\sigma|x, \tau) = pP(y - \Delta y, \sigma|x, \tau) + pP(y + \Delta y, \sigma|x, \tau) + (1 - 2p)P(y, \sigma|x, \tau), \quad (2.1)$$

where $\Delta\sigma > 0$, p is the probability of hopping to the left or right, $1 - 2p$ is the probability of staying at the same position without hopping. Equation (2.1) can be explained as

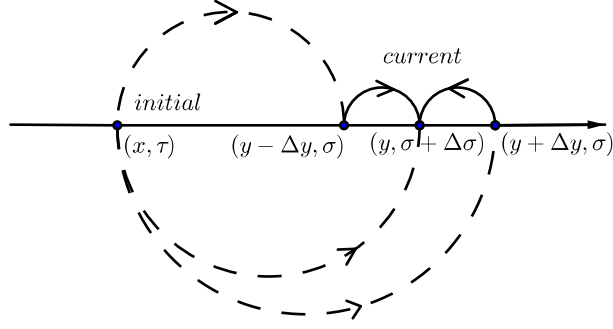


Figure 2.1: Diagram for forward equation

follows. Given initial position and time (x, τ) , the probability of the random walker being at $(y, \sigma + \Delta\sigma)$ is equal the sum of three probabilities: (1) the random walker starts at (x, τ) and arrives at $(y - \Delta y, \sigma)$, then takes time $\Delta\sigma$ to hop to y with probability p ; (2) the random walker starts from x at time τ and arrives at $y + \Delta y$ at time σ , then takes time $\Delta\sigma$ to hop to y with probability p ; (3) the random walker starts from (x, τ) and arrives at (y, σ) , then stays at y for time $\Delta\sigma$ with probability $1 - 2p$. See Figure 2.1.

Then applying Taylor's formula to equation (2.1) about (y, σ) , we find that

$$\begin{aligned}
& P(y, \sigma + \Delta\sigma | x, \tau) - P(y, \sigma | x, \tau) \\
&= p \left[P(y - \Delta y, \sigma | x, \tau) + P(y + \Delta y, \sigma | x, \tau) - 2P(y, \sigma | x, \tau) \right], \\
&= p \left[P(y, \sigma | x, \tau) - \frac{\partial}{\partial y} P(y, \sigma | x, \tau) \Delta y + \frac{(\Delta y)^2}{2} \frac{\partial^2 P(y, \sigma | x, \tau)}{\partial y^2} + O((\Delta y)^3) \right. \\
&\quad \left. + P(y, \sigma | x, \tau) + \frac{\partial}{\partial y} P(y, \sigma | x, \tau) \Delta y + \frac{(\Delta y)^2}{2} \frac{\partial^2 P(y, \sigma | x, \tau)}{\partial y^2} + O((\Delta y)^3) \right. \\
&\quad \left. - 2P(y, \sigma | x, \tau) \right], \\
&= p \left[\frac{\partial^2 P(y, \sigma | x, \tau)}{\partial y^2} (\Delta y)^2 + O((\Delta y)^3) \right]. \tag{2.2}
\end{aligned}$$

Divide equation (2.2) by $\Delta\sigma$, and assume that

$$\lim_{\Delta\sigma, \Delta y \rightarrow 0} \frac{(\Delta y)^2}{\Delta\sigma} = D, \quad \lim_{\Delta\sigma, \Delta y \rightarrow 0} \frac{(\Delta y)^3}{\Delta\sigma} = 0.$$

Then we have

$$\frac{\partial}{\partial\sigma} P(y, \sigma|x, \tau) = \mathcal{L}P(y, \sigma|x, \tau),$$

where

$$\mathcal{L} = pD \frac{\partial^2}{\partial y^2},$$

and pD is the diffusion coefficient.

The Kolmogorov backward equation addresses the backward problem: suppose we know the probability distribution of y at time σ , and would like to know the probability of the random walk initially starting at x at time τ . Thus, the Kolmogorov backward equation is a differential equation describing the dynamics of the transition probability at initial position and time (x, τ) given the current position and time (y, σ) . The “backward” refers to the fact that the PDE is integrated backward in time. Again,

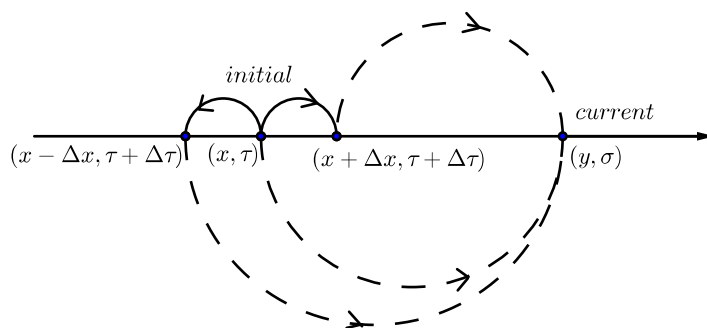


Figure 2.2: Diagram for backward equation

we can apply the Chapman-Kolmogorov equation to $P(y, \sigma|x, \tau)$:

$$P(y, \sigma|x, \tau) = pP(y, \sigma|x+\Delta x, \tau+\Delta\tau) + pP(y, \sigma|x-\Delta x, \tau+\Delta\tau) + (1-2p)P(y, \sigma|x, \tau+\Delta\tau). \quad (2.3)$$

Equation (2.3) can be explained as follows. Given current position and time (y, σ) , the probability of the random walker initially being at (x, τ) is equal the sum of three probabilities: (1) the random walker takes time $\Delta\tau$ to hop to $x + \Delta x$ from x with probability p , then continues random walk from $(x + \Delta x, \tau + \Delta\tau)$ to the current position and time (y, σ) ; (2) the random walker takes time $\Delta\tau$ to hop to $x - \Delta x$ from x with probability p , then continues random walk from $(x - \Delta x, \tau + \Delta\tau)$ to the current position and time (y, σ) ; (3) the random walker starts from (x, τ) and stay at x for time $\Delta\tau$ with probability $1 - 2p$, then continues the random walk from $(x, \tau + \Delta\tau)$ to the current position and time (y, σ) . See Figure 2.2. Using Taylor's expansion,

$$\begin{aligned}
& P(y, \sigma|x, \tau) - P(y, \sigma|x, \tau + \Delta\tau) \\
&= p \left[P(y, \sigma|x + \Delta x, \tau + \Delta\tau) + P(y, \sigma|x - \Delta x, \tau + \Delta\tau) - 2P(y, \sigma|x, \tau + \Delta\tau) \right], \\
&= p \left[P(y, \sigma|x, \tau + \Delta\tau) - \frac{\partial}{\partial y} P(y, \sigma|x, \tau + \Delta\tau) \Delta x + \frac{(\Delta x)^2}{2} \frac{\partial^2 P(y, \sigma|x, \tau + \Delta\tau)}{\partial x^2} \right. \\
&\quad + O((\Delta x)^3) + P(y, \sigma|x, \tau + \Delta\tau) + \frac{\partial}{\partial y} P(y, \sigma|x, \tau + \Delta\tau) \Delta x \\
&\quad \left. - \frac{(\Delta x)^2}{2} \frac{\partial^2 P(y, \sigma|x, \tau + \Delta\tau)}{\partial x^2} + O((\Delta x)^3) - 2P(y, \sigma|x, \tau + \Delta\tau) \right], \\
&= p \frac{\partial^2 P(y, \sigma|x, \tau + \Delta\tau)}{\partial x^2} \Delta x^2 + O((\Delta x)^3). \tag{2.4}
\end{aligned}$$

Divide equation (2.4) by $\Delta\tau$, and assume that

$$\lim_{\Delta\tau, \Delta x \rightarrow 0} \frac{(\Delta x)^2}{\Delta\tau} = D, \quad \lim_{\Delta\tau, \Delta x \rightarrow 0} \frac{(\Delta y)^3}{\Delta\tau} = 0,$$

we have

$$-\frac{\partial}{\partial \tau} P(y, \sigma|x, \tau) = \mathcal{L}^* P(y, \sigma|x, \tau),$$

where

$$\mathcal{L}^* = pD \frac{\partial^2}{\partial x^2},$$

pD is the diffusion coefficient.

We see that both Kolmogorov forward and backward equations describe the Brownian process, and the backward operator is the adjoint of the forward operator,

the forward and backward operators are the same in this case. But the backward operator is especially helpful in obtaining the exit time distribution from the survival probability of the Brownian process. Let A and B be two positions on the interval, where $A < B$, we define the exit time as the time it takes for the Brownian process to reach either position A or B , $S(x, t) = \text{Prob}(A < x < B)$ be the probability that the process doesn't reach positions A or B at time t given that it starts from x at time 0. $S(x, t)$ is also called the survival probability, and is given by integrating over all possible current positions y :

$$S(x, t) = \int_A^B P(y, t|x, 0) dy,$$

where $P(y, t|x, 0)$ is the transition probability. If the particle has survived until t but exits at time $t + dt$, $w(x, t)dt$ represents the probability of first exit in time interval $(t, t + dt)$, then the exit time distribution $w(x, t)$ can be obtained by

$$\begin{aligned} \text{Prob}(t \leq \text{exit time} \leq t + dt \mid \text{initial position } x) &= w(x, t)dt = S(x, t) - S(x, t + dt), \\ \Rightarrow w(x, t) &= -\frac{\partial}{\partial t}S(x, t). \end{aligned} \quad (2.5)$$

2.2 Derivation of Backward Equation for Broadwell Process

In this section, we derive the backward equation from the forward equation of the Broadwell process using the fact that the backward equation is the adjoint of the forward equation. The two-state Broadwell model can be described as a particle's random walk parameterized by a starting position $x \in [-L/2, L/2]$ at time τ , a velocity $+v$ (state 1, where v is a positive constant) or $-v$ (state 2), and a flip rate $F(y)$, where $y \in [-L/2, L/2]$ represents the current position at time σ . While traveling with speed v , the particle shifts between the two states with probability $F(y)d\sigma$ within time interval $(\sigma, \sigma + d\sigma)$. We define l and k as the initial state and the current state respectively, where $l, k \in \{1, 2\}$. $P_{kl}(y, \sigma|x, \tau)dy$ is the probability that the particle lies in the interval $(y, y + dy)$ in state k at time σ , given that the particle initially starts at x in state l at time τ .

Given a starting position x , when the particle exits from either endpoint, the total travel time is recorded. When the Broadwell process is repeated a large number of times, we obtain the exit time distributions. Define $w_1(x, t)$, $w_2(x, t)$ to be exit time distributions conditioned on the particle initially starting from x in state 1 or state 2 respectively, where t is the exit time. We now derive equations for $w_1(x, t)$ and $w_2(x, t)$.

Let $P_{1l}(y, \sigma|x, \tau)$ and $P_{2l}(y, \sigma|x, \tau)$ represent the probability that the particle is at y in state 1 and 2 at time σ respectively, given that the particle initially starts at x in state l at time τ . Consider the forward equations for the transition probabilities $P_{1l}(y, \sigma|x, \tau)$ and $P_{2l}(y, \sigma|x, \tau)$ of the Broadwell process:

$$\frac{\partial}{\partial \sigma} P_{1l}(y, \sigma|x, \tau) = -v \frac{\partial}{\partial y} P_{1l}(y, \sigma|x, \tau) + F(y)(P_{2l}(y, \sigma|x, \tau) - P_{1l}(y, \sigma|x, \tau)), \quad (2.6)$$

$$\frac{\partial}{\partial \sigma} P_{2l}(y, \sigma|x, \tau) = v \frac{\partial}{\partial y} P_{2l}(y, \sigma|x, \tau) + F(y)(P_{1l}(y, \sigma|x, \tau) - P_{2l}(y, \sigma|x, \tau)), \quad (2.7)$$

$$P_{1l}(-L/2, \sigma|x, \tau) = 0, \quad (2.8)$$

$$P_{2l}(L/2, \sigma|x, \tau) = 0, \quad (2.9)$$

for $\sigma > \tau$, $-L/2 < y < L/2$, and

$$P_{1l}(y, \sigma|x, \tau) = \delta_{1l} \delta(y - x), \quad (2.10)$$

$$P_{2l}(y, \sigma|x, \tau) = \delta_{2l} \delta(y - x), \quad (2.11)$$

for $\sigma \leq \tau$, $-L/2 < y < L/2$, where δ_{1l} and δ_{2l} are Kronecker delta functions, and $\delta(\cdot)$ is Dirac delta function.

Equation (2.6) can be explained by the two equations below:

$$\frac{\partial}{\partial \sigma} P_{1l}(y, \sigma|x, \tau) = -v \frac{\partial}{\partial y} P_{1l}(y, \sigma|x, \tau), \quad (2.12)$$

$$\frac{\partial}{\partial \sigma} P_{1l}(y, \sigma|x, \tau) = F(y)(P_{2l}(y, \sigma|x, \tau) - P_{1l}(y, \sigma|x, \tau)). \quad (2.13)$$

Equation (2.12) is actually a transport equation, which means that the particle is advecting to the right with constant speed v . In equation (2.13), when the right-hand side is positive, the particle is currently more likely to be in state 2 than state 1, and $P_{1l}(y, \sigma|x, \tau)$ on the left-hand side increases, which means that the particle is more

likely to flip from current state 2 to state 1. We can combine equations (2.12) and (2.13) into equation (2.6), which means that when the particle is in state 1, advecting to the right with constant speed v , it is more likely to flip from current state 1 to state 2. Equation (2.7) means that when the particle is in state 2, advecting to the left with constant speed v , it is more likely to flip from current state 2 to state 1. Equations (2.8) and (2.9) state that no matter where the Broadwell process starts, given $\sigma > \tau$, the probability of observing a particle at $y = -L/2$ in state 1 (moving to the right) and the probability of observing a particle at $y = L/2$ in state 2 (moving to the left) are zero. Hence, equations (2.8) and (2.9) are “absorbing” boundary conditions. When $l = 1$, equations (2.10) and (2.11) become $P_{11}(y, \sigma|x, \tau) = \delta(y - x)$ and $P_{21}(y, \sigma|x, \tau) = 0$, saying that the particle is in state 1 and position x before the Broadwell process really starts, i.e. $\sigma \leq \tau$. Similarly, taking $l = 2$ yields $P_{12}(y, \sigma|x, \tau) = 0$ and $P_{22}(y, \sigma|x, \tau) = \delta(y - x)$, saying that the particle is in state 2 and position x before the Broadwell process really starts. In other words, equations (2.10) and (2.11) state that the particle is in position x state l when $\sigma \leq \tau$.

We rewrite equations (2.6) and (2.7) in operator form as

$$\frac{\partial}{\partial \sigma} P_{kl}(y, \sigma|x, \tau) = \mathcal{L}(y, k) P_{kl}(y, \sigma|x, \tau), \quad k = 1, 2, \quad (2.14)$$

where

$$\mathcal{L}(y, k) P_{kl}(y, \sigma|x, \tau) = \sum_{k'=1}^2 L_{kk'}(y) P_{k'l}(y, \sigma|x, \tau), \quad (2.15)$$

$$L_{11}(y) = -v \frac{\partial}{\partial y} - F(y), \quad L_{12}(y) = F(y), \quad (2.16)$$

$$L_{21}(y) = F(y), \quad L_{22}(y) = v \frac{\partial}{\partial y} - F(y). \quad (2.17)$$

The backward equation is given in terms of the adjoint operator \mathcal{L}^* [90, 14] operating on the initial position and state:

$$-\frac{\partial}{\partial \tau} P_{kl}(y, \sigma|x, \tau) = \mathcal{L}^*(x, l) P_{kl}(y, \sigma|x, \tau), \quad l = 1, 2, \quad (2.18)$$

where

$$\mathcal{L}^*(x, l)P_{kl}(y, \sigma|x, \tau) = \sum_{l'=1}^2 L_{ll'}^*(x)P_{kl'}(y, \sigma|x, \tau), \quad (2.19)$$

$$L_{11}^*(x) = v\frac{\partial}{\partial x} - F(x), \quad L_{12}^*(x) = F(x), \quad (2.20)$$

$$L_{21}^*(x) = F(x), \quad L_{22}^*(x) = -v\frac{\partial}{\partial x} - F(x). \quad (2.21)$$

Let $t = \sigma - \tau$. Because the Broadwell process is a time homogeneous process, given a previous configuration (l, x) , the probability of finding the particle in configuration (state k , position y) depends only on the length of time separating the two configurations. We have $P_{kl}(y, t|x, 0) = P_{kl}(y, \sigma|x, \tau)$ and $-\frac{\partial}{\partial \tau} = \frac{\partial}{\partial t}$. Hence, the backward equations become

$$\frac{\partial}{\partial t}P_{k1}(y, t|x, 0) = (v\partial_x - F(x))P_{k1}(y, t|x, 0) + F(x)P_{k2}(y, t|x, 0), \quad (2.22)$$

$$\frac{\partial}{\partial t}P_{k2}(y, t|x, 0) = F(x)P_{k1}(y, t|x, 0) + (-v\partial_x - F(x))P_{k2}(y, t|x, 0), \quad (2.23)$$

$$P_{k1}(y, t|L/2, 0) = 0, \quad (2.24)$$

$$P_{k2}(y, t|-L/2, 0) = 0, \quad (2.25)$$

for $t > 0$, $y \in D$ and

$$P_{k1}(y, t|x, 0) = \delta_{k1}\delta(y - x), \quad (2.26)$$

$$P_{k2}(y, t|x, 0) = \delta_{k2}\delta(y - x), \quad (2.27)$$

for $t \leq 0$, $y \in D$. Equations (2.24) and (2.25) mean that when the particle initially starts at $x = L/2$ or $x = -L/2$ at $t = 0$, advecting to the right or left respectively, it exits as long as $t > 0$. The probability of observing the particle in position y at time $t > 0$ is zero.

Let $S_1(x, t)$ be the probability that the particle is in $[-L/2, L/2)$ at time t given that it starts at position x in state 1, $S_2(x, t)$ be the probability that the particle is in $(-L/2, L/2]$ at time t given that it starts at position x in state 2. Then the survival probabilities are given by integrating over all possible current positions y and states:

$$S_i(x, t) = \int_{-\frac{L}{2}}^{\frac{L}{2}} \sum_{k=1}^2 P_{ki}(y, t|x, 0) dy, \quad i = 1, 2. \quad (2.28)$$

Then equations (2.22) - (2.25) transform to

$$\frac{\partial S_1}{\partial t} - v(x) \frac{\partial S_1}{\partial x} = F(x)(S_2 - S_1), \quad (2.29)$$

$$\frac{\partial S_2}{\partial t} + v(x) \frac{\partial S_2}{\partial x} = F(x)(S_1 - S_2), \quad (2.30)$$

$$S_1(L/2, t) = 0, \quad (2.31)$$

$$S_2(-L/2, t) = 0, \quad (2.32)$$

for $t > 0$, $-L/2 < x < L/2$, and equations (2.26), (2.27) become

$$S_1(x, t) = 1, \quad (2.33)$$

$$S_2(x, t) = 1, \quad (2.34)$$

for $x \in [-L/2, L/2]$, $t \leq 0$.

In fact, we observe that $S_1(L/2, t) = S_2(-L/2, t) = H(-t)$ for any t . Let $w_i(x, t)$, $i = 1, 2$ be the exit time distribution. Then we have

$$w_i(x, t)dt = S_i(x, t) - S_i(x, t + dt), \quad (2.35)$$

$$\Rightarrow w_i(x, t) = -\frac{\partial S_i}{\partial t}, \quad (2.36)$$

which are analogues of equation (2.5) used for deriving the exit time distribution of Brownian process. Taking the derivative of equations (2.29) - (2.34) with respect to t , we finally obtain the equations for exit time distribution:

$$\frac{\partial w_1}{\partial t} - v \frac{\partial w_1}{\partial x} = F(x)(w_2 - w_1), \quad (2.37)$$

$$\frac{\partial w_2}{\partial t} + v \frac{\partial w_2}{\partial x} = F(x)(w_1 - w_2), \quad (2.38)$$

$$w_1(L/2, t) = \delta(t), \quad (2.39)$$

$$w_2(-L/2, t) = \delta(t), \quad (2.40)$$

for $t > 0$, $-L/2 < x < L/2$, and

$$w_1(x, t) = 0, \quad (2.41)$$

$$w_2(x, t) = 0. \quad (2.42)$$

for $t \leq 0$, where $\delta(t)$ is the Dirac delta function. Equations (2.37) - (2.42) will be used extensively throughout the dissertation.

Chapter 3

MONTE-CARLO SIMULATION FOR THE BROADWELL PROCESS

In this Chapter, we present a Monte-Carlo method to simulate the Broadwell process and obtain the exit time distributions. One important advantage of studying the Broadwell model is the ease with which it can be simulated. Accurate simulations are critical for comparisons between reconstructed flip-rate functions and the underlying target functions that produced the exit time data. When generating the exit time distribution from our simulations, the dominant error (besides round-off) stems from using a finite number of realizations.

3.1 Monte-Carlo Simulation Using Rejection-Acceptance

We now give details of our Monte-Carlo method in Algorithm 2. This method can be used to simulate a Broadwell particle with spatially dependent velocity, even though for our inverse problem, the particles always have constant velocity. The method is based on the Rejection-Acceptance method [91], a common method for drawing random variables from a probability density function (pdf) whose functional form is known, but non-standard. For example, we can use Rejection-Acceptance method to generate a random variable having pdf: $f_X(x) = \frac{2}{3\pi}\sqrt{9-x^2}$, $-3 \leq x \leq 3$. The Rejection-Acceptance method is described in Algorithm 1.

We note four important points about the Monte-Carlo method.

1. The algorithm samples from $w_1(y_0, t)$ or $w_2(y_0, t)$ depending on the initial velocity/state: see equation (3.3).
2. The algorithm generates random variables for the time periods in between the state transitions θ (the “flip times”). For a Broadwell process with a constant

Algorithm 1 Rejection-Acceptance Algorithm

- 1: Require: we have known a method for simulating a random variable Y having pdf $g(\cdot)$, and would like to generate a random variable X with pdf $f(\cdot)$. Also, suppose there exists a constant C such that

$$\frac{f(x)}{g(x)} \leq C \quad \text{for all } x.$$

- 2: Generate a random variable Y distributed as $g(\cdot)$.
3: Generate $U \sim U(0, 1)$, where U is independent from Y .
4: **if** $U \leq \frac{f(Y)}{Cg(Y)}$, **then**
5: set $X = Y$ (“acceptance”);
6: **else**
7: Goto 2.
8: **end if**
-

transition rate, the flip times are exponentially distributed. For a *spatially-dependent* transition rate $F(y)$, the flip time $\theta \equiv t_{j+1} - t_j$ is distributed according to

$$\begin{aligned} \theta \sim Q(t) &\equiv F[y(t)] \exp[-p(t)], \\ p(t) &= \int_0^t F[y(t')] dt', \end{aligned} \tag{3.1}$$

where the position of the particle satisfies $dy(t)/dt = v(y)$. We sample from $Q(t)$ using a Rejection-Acceptance method [91]: suppose there exist constants F_{\min} and F_{\max} satisfying $0 < F_{\min} \leq F(y) \leq F_{\max} < \infty$ for $-L/2 < y < L/2$. Then

$$Q(t) \leq CF_{\min} \exp(-F_{\min}t) \equiv P(t),$$

where $C = F_{\max}/F_{\min}$ and so an exponential distribution can be used as an envelope function.

3. Once the flip time θ is generated, the flip position y_{j+1} can be found by solving $\int_{y_j}^{y_{j+1}} v^{-1}(y) dy = \theta$. This integral could be expensive to calculate if it has to be done many times. Also, every evaluation of $Q(t)$ requires computing the integral $p(t)$ in equation (3.1). Both of these issues are handled simultaneously

in our algorithm through the solution of the pair of ordinary differential equations (3.2)-(3.3). For the special case where v is a constant, equations (3.2) and (3.3) should be replaced with $dp/dt = F(y_j + vt)$ and $y(t) = y_j + vt$.

4. When solving the differential equations (3.2) and (3.3), F may have to be evaluated outside of the interval $[-L/2, L/2]$. Because the form of $F(y)$ outside $[-L/2, L/2]$ does not affect the exit time, we simply take $F(y) = F(L/2)$ for $y > L/2$ and $F(y) = F(-L/2)$ for $y < -L/2$.

3.2 Generation of Noisy Distributions from a Finite Number of Exit Times

Because the solutions to equations (2.37) - (2.42) are highly singular, equations (2.37) - (2.42) are not useful in practice for inferring $F(x)$. Related quantities that are more regular and whose governing equations are more amenable to numerical methods are the cumulative density functions (cdfs) and Laplace-transformed probability density functions. We now define the noisy cdfs as $W_{1,\text{data}}(t)$ and $W_{2,\text{data}}(t)$, the noisy Laplace-transformed pdfs as $\tilde{w}_{1,\text{data}}(s)$ and $\tilde{w}_{2,\text{data}}(s)$.

We always use Algorithm 2 to generate two sets of N exit times $\{\tau_j^{(1)}\}$ and $\{\tau_j^{(2)}\}$. With this notation, $\tau_j^{(i)}$ ($1 \leq j \leq N$, $i = 1, 2$) is the j th exit time conditioned on the particle having initial velocity $(-1)^{i+1}v$. Assuming that $\{\tau_j^{(1)}\}$ and $\{\tau_j^{(2)}\}$ are sorted in ascending order, noisy cumulative densities $W_{1,\text{data}}(t)$ and $W_{2,\text{data}}(t)$ are computed as

$$W_{i,\text{data}}(t) = \begin{cases} 0 & \text{if } t \leq \tau_1^{(i)}, \\ \frac{m}{N} & \text{if } \tau_1^{(i)} < t < \tau_N^{(i)}, \\ 1 & \text{if } t \geq \tau_N^{(i)}, \end{cases} \quad (3.4)$$

where m is the unique index satisfying $\tau_m^{(i)} < t < \tau_{m+1}^{(i)}$.

Algorithm 2 Generating exit times from a Broadwell process

- 1: Require: an interval size L , a starting position $-L/2 \leq y_0 \leq L/2$, functions $F(y), v(y) \in C(-\infty, +\infty)$, $F_{\min}, F_{\max} > 0$ where $F_{\min} \leq F(y) \leq F_{\max}$ for $y \in [-L/2, L/2]$.
- 2: Let $P(t) \equiv F_{\max} \exp(-F_{\min} t)$.
- 3: Set $j = 0$ and $t_j = 0$.
- 4: **while** $-L/2 < y_j < L/2$ **do**
- 5: Draw $\theta \sim \exp(F_{\min})$
- 6: Compute $p(\theta)$ and $y(\theta)$ by numerically solving

$$\frac{dp(t)}{dt} = F(y), \quad (3.2)$$

$$\frac{dy(t)}{dt} = \begin{cases} (-1)^j v(y), & \{\text{for positive velocity at } t = 0\} \\ (-1)^{j+1} v(y), & \{\text{for negative velocity at } t = 0\} \end{cases} \quad (3.3)$$

on $t \in [0, \theta]$, subject to initial conditions $p(0) = 0$ and $y(0) = y_j$.

- 7: Set $Q(\theta) = F[y(\theta)] \exp[-p(\theta)]$
 - 8: Draw $\rho \sim U(0, 1)$
 - 9: **if** $\rho < Q(\theta)/P(\theta)$ **then**
 - 10: $j \leftarrow j + 1$ {acceptance}
 - 11: Set $y_j = y(\theta)$ and $t_j = t_{j-1} + \theta$
 - 12: Goto 4
 - 13: **else**
 - 14: Goto 5 {rejection}
 - 15: **end if**
 - 16: **end while**{Particle has left interval}
 - 17: **if** $y_j > L/2$ **then**
 - 18: Output the exit time as $t_j + \int_{y_j}^{L/2} v^{-1}(y)dy$.
 - 19: **else**
 - 20: Output the exit time as $t_j + \int_{y_j}^{-L/2} (-v^{-1}(y))dy$.
 - 21: **end if**
-

Then the noisy Laplace transform of a finite number of exit times is calculated through

$$\tilde{w}_{j,\text{data}}(s) = \begin{cases} \int_0^\infty e^{-st} \frac{dW_{j,\text{data}}(t)}{dt} dt = s\tilde{W}_{j,\text{data}}(s), & s > 0, \\ 1, & s = 0, \end{cases} \quad (3.5)$$

where

$$\tilde{W}_{j,\text{data}}(s) = \int_0^\infty e^{-st} W_{j,\text{data}}(t) dt = \int_0^1 e^{-st[\eta]} W_{j,\text{data}}(t[\eta]) \frac{d\eta}{(1-\eta)^2}, \quad (3.6)$$

where $j = 1, 2$ and $t[\eta] = \eta/(1-\eta)$. We avoid “binning” when calculating $\tilde{w}_{j,\text{data}}$, because this introduces a corresponding discretization error. The integral in equation (3.6) can be calculated using the trapezium rule on equally spaced abscissae in η .

Using the Monte-Carlo method (Algorithm 2) and equations (3.4) - (3.6), we are able to generate the probability density functions $w_1(x, t)$, $w_2(x, t)$ and their Laplace transforms with initial position $x \in (-L/2, L/2)$ and $x = \pm L/2$. Figure 3.1 shows the probability density functions $w_1(0, t)$ generated by the algorithm for two different $F(y)$ when $v(y) = \text{constant}$. By definition, w_1 is the exit time density for a particle that initially has velocity $v > 0$. Therefore the solution $w_1(x, t)$ in equation (2.37) contains delta functions that correspond to an immediate particle exit at a time $t_c \equiv (L/2 - x)/v$. The reason is if t is the particle exit time and θ is the time before the *first* state transition, then

$$P(t = t_c) = P(\theta \geq t_c) = \int_{t_c}^\infty Q(t') dt' > 0. \quad (3.7)$$

Hence the probability distribution of the exit times will always contain point masses (delta functions) of probability located at $t = t_c$ [32]. In Figure 3.1(b) a numerical approximation of this delta function can be seen at $t = 0.5$. The height of this “spike” is controlled by the size of the bins used when creating the histogram and becomes unbounded as the bin size tends to zero and the number of trials tends to infinity. These delta distributions are always present in the exact solution but they may not always be visible in the numerical solution if the number of trials is small or the bin size is large; see Figure 3.1(a) for example.

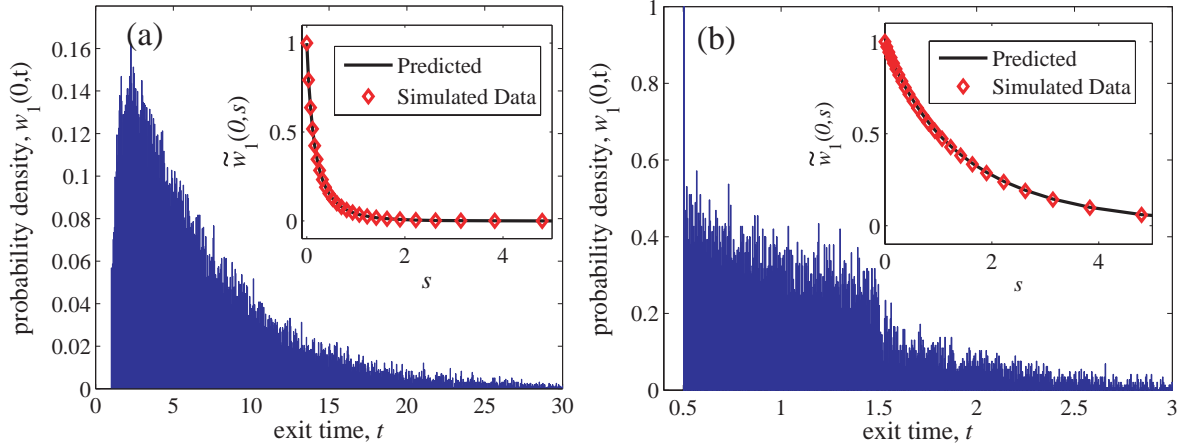


Figure 3.1: Simulated exit times of a Broadwell process starting from $x = 0$. (a) $F(y) = 10y^3 + 5e^y + 1$, $v = 1/2$ and (b) $F(y) = 1 + y^2$, $v = 1$. Insets show Laplace-transformed data. Solid line: solution to equations (4.5), (4.6). Diamonds: Laplace transform of histogram data. The number of realizations was $N = 40,000$ in each case.

Similarly, Figure 3.2 shows the simulated exit time distributions $w_1(-L/2, t)$ and $w_2(L/2, t)$ of a Broadwell process with a given flip rate function $F(y)$ and constant velocity $v = 1$. Notice that Figure 3.2(b) and Figure 3.2(c) contain ‘spikes’ as well. The spike is a numerical approximation of a Dirac delta function, which corresponds to an immediate particle exit at time $t_c = L/v$. Although probability densities are shown in Figure 3.1 and Figure 3.2, cumulative density functions $W_1(0, t)$, $W_2(0, t)$ or $\widetilde{W}_1(s)$, $\widetilde{W}_2(s)$ are used to infer the flip rate function in Chapter 4, while $W_1(-L/2, t)$ and $W_2(L/2, t)$ are used to infer the flip rate function in Chapter 5.

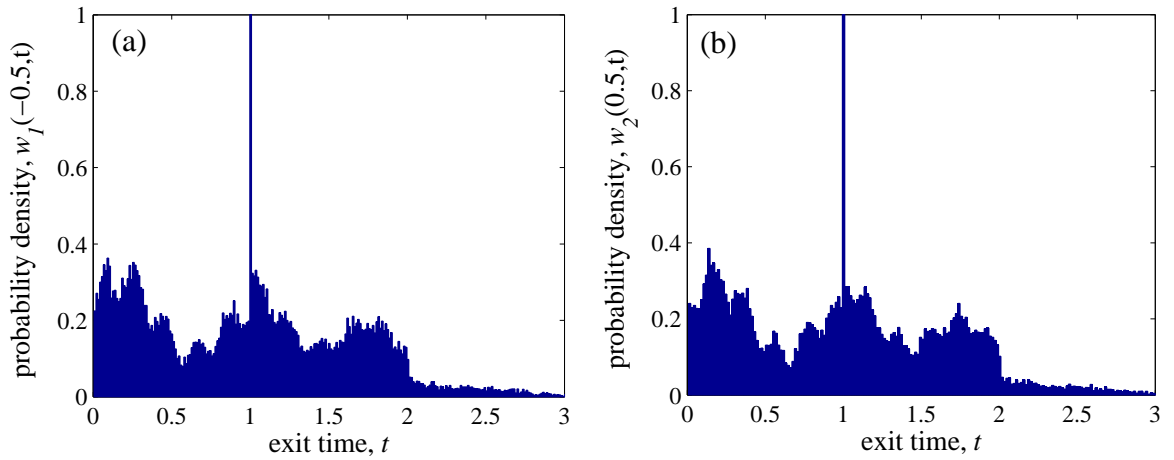


Figure 3.2: Simulated exit time distributions of a Broadwell process with flip rate $F(y) = 0.5 + 0.2 \cos(16y) + 0.1 \sin(64y)$, constant velocity $v = 1$, and $L = 1$. (a) The flip rate function $F(y)$. (b) Exit time distribution w_1 starting from $x = -0.5$ with velocity $+v$, generated by $F(y)$ in (a). (c) Exit time distribution w_2 starting from $x = 0.5$ with velocity $-v$, generated by flip rate $F(y)$ in (a). The number of exit times to generate each distribution is $N = 10^5$.

Chapter 4

RECONSTRUCTION OF THE FLIP RATE IN A BROADWELL PROCESS USING PROJECTION METHODS

Inverse problems arise in many applications such as medical imaging [20], high energy particle physics [92], and seismology [93]. Some of these applications involve measurement of waves at the boundary of a domain; from this boundary data one may wish to reconstruct spatially-dependent properties within the domain such as the density and/or wave speed. In this chapter, we will study inverse stochastic problem, where the underlying physics involves an intrinsic random process, the Broadwell process. The corresponding “boundary data” for the problem are exit time distributions and we wish to infer the flip rate from the exit distributions.

In Section 4.1, we state the inverse problem of reconstructing the flip-rate function from the exit time distributions. The associated optimization problem involves minimizing the distance between the solution of the backward Kolmogorov equation and the exit time data (derived from simulations or from the solution of the backward Kolmogorov equation with a given flip rate function). In Section 4.2 and 4.3 we discuss the numerical aspects of our work. In particular, we present two reconstruction methods. The first involves minimizing the difference between the solution to the backward Kolmogorov equation and the target data in the time domain. The second involves minimizing the difference between the Laplace-transformed solution of the backward Kolmogorov equation and transformed exit time data. In Section 4.4 we present the results of our reconstruction using noisy data and compare the two methods. We show that for a finite number of exit times, the most reliable reconstruction of the flip rate occurs at an intermediate advection speed, no matter which method is used. In Section 4.5, we discuss general implications of our results and summarize our findings.

4.1 Two-state Broadwell Model and The Statement of Inverse Problem

A two-state Broadwell model describes a particle that can take one of two states. Initially, the particle is at position x and in state $i \in \{1, 2\}$. The particle advects within an interval $(-L/2, L/2)$ with velocity $+v$ if $i = 1$ and $-v$ if $i = 2$. While advecting, the particle may change state with probability $F(y)dt$ within time interval $(t, t + dt)$ where y is the current particle position.

Let $w(t|x, 1, 0) \equiv w_1(x, t)$ and $w(t|x, 2, 0) = w_2(x, t)$ be the exit time distributions conditioned on the particle initially being at position x and having a positive ($+v$) and negative ($-v$) velocity respectively. Then the exit time distributions satisfy equations (2.37)-(2.42). A full derivation of the backward equation for the exit time distribution for a two state Broadwell process can be found in Chapter 2.

Given $F(x)$, one can solve the well-posed hyperbolic initial boundary value problem (2.37) - (2.42) (the “forward problem”) to find $w_1(x, t)$ and $w_2(x, t)$ for all $-L/2 < x < L/2$ and $t > 0$. Note that equations (2.37) and (2.38) constitute Kolmogorov’s backward equations for the exit time distributions, and that solving this backward equation defines the *forward* problem for computing $w_1(x, t), w_2(x, t)$ from a known $F(x)$. However here we are interested in the *inverse* problem:

Problem Statement: Let $w_1(x, t), w_2(x, t)$ be the unique solution of (2.37) - (2.42), for a given v and a known $F(x)$, on the region $-L/2 \leq x \leq L/2, t \in \mathbb{R}$. Fix a known $x_0 \in (-L/2, L/2)$, given $w_1(x_0, t), w_2(x_0, t)$ and v , find flip rate function $F(x) \in C[-L/2, L/2]$.

In practice, the exit time distributions could come from simulating a Broadwell process directly or from a single solution of the forward problem. For particles that initially advect with velocities $+v$ and $-v$, we refer to associated exit time distributions $w_{1,\text{data}}(x_0, t)$ and $w_{2,\text{data}}(x_0, t)$, respectively; note that $w_{1,\text{data}}(x_0, t)$ and $w_{2,\text{data}}(x_0, t)$ may or may not be noisy. Details on how $w_{1,\text{data}}$ and $w_{2,\text{data}}$ are computed are given in Chapter 3.

Unfortunately, equations (2.37) - (2.42) are not useful in practice for inferring $F(x)$ because the solutions are highly singular. Related quantities that are more regular and whose governing equations are more amenable to numerical methods are the cumulative density functions and Laplace-transformed probability density functions. We now give explicit forms for these equations because we make frequent use of them later on.

The cdfs are related to the pdfs by $W_1(x, t) = \int_0^t w_1(x, t')dt'$ and $W_2(x, t) = \int_0^t w_2(x, t')dt'$. Therefore, upon integrating equations (2.37) - (2.38) in time, we find

$$\frac{\partial W_1}{\partial t} - v \frac{\partial W_1}{\partial x} = F(x)(W_2 - W_1), \quad (4.1)$$

$$\frac{\partial W_2}{\partial t} + v \frac{\partial W_2}{\partial x} = F(x)(W_1 - W_2), \quad (4.2)$$

for $-L/2 < x < L/2$, $t \geq 0$, subject to the boundary conditions

$$W_1(L/2, t) = H(t), \quad W_2(-L/2, t) = H(t), \quad (4.3)$$

and initial conditions

$$W_1(x, 0) = 0, \quad W_2(x, 0) = 0. \quad (4.4)$$

In equations (4.3), $H(t)$ is the Heaviside step function satisfying $H(t) = 1$ if $t > 0$ and $H(t) = 0$ if $t \leq 0$. The corresponding inverse problem is to find $F(x) \in C[-L/2, L/2]$ given $-L/2 < x_0 < L/2$, v and $W_{j,\text{data}}(x_0, t) = \int_0^t w_{j,\text{data}}(x_0, t')dt'$ for $t > 0$ and $j = 1, 2$. Alternatively, we can also take Laplace transforms of equations (2.37) - (2.38) to find

$$s\tilde{w}_1(x, s) = v \frac{\partial \tilde{w}_1}{\partial x} + F(x)(\tilde{w}_2 - \tilde{w}_1), \quad (4.5)$$

$$s\tilde{w}_2(x, s) = -v \frac{\partial \tilde{w}_2}{\partial x} + F(x)(\tilde{w}_1 - \tilde{w}_2), \quad (4.6)$$

subject to boundary conditions

$$\tilde{w}_1(x = L/2, s) = 1, \quad \tilde{w}_2(x = -L/2, s) = 1. \quad (4.7)$$

The corresponding inverse problem is to find $F(x) \in C[-L/2, L/2]$ given $-L/2 < x_0 < L/2$, v and $\tilde{w}_{j,\text{data}}(x_0, s)$ for $s > 0$ and $j = 1, 2$.

4.2 Solution to the Forward Problems

In this section, we give details on solving the forward problem (4.5)-(4.7) and (4.1)-(4.4).

Solution to (4.5)-(4.7): Our method for finding $\tilde{w}_1(x_0, s)$ and $\tilde{w}_2(x_0, s)$ from equations (4.5)-(4.7) is based on solving the boundary value problem using a pseudospectral method [94] for different values of $s \geq 0$: see Algorithm 3. The solutions $\tilde{w}_1(x_0, s)$ and $\tilde{w}_2(x_0, s)$ are always infinitely differentiable, monotonically decreasing functions in s that $\rightarrow 0$ as $s \rightarrow \infty$.

Algorithm 3 Algorithm for solving the forward problem (4.5)-(4.7).

- 1: Require: flip rate function $F(x)$, velocity $v > 0$, interval size L , starting position $-L/2 < x_0 < L/2$ and integer $N \gg 1$.
 - 2: **for** $i = 1, 2, \dots, N$ **do**
 - 3: let $\xi_i = (i - 1)/N$ and $s_i = \xi_i/(1 - \xi_i)$.
 - 4: With $s = s_i$, solve (4.5)-(4.7) using a pseudospectral discretization [94] in x .
 - 5: Interpolate the solution at $x = x_0$ to find $\tilde{w}_1(x_0, s_i)$ and $\tilde{w}_2(x_0, s_i)$.
 - 6: **end for**
 - 7: Output: Laplace transformed exit time distributions $\tilde{w}_1(x_0, s_i)$ and $\tilde{w}_2(x_0, s_i)$, $i = 1, \dots, N$.
-

Solution to (4.1)-(4.4): In contrast to $\tilde{w}_1(x_0, s)$ and $\tilde{w}_2(x_0, s)$, the solutions $W_1(x, t)$ and $W_2(x, t)$ contain jump discontinuities that propagate into the domain of solution with velocity $\pm v$: the jump discontinuity in $W_1(x, t)$ ($W_2(x, t)$) propagates along the characteristic line $t = -x/v + L/(2v)$ ($t = +x/v + L/(2v)$). This behavior in the singularities is illustrated by the following theorem which uses an eigenfunction expansion to construct an explicit solution to (4.1)-(4.4).

Theorem 1 (Series solution to the forward problem (4.1)-(4.4)). *For $0 < t < L/v$, the solution to (4.1)-(4.4) is*

$$W_1(x, t) = a_1(x)H[t + x/v - L/(2v)] + Z_1(x, t), \quad (4.8)$$

$$W_2(x, t) = a_2(x)H[t - x/v - L/(2v)] + Z_2(x, t), \quad (4.9)$$

where $H[\cdot]$ is the heaviside step function and $Z_1(x, t)$, $Z_2(x, t)$ are continuous functions given by the series (at least formally)

$$\mathbf{Z}(x, t) = - \sum_{m=1}^{\infty} \frac{\mathbf{u}_m(x)}{s_m D_m} [h_m^{(1)}(t) + h_m^{(2)}(t)], \quad (4.10)$$

where:

$$h_m^{(1)}(t) = \int_{-L/2}^{-L/2+vt} p_m^{(1)*}(y) a_2(y) F(y) (1 - e^{(t-\frac{y}{v}-\frac{L}{2v})s_m}) dy, \quad (4.11)$$

$$h_m^{(2)}(t) = \int_{L/2-vt}^{L/2} p_m^{(2)*}(y) a_1(y) F(y) (1 - e^{(t+\frac{y}{v}-\frac{L}{2v})s_m}) dy, \quad (4.12)$$

$$a_1(x) = \exp \left[-\frac{1}{v} \int_x^{L/2} F(x') dx' \right], \quad (4.13)$$

$$a_2(x) = \exp \left[-\frac{1}{v} \int_{-L/2}^x F(x') dx' \right], \quad (4.14)$$

$$D_m = \langle \mathbf{p}_m(x), \mathbf{u}_m(x) \rangle = \int_{-L/2}^{L/2} \mathbf{p}_m^*(x) \mathbf{u}_m(x) dx. \quad (4.15)$$

In (4.10), $s_m \in \mathbb{C}$ and $\mathbf{u}_m(x) \in \mathbb{C}^2$ are the eigenvalues and eigenfunctions of \mathbf{A} where

$$\mathbf{A} \begin{pmatrix} u_1 \\ u_2 \end{pmatrix} = \left\{ \begin{bmatrix} v \frac{d}{dx} & 0 \\ 0 & -v \frac{d}{dx} \end{bmatrix} + F(x) \begin{bmatrix} -1 & 1 \\ 1 & -1 \end{bmatrix} \right\} \begin{pmatrix} u_1(x) \\ u_2(x) \end{pmatrix}, \quad (4.16)$$

along with the boundary conditions $u_1(L/2) = u_2(-L/2) = 0$. $\mathbf{p}_m(x) = [p_m^{(1)}(x), p_m^{(2)}(x)]^T$ are the eigenfunctions of the adjoint operator \mathbf{A}^* .

We now discuss the behavior of the solutions $W_1(x, t)$ and $W_2(x, t)$ in light of equations (4.8)-(4.9) and defer the proof of the theorem to the end of this section. From (4.8) and (4.9) it is clear that discontinuities in the boundary conditions (4.3) propagate into the interior. In Figure 4.1(a), W_1 is discontinuous on the diagonal line separating A, C and B, D while W_2 is discontinuous on the line separating A, D and B, C . Because the hyperbolic system (4.1)-(4.4) has a finite wave speed $v > 0$, region C is outside the region of influence of the disturbances originating at $(x, t) = (L/2, 0)$ and $(-L/2, 0)$ and we expect that $W_1(x, t) = W_2(x, t) = 0$ in C . This behavior is confirmed in Figure 4.1(b) which shows the cumulative distribution functions $W_1(x = -L/4, t)$

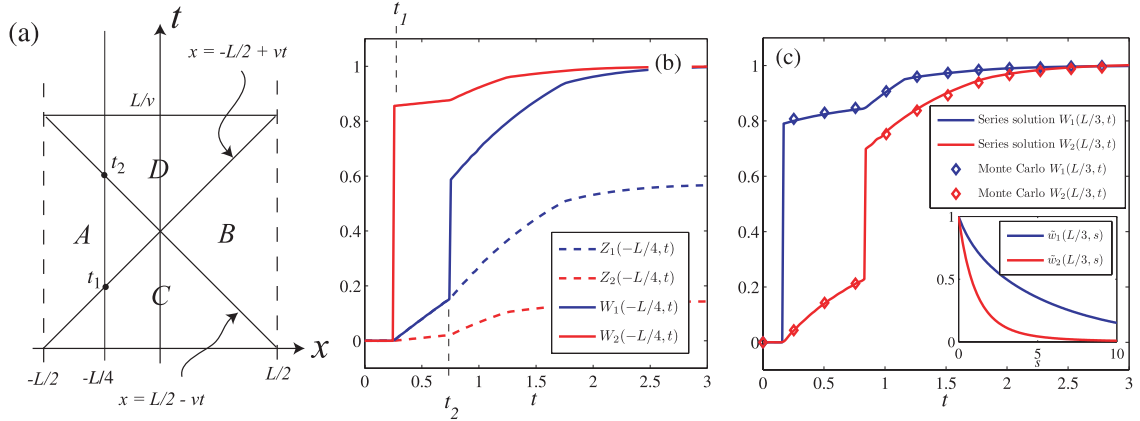


Figure 4.1: (a) Propagation of discontinuities of equations (2.37) - (2.42) in the x - t plane. The solution $w_1(x, t)$ is formally infinite on $x = L/2 - vt$ while $w_2(x, t)$ is infinite on $x = -L/2 + vt$. These singularities give rise to discontinuities in W_1 and W_2 that can be seen in (b,c). (b) Numerical computation of cumulative probability densities (cdfs) $W_1(x_0 = -L/4, t)$, $W_2(x_0 = -L/4, t)$ and auxiliary functions $Z_1(x_0 = -L/4, t)$, $Z_2(x_0 = -L/4, t)$ computed through (4.10) and Algorithm 4 using using 101 Chebyshev grid points and 51 eigenfunctions $\mathbf{u}_1, \mathbf{u}_2, \dots, \mathbf{u}_{51}$. (c) Numerical computation of cdfs $W_1(x_0 = L/3, t)$ and $W_2(x_0 = L/3, t)$ (solid) along with results from Monte Carlo simulations (diamond). Inset shows Laplace-transformed probability densities $\tilde{w}_1(x_0 = L/3, s)$ and $\tilde{w}_2(x_0 = L/3, s)$. Common parameters in (b,c) are $v = 1$, $F(y) = 1 + y$ and $L = 1$.

and $W_2(x = -L/4, t)$ calculated using (4.8)-(4.10). The function $W_1(-L/4, t)$ has a discontinuous derivative at $t_1 = L/(4v)$ and a jump discontinuity at $t_2 = 3L/(4v)$ while $W_2(-L/4, t)$ has a jump discontinuity at t_1 and a discontinuous derivative at t_2 . Figure 4.1(c) shows cdfs evaluated at $x_0 = L/3$. The inset shows associated Laplace-transformed probability density functions $\tilde{w}_1(L/3, s)$ and $\tilde{w}_2(L/3, s)$, found by solving equations (4.5)-(4.7) using Algorithm 3. Cumulative density functions from Monte-Carlo simulations are superposed to validate our numerical method; details of how these simulations are performed are described in Chapter 3.

The expansions (4.8)-(4.9) in Theorem 1 are commonly used to analyze seismic waves [93, 95, 96] and form the basis of our numerical method for the forward problem

in t : see Algorithm 4. Numerically, the cdfs W_1 and W_2 are computed by taking a finite number of terms in (4.10) and adding on a step discontinuity at $t = \mp x/v + L/(2v)$ with strength given by (4.13) and (4.14). A pseudo-spectral collocation method on a Chebyshev grid was used to find the eigenvectors \mathbf{u}_j and Clenshaw-Curtis quadrature [94] was used to quickly evaluate the integrals (4.11) and (4.12) for $0 < t < L/v$. The strength of this numerical method is that no integration in time is required to find $W_1(x_0, t)$, $W_2(x_0, t)$, and the method allows quick evaluation of the cdfs at one fixed value of $x = x_0$. Its weakness is that many terms are usually required ($\gtrsim 100$) in the expansion to obtain accurate results when x_0 is close to $\pm L/2$. Furthermore we found that when $x_0 = \pm L/2$, the expansion (4.10) converged to a discontinuous function, giving $W_1(x_0, t) > 1$ and $W_2(x_0, t) > 1$ as $t \rightarrow \infty$; hence the properties of the series (4.10) still require further investigation at the domain boundaries.

Another important reason for separating out W_1 and W_2 into continuous and discontinuous components is to avoid Gibbs oscillations when solving for $\mathbf{Z}(x, t)$ as superpositions of eigenfunctions \mathbf{u}_n . These oscillations would introduce large errors into the solution to the forward problem (4.1)-(4.4) and therefore hinder the solution of the inverse problem.

Proof of Theorem 1. Upon substituting (4.8), (4.9) into (4.1), (4.2), we find that $Z_1(x, t)$ and $Z_2(x, t)$ satisfy

$$\frac{\partial Z_1}{\partial t} - v \frac{\partial Z_1}{\partial x} - F(x)(Z_2 - Z_1) = a_2(x)F(x)H[t - x/v - L/(2v)], \quad (4.18)$$

$$\frac{\partial Z_2}{\partial t} + v \frac{\partial Z_2}{\partial x} - F(x)(Z_1 - Z_2) = a_1(x)F(x)H[t + x/v - L/(2v)], \quad (4.19)$$

subject to the *homogeneous* boundary conditions $Z_1(L/2, t) = 0$, $Z_2(-L/2, t) = 0$ and initial conditions $Z_1(x, 0) = 0$, $Z_2(x, 0) = 0$ and $a_{1,2}$ are defined by (4.13) and (4.14). We now find a series representation for $Z_1(x, t)$ and $Z_2(x, t)$. After taking Laplace

Algorithm 4 Algorithm for solving the forward problem (4.1)-(4.4). The same symbol is used to refer to quantities in (4.10)-(4.15) as well as their numerical approximations. For example, \mathbf{A} refers to the differential operator as well as its matrix approximation.

1: Require: A target flip rate $F(x)$, velocity $v > 0$, an integer N , a starting position $-L/2 < x_0 < L/2$ and a discretization of the interval $[-L/2, L/2]$, $\{\chi_0, \chi_1, \dots, \chi_n\}$.

2: Discretize the differential operators \mathbf{A} and the adjoint \mathbf{A}^* where

$$\mathbf{A} \begin{pmatrix} u_1 \\ u_2 \end{pmatrix} = \left\{ \begin{bmatrix} v \frac{d}{dx} & 0 \\ 0 & -v \frac{d}{dx} \end{bmatrix} + F(x) \begin{bmatrix} -1 & 1 \\ 1 & -1 \end{bmatrix} \right\} \begin{pmatrix} u_1(x) \\ u_2(x) \end{pmatrix},$$

$$\mathbf{A}^* \begin{pmatrix} p_1 \\ p_2 \end{pmatrix} = \left\{ \begin{bmatrix} -v \frac{d}{dx} & 0 \\ 0 & v \frac{d}{dx} \end{bmatrix} + F(x) \begin{bmatrix} -1 & 1 \\ 1 & -1 \end{bmatrix} \right\} \begin{pmatrix} p_1(x) \\ p_2(x) \end{pmatrix}.$$

Note that \mathbf{A} must account for the boundary conditions $u_1(L/2) = 0$ and $u_2(-L/2) = 0$ respectively and \mathbf{A}^* must account for the adjoint boundary conditions $p_1(-L/2) = 0$ and $p_2(L/2) = 0$.

- 3: Compute s_1, \dots, s_N , the first N complex eigenvalues of \mathbf{A} with smallest absolute value.
- 4: Compute the corresponding N eigenvectors of $\mathbf{u}_1, \dots, \mathbf{u}_N$ of \mathbf{A} and $\mathbf{p}_1, \dots, \mathbf{p}_N$ of \mathbf{A}^* .
- 5: Compute the inner products $D_m = \int_{-L/2}^{L/2} \mathbf{p}_m^*(x) \mathbf{u}_m(x) dx$ for $m = 1, \dots, N$.
- 6: Compute the functions $h_m^{(1)}(t)$ and $h_m^{(2)}(t)$ in (4.11) and (4.12) for $m = 1, \dots, N$.
- 7: Compute $a_1(x)$ and $a_2(x)$ in (4.13) and (4.14).
- 8: Compute

$$\mathbf{Z}(x_0, t) = - \sum_{m=1}^N \frac{\mathbf{u}_m(x_0)}{s_m D_m} [h_m^{(1)}(t) + h_m^{(2)}(t)], \quad (4.17)$$

as the N -term approximation to (4.10). If x_0 does not coincide with a grid point χ_j , use interpolation to find $\mathbf{u}_m(x_0)$.

- 9: Compute $W_1(x_0, t)$ and $W_2(x_0, t)$ by adding discontinuities of strength $a_1(x_0)$ and $a_2(x_0)$ at $t = -x_0/v + L/(2v)$ and $t = x_0/v + L/(2v)$ respectively to Z_1 and Z_2 : see equations (4.8) and (4.9).
- 10: Output $W_1(x_0, t)$ and $W_2(x_0, t)$.
-

transforms of (4.18) and (4.19), we find that $\tilde{\mathbf{Z}}(x, s) = [\tilde{Z}_1(x, s), \tilde{Z}_2(x, s)]^T$ satisfies

$$(\mathbf{A} - s\mathbf{I})\tilde{\mathbf{Z}}(x, s) = -\frac{\tilde{\mathbf{N}}(x, s)}{s}, \quad (4.20)$$

$$\tilde{\mathbf{N}}(x, s) = F(x) \begin{bmatrix} a_2(x)e^{-\left(\frac{L}{2v} + \frac{x}{v}\right)s} \\ a_1(x)e^{-\left(\frac{L}{2v} - \frac{x}{v}\right)s} \end{bmatrix}. \quad (4.21)$$

with boundary conditions $\tilde{Z}_1(L/2, s) = 0, \tilde{Z}_2(-L/2, s) = 0$. Equation (4.20) has a solution of the form

$$\tilde{\mathbf{Z}}(x, s) = \sum_{n=1}^{\infty} \frac{c_n(s)\mathbf{u}_n(x)}{s - s_n}, \quad (4.22)$$

where the vector eigenfunctions $\mathbf{u}_n(x) \in \mathbb{C}^2$ satisfy $\mathbf{A}\mathbf{u}_n = s_n\mathbf{u}_n$ for eigenvalues $s_n \in \mathbb{C}$. As an aside, when $F(x) = F_0$ is a constant, one can show that the eigenfunctions are proportional to $[-(\alpha^2 + \lambda_n^2)^{1/2} \sinh \lambda_n(x+1/2) + \lambda_n \cosh \lambda_n(x+1/2), \alpha \sinh \lambda_n(x+1/2)]^T$ with $\alpha \equiv F_0L/v$, the $\lambda_n \in \mathbb{C}$ satisfy the transcendental equation $-(\alpha^2 + \lambda_n^2)^{1/2} \tanh \lambda_n + \lambda_n = 0$, and the eigenvalues are given by $s_n = -\alpha - (\alpha^2 + \lambda_n^2)^{1/2}$.

Recall that if $\{\mathbf{u}_n\}$ are the eigenfunctions of \mathbf{A} and $\{\mathbf{p}_m\}$ are the eigenfunctions of the adjoint operator \mathbf{A}^* , then $\langle \mathbf{p}_m, \mathbf{u}_n \rangle = 0$ unless $m = n$. Substituting (4.22) into (4.20), left-multiplying both sides of by \mathbf{p}_m^* and integrating, we find that

$$c_n(s) = \frac{\langle \mathbf{p}_m(x), \tilde{\mathbf{N}}(x, s) \rangle}{sD_m},$$

where D_m is defined by (4.15). (One cannot obtain c_n by invoking orthogonality of $\{\mathbf{u}_n\}$ because \mathbf{A} is not self-adjoint.) We now take the inverse Laplace transform of (4.22) and switch the order of integration to obtain the continuous parts of the cdfs:

$$\begin{aligned} \mathbf{Z}(x, t) &= \sum_{m=1}^{\infty} \frac{\mathbf{u}_m(x)}{D_m} \left\{ \int_{-L/2}^{L/2} dy p_m^{(1)*}(y) a_2(y) F(y) \int_{\gamma-i\infty}^{\gamma+i\infty} \frac{ds}{2\pi i} \frac{e^{(t-\frac{y}{v}-\frac{L}{2v})s}}{s(s-s_m)} + \right. \\ &\quad \left. \int_{-L/2}^{L/2} dy p_m^{(2)*}(y) a_1(y) F(y) \int_{\gamma-i\infty}^{\gamma+i\infty} \frac{ds}{2\pi i} \frac{e^{(t+\frac{y}{v}-\frac{L}{2v})s}}{s(s-s_m)} \right\}, \quad \text{Re } \gamma > 0, \\ &= -\sum_{m=1}^{\infty} \frac{\mathbf{u}_m(x)}{s_m D_m} [h_m^{(1)}(t) + h_m^{(2)}(t)]. \end{aligned}$$

where $h_m^{(1)}(t)$ and $h_m^{(2)}(t)$ are given by equations (4.11) and (4.12) respectively. \square

4.3 Projection Method to Solve Inverse Problem

In this section, we describe our algorithms for reconstructing the flip rate function $F(x)$ from the two distributions of exit times $w_{1,\text{data}}(t)$ and $w_{2,\text{data}}(t)$. These distributions can come from simulating the Broadwell process directly through Algorithm 2 or through a one-time solution of the forward problems (4.5)-(4.7) or (4.1)-(4.4). We implement two related algorithms. The first method uses the exit time data directly (t -method) and the second method uses Laplace-transformed exit time data (s -method). Pseudocodes for the two methods are given in Algorithms 5 and 6.

In both methods, we represent the trial flip rate function $F_M(x)$ and the target flip rate function $F^*(x)$ as linear combination of Legendre polynomials on $[-L/2, L/2]$:

$$F_M(x) = \sum_{j=0}^{M-1} a_j \phi_j(x), \quad (4.23)$$

For example, $\phi_0(x) = 1$, $\phi_1(x) = 2x/L$, $\phi_2(x) = 6\left(\frac{x}{L}\right)^2 - \frac{1}{2}$.

Our aim is to find coefficients a_1, \dots, a_M to minimize the objective functions for the t -method and s -methods, Π_1 and Π_2 respectively. These take the form

$$\begin{aligned} \Pi_1(\mathbf{a}) &= \int_0^{L/v} |W_1(x_0, t; \mathbf{a}) - W_{1,\text{data}}(x_0, t)|^2 dt + \int_0^{L/v} |W_2(x_0, t; \mathbf{a}) - W_{2,\text{data}}(x_0, t)|^2 dt, \\ \Pi_2(\mathbf{a}) &= \int_0^\infty |\tilde{w}_1(x_0, s; \mathbf{a}) - \tilde{w}_{1,\text{data}}(x_0, s)|^2 ds + \int_0^\infty |\tilde{w}_2(x_0, s; \mathbf{a}) - \tilde{w}_{2,\text{data}}(x_0, s)|^2 ds. \end{aligned}$$

The data sets $W_{j,\text{data}}(x_0, t)$, $\tilde{w}_{j,\text{data}}(x_0, s)$ associated with $F^*(x)$ can be computed from individual exit times using (3.4) and (3.5) respectively.

Minimization of Π_1 and Π_2 with respect to \mathbf{a} was performed using the Matlab routines `fminunc.m` and `lsqnonlin.m` for the t and s methods respectively, with the tolerances `TolFun` and `TolX` set to 10^{-14} . The initial guess for the coefficients was always $a_j = 1$ for $j = 1, \dots, M$, unless otherwise stated. The minimizing coefficients \hat{a}_j then define the reconstructed flip rate through $\hat{F}(x) = \sum_{j=1}^N \hat{a}_j \phi_j(x)$.

An obvious limitation of the projection method is that the method does not converge for non-polynomial F^* and polynomial F^* with degree greater than M . However, as we shall see in section 4.4, the method may still be used to find reasonable approximations in these cases.

Algorithm 5 Reconstruction of flip rate coefficients using the t -method

- 1: Require: An integer M , an interval length L , target flip rate function $F^*(x)$, a particle speed $v > 0$, a starting position $-L/2 < x_0 < L/2$ and the first M Legendre polynomials on $(-L/2, L/2)$, ϕ_1, \dots, ϕ_M (see text for details).
- 2: Generate noisy cdfs of the exit time $W_{1,\text{data}}(x_0, t)$ and $W_{2,\text{data}}(x_0, t)$ for $F^*(x)$ using Algorithm 2.
- 3: For a given $\mathbf{a} = (a_0, a_1, \dots, a_{M-1}) \in \mathbb{R}^M$, define $F_M(x) = \sum_{j=0}^{M-1} a_j \phi_j(x)$. Let $W_1(x_0, t; \mathbf{a})$ and $W_2(x_0, t; \mathbf{a})$ be the solution to the forward problem (4.1)-(4.4) with $F = F_M$, calculated using Algorithm 4.
- 4: Find $\mathbf{a} = \hat{\mathbf{a}}$ that minimizes

$$\Pi_1(\mathbf{a}) = \int_0^{L/v} |W_1(x_0, t; \mathbf{a}) - W_{1,\text{data}}(x_0, t)|^2 dt + \int_0^{L/v} |W_2(x_0, t; \mathbf{a}) - W_{2,\text{data}}(x_0, t)|^2 dt. \quad (4.24)$$

Integrating through discontinuities can be avoided by noting that $W_1(x, t) = 0$ and $W_2(x, t) = 0$ when $t < \min(\frac{L}{2v} - \frac{x}{v}, \frac{x}{v} + \frac{L}{2v})$. The lower limits of integration in (4.24) can be replaced with $(\frac{L}{2v} - \frac{x_0}{v})^+$ when $0 \leq x_0 < L/2$ and $(\frac{x_0}{v} + \frac{L}{2v})^+$ when $-L/2 < x_0 \leq 0$.

- 5: Output $\hat{F}(x) \equiv \sum_{j=0}^{M-1} \hat{a}_j \phi_j(x)$ as the estimate of the flip rate function for the exit time distributions $W_{1,\text{data}}(x_0, t)$ and $W_{2,\text{data}}(x_0, t)$.
-

4.4 Results and Discussion

4.4.1 Flip Rate Reconstruction

We used the projection algorithm discussed in section 4.3 to reconstruct flip rate functions from data generated using Monte-Carlo simulation (see Chapter 3). In the following discussion, let N be the number of exit times for each initial velocity $+v, -v$, so that the total number of exit times is always $2N$. We also take the starting position $x_0 = 0$, interval length $L = 1$ and particle speed $v = 1$ unless otherwise stated.

For Figure 4.2, we reconstruct some “structurally simple” smooth functions that have few extrema within $(-L/2, L/2)$ and find that the accuracy of the reconstructions improves as the noise in the data decreases. For the “ $N = \infty$ ” cases, artificial, noiseless data is generated by solving the forward problems equations (4.1)-(4.4) and (4.5)-(4.7) with $F = F^*$. Panels (a-f) indicate that for a given N , the t -method generally outperforms the s -method because the associated errors are smaller. In (a,b) we reconstruct a cubic polynomial by recovering $M = 4$ Legendre coefficients. In (c,d) we attempt to

Algorithm 6 Reconstruction of flip rate coefficients using the s -method

- 1: Require: An integer M , an interval length L , a target flip rate function $F^*(x)$, a particle speed $v > 0$ and a starting position $-L/2 < x_0 < L/2$ and the first M Legendre polynomial on $(-L/2, L/2)$, ϕ_1, \dots, ϕ_M (see text for details).
- 2: Use $F^*(x)$ to generate Laplace-transformed exit time pdfs $\tilde{w}_{1,\text{data}}(x_0, s)$ and $\tilde{w}_{2,\text{data}}(x_0, s)$ through Algorithm 2.
- 3: For a given $\mathbf{a} \in \mathbb{R}^M$, let $\tilde{w}_1(x_0, s; \mathbf{a})$ and $\tilde{w}_2(x_0, s; \mathbf{a})$ be the solution to the forward problem (4.5)-(4.7) calculated using Algorithm 3 with flip rate function defined by $\mathbf{a} = \{a_0, a_2, \dots, a_{M-1}\}$:

$$F_M(x) = \sum_{j=0}^{M-1} a_j \phi_j(x).$$

- 4: Find $\mathbf{a} = \hat{\mathbf{a}}$ that minimizes

$$\Pi_2(\mathbf{a}) = \int_0^\infty |\tilde{w}_1(x_0, s; \mathbf{a}) - \tilde{w}_{1,\text{data}}(x_0, s)|^2 ds + \int_0^\infty |\tilde{w}_2(x_0, s; \mathbf{a}) - \tilde{w}_{2,\text{data}}(x_0, s)|^2 ds, \quad (4.25)$$

The integral in (4.25) is calculated using using a change of variable $s[\xi] = \xi/(1 - \xi)$ so that

$$\Pi_2 = \sum_{j=1}^2 \int_0^1 [\tilde{w}_j(x_0, s[\xi], \mathbf{a}) - \tilde{w}_{j,\text{data}}(x_0, s[\xi])]^2 \frac{d\xi}{(1 - \xi)^2},$$

which can be computed using the trapezium rule on equally spaced abscissae on $[0, 1]$.

- 5: Output $\hat{F}(x) \equiv \sum_{j=0}^{M-1} \hat{a}_j \phi_j(x)$ as the estimate of the flip rate function for the exit time distributions $\tilde{w}_1(x_0, s)$ and $\tilde{w}_2(x_0, s)$.
-

reconstruct a transcendental function by representing $F^*(x)$ with $M = 5$ coefficients. Although $\|F_M - F^*\|_\infty \rightarrow 0$ as the noise decreases, we are still able to find a reasonable approximation F_M so that $\|F_M - F^*\|_\infty$ is not too large. The s -method converges to the correct solution for perfect data but the inclusion of a small amount of noise renders the method unstable, resulting in a large error. This kind of behavior also occurs with the t -method when $M \gtrsim 5$ and is typical in many ill-posed problems (see below). In (e) and (f), we reconstruct flip rate functions from a relatively small number of exit times by taking $M = 3$ basis functions; however, smaller M restricts the range of admissible target functions.

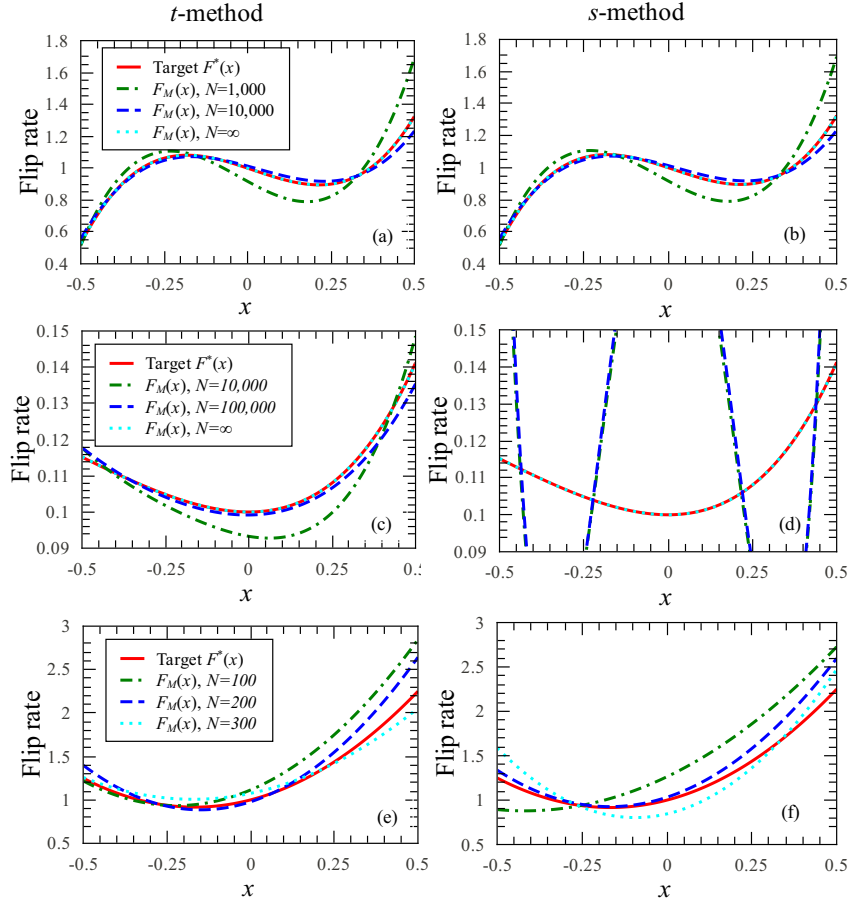


Figure 4.2: Reconstructed approximations to flip rate functions $F^*(x)$ from noisy exit time data. (a,b) $F^*(x) = 1 - 0.7x - 0.3x^2 + 6x^3$, $M = 4$; (c,d) $F^*(x) = x^2e^{-x}/10 + 1/10$, $M = 5$; (e,f) $F^*(x) = 1 + x + 3x^2$, $M = 3$. The *t*-method was used in the left panels and the *s*-method was used in the right panels. $N = \infty$ corresponds to perfect, noiseless data, which is generated by solving the forward problems (4.1)-(4.4) and (4.5)-(4.7).

If we have no *a-priori* knowledge on $F^*(x)$ (e.g. it may be a high-degree polynomial, have many extrema or be discontinuous), our method may not capture $F^*(x)$ accurately. For our method to be successful, it is important that we know beforehand that $F^*(x)$ is smooth and structurally not too complex. Increasing the number of basis functions M increases the range of functions we can accurately represent. Providing F^* is smooth enough, it can always be represented through its Taylor series and our method strives to capture its first M coefficients. Ideally, we would like M to be as

large as possible to represent any $F^*(x) \in C^\infty(-L/2, L/2)$. However in practice it is difficult to reliably reconstruct $F^*(x)$ (even polynomials) when $M \gtrsim 5$. The reason, which is common with all projection methods [13, 97], is that as the finite-dimensional approximation to $F^*(x)$ improves with $M \rightarrow \infty$, the method becomes more unstable due to ill-posedness of the inverse problem. In this limit, minimizing the objective functions (4.24), (4.25) is prone to large errors.

4.4.2 Instability of Projection Method

Numerically, the instability discussed above may be quantified by examining the condition number of the objective function near its minimum. Specifically, we study the Hessian (matrix of second partial derivatives) of the objective functions Π_1 and Π_2 in (4.24) and (4.25) with respect to the coefficients a_j , $j = 0, \dots, M - 1$:

$$H_{ij}^{(1)} \equiv \left. \frac{\partial^2 \Pi_1}{\partial a_i \partial a_j} \right|_{a_i=a_i^*, a_j=a_j^*}, \quad H_{ij}^{(2)} \equiv \left. \frac{\partial^2 \Pi_2}{\partial a_i \partial a_j} \right|_{a_i=a_i^*, a_j=a_j^*}, \quad (4.26)$$

for $i, j = 0, \dots, M - 1$. In (4.26), a_i^* are the target coefficients of a polynomial flip rate function: $F^*(x) = \sum_{i=0}^{M-1} a_i^* \phi_i(x)$. The condition number of a matrix A is defined as the ratio of its largest eigenvalue to its smallest: $\kappa = \lambda_{\max}(A)/\lambda_{\min}(A)$. Because the eigenvalues represent the principle curvatures of Π_1 and Π_2 at the point \mathbf{a}^* , they are always positive; a very large condition number indicates that Π_1 or Π_2 is locally very flat at $\mathbf{a} = \mathbf{a}^*$ and finding \mathbf{a}^* numerically is prone to errors. On the other hand, a moderate-sized condition number indicates only a small difference in curvatures near \mathbf{a}^* and so finding the minimum numerically should not be difficult. Table 4.1 shows that both condition numbers for the t - and s -methods grow exponentially as the number of basis functions M increases. For $M = 5$ basis functions, the condition numbers for the t -method are consistently two orders of magnitude smaller than those for the s -method. This suggests that fitting to the exit time data directly (as opposed to its Laplace transform) leads to more effective algorithms and better estimates for the flip rate function. This is confirmed in our numerical experiments because occasionally the

t -method is able to recover $M = 5$ coefficients of a quartic polynomial $F(x)$, but the s -method is seldom able to do so.

Table 4.1: Local condition numbers κ_s and κ_t for $F^*(x)$ corresponding to the objective functions (4.25) and (4.24) respectively. M denotes the number of basis functions used in (4.23).

$F^*(x)$	M	κ_t	κ_s
$F^*(x) = 1 + x$	2	5.3×10^2	3.1×10^2
	3	1.0×10^4	3.3×10^4
	4	1.4×10^5	3.5×10^6
	5	1.0×10^6	1.6×10^8
$F^*(x) = 1 - x + x^2$	3	5.0×10^5	1.8×10^5
	4	3.5×10^6	1.6×10^7
	5	6.7×10^6	5.2×10^8

4.4.3 Sensitivity of Reconstruction to Advection Speed

We also explore the accuracy of our reconstruction for different advection speeds v , given a fixed number of exit times when $F^*(x)$ is a polynomial of degree $\leq M$. In Figure 4.3, we see that, for both methods, when the velocity is either much less or much larger than unity, the associated error is large. (Although the upper limit of the objective function (4.24) depends on the value of v used, we checked that the non-monotonic behavior in $\|F_M - F^*\|_\infty$ was not sensitive to the upper limit of integration.)

In practice, there are always two sources of error in the reconstruction of F^* : the first is from noise in the data and the second stems from the minimization procedure itself:

$$\text{Total error} = \text{error from noise in data} + \text{error from minimization.} \quad (4.27)$$

If the minimization of the objective functions (4.24) or (4.25) was achieved with zero error, noisy exit times would still produce an error in the reconstructed F . On the other hand, for noiseless data, the flat minima and large condition numbers discussed above would produce an erroneous F from the minimization. It is hard to separate the two

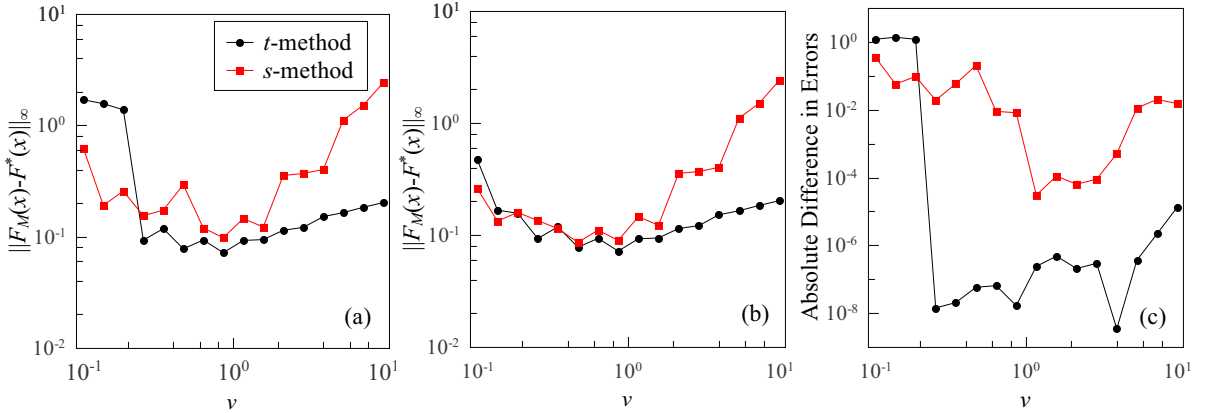


Figure 4.3: Error in reconstructed flip rate as a function of particle velocity. Each point is an average over 10 sets of $2N = 20,000$ exit times. Target flip rate $F^*(x) = \frac{9}{4}x^2 - \frac{3}{4}x + \frac{9}{16}$, corresponding to target coefficients $\mathbf{a}^* = [0.75, -0.375, 0.375, 0]$. Initial guesses are (a) $\mathbf{a} = [1, 1, 1, 1]$, (b) $\mathbf{a} = [0.76, -0.385, 0.365, 0.01]$. The same exit times were used for both (a) and (b). The difference in the errors is shown in (c).

types of error in (4.27), but some insight can be gained by comparing Figure 4.3(a) and Figure 4.3(b) which differ only in the starting values for the coefficients a_0, \dots, a_{M-1} ; in particular the exit times for each value of v for each figure are identical. When we move the initial guess for the coefficients closer to their target values in (b), we greatly reduce the error in minimization because the accuracy of minimization algorithms depends on the quality of the initial guess. Therefore, the error in (b) comes mainly from *noise in the data*. Because the exit times were identical for (a) and (b), the difference of the errors in (a) and (b) – shown in (c) – represents the *error from minimization* which is associated with large condition numbers, flat extrema and perhaps multiple local minima. We note that the error from minimization by the s -method is much larger than the corresponding error by the t -method for a wide range of v values.

When the dominant error stems from noise in the data (as is the case in Figure 4.3(b)), we can understand why $v = O(1)$ provides the most accurate reconstruction by analyzing how well the Monte-Carlo simulations approximate the moments of the exit time distribution. We prove

Theorem 2. Let $T_1^{(n)}(x)$ and $T_2^{(n)}(x)$ be the n th moments of the exit time conditioned on the particle starting at position x with initial velocity $+v$ and $-v$ respectively. Then the moments have the asymptotic behavior

$$T_j^{(k)}(x) = \begin{cases} O\left(\frac{k!}{v^{2k}}\right), & v \ll 1, \\ O\left(\frac{k!}{v^k}\right), & v \gg 1, \end{cases} \quad (4.28)$$

where $i = 1, 2$.

Proof. We have $T_i^{(n)}(x) = (-\partial/\partial s)^n \tilde{w}_i(x, s)|_{s=0}$ for $n \geq 0$, $i = 1, 2$ and from Equations (4.5) and (4.6), these moments satisfy the coupled equations

$$\begin{aligned} -v \frac{dT_1^{(n)}}{dx} - F(x)(T_2^{(n)} - T_1^{(n)}) &= nT_1^{(n-1)}, \\ v \frac{dT_2^{(n)}}{dx} - F(x)(T_1^{(n)} - T_2^{(n)}) &= nT_2^{(n-1)}, \end{aligned}$$

subject to the boundary conditions $T_1^{(n)}(L/2) = 0$ and $T_2^{(n)}(-L/2) = 0$ where $n \geq 1$ and $T_i^{(0)}(x) = 1$. After some algebra, we find expressions for the moments in terms of indefinite integrals:

$$T_1^{(n)}(x) = -\frac{n}{v^2} \int dx F(x) \int dx [T_1^{(n-1)}(x) + T_2^{(n-1)}(x)] - \frac{n}{v} \int dx T_1^{(n-1)}(x), \quad (4.29)$$

$$T_2^{(n)}(x) = -\frac{n}{v^2} \int dx F(x) \int dx [T_1^{(n-1)}(x) + T_2^{(n-1)}(x)] + \frac{n}{v} \int dx T_2^{(n-1)}(x). \quad (4.30)$$

When $v \ll 1$, we retain the first integral in each of equations (4.29) and (4.30) to find to obtain $T_i^{(k)} = O(k!/v^{2k})$. If $v \gg 1$, we retain the second integral to find $T_i^{(k)} = O(k!/v^k)$. \square

In (4.28), we see that the moments have a different asymptotic form depending on whether v is small or large. When $v \ll 1$, the random walker is the diffusive limit where all the moments (except for the zeroth moment) diverge. On the other hand, when $v \gg 1$, the particle is in the ballistic limit: all moments except for the zeroth moment are asymptotically small and, to leading order, independent of $F(x)$.

Now consider approximating $w_1(x_0, t)$ or $w_2(x_0, t)$ with their noisy counterparts generated by the Monte-Carlo simulations. How well are the $w_1(x_0, t)$ and $w_2(x_0, t)$ approximated? One way to quantify the accuracy is by calculating the error in the moments of the noisy distribution. Given an initial velocity $+v$, let $\{\tau_j\}$, $1 \leq j \leq N$ be the N generated exit times (the following argument with initial velocity $-v$ is almost identical). Then by the central limit theorem, the k th moment is approximately distributed according to

$$\frac{1}{N} \sum_{j=1}^N \tau_j^k \sim \mathcal{N} \left(T_1^{(k)}, \frac{\text{Var}(\tau_j^k)}{N} \right),$$

where $\mathcal{N}(\mu, \nu)$ is a normal distribution with mean μ and variance ν . Therefore a measure of the error incurred when calculating the k th sample moment is

$$N^{-1/2} \sqrt{\text{Var}(\tau_j^k)} = N^{-1/2} \sqrt{T_1^{(2k)} - T_1^{(k)2}} = \begin{cases} O(N^{-1/2} v^{-2k}), & v \ll 1, \\ O(N^{-1/2} v^{-k}), & v \gg 1, \end{cases} \quad (4.31)$$

using (4.28) and $\text{Var}(\tau_j^k) = E[(\tau_j^k - T_1^{(k)})^2]$. Therefore from (4.31), a quick rule-of-thumb for the accuracy of the Monte-Carlo generated exit time distribution is that the error scales as $N^{-1/2}$ where N is the number of trials.

It is evident from (4.31) that for a fixed number of realizations, the error in the k th moment diverges as v^{-2k} as $v \rightarrow 0$ and the underlying exit time distribution is badly approximated in the limit of small v . On the other hand, as $v \rightarrow \infty$, although the error in the moments tend to zero, the moments themselves also tend to zero. From equation (3.7) the probability that a Broadwell particle with initial velocity $+v$ exits in time t_c tends to 1 as $v \rightarrow \infty$: for large v , the generated list of exit times is populated almost exclusively by t_c (and $t_c \rightarrow 0$ as $v \rightarrow \infty$). From a single exit time it is very difficult to infer any information about $F(x)$. In both limiting cases, because the distribution of exit times is poorly captured by a finite number of realizations, the quality of the reconstruction suffers.

Finally, we systematically explore the effect of noise on the reconstruction quality. In Figure 4.4, we plot the error of the reconstructed $F_M(x)$ against the number of

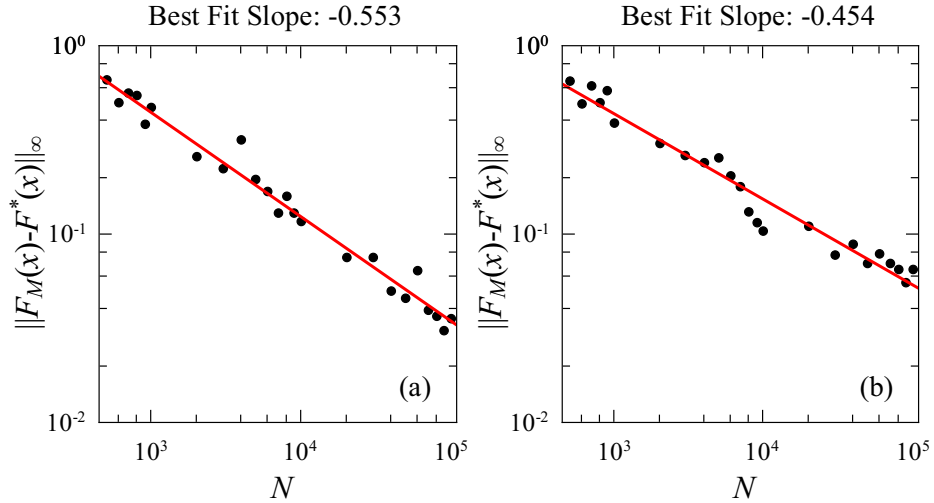


Figure 4.4: Dependence of error in reconstructed flip rate function $F(x)$ on the number of exit times per initial particle state N when $F(x) = 1 - 0.7x - 0.3x^2 + 6x^3$ using (a) t -method and (b) s -method. For each N , the error is calculated by performing minimizations for 10 data sets and taking the average, with each set containing $2N$ exit times.

exits. For a wide range of polynomials $F^*(x)$, using both the t - and s -methods, we find that the error in the reconstructed function scales as $O(N^{-1/2})$. In particular, we see that for $N = O(10^4)$, the error $\|F_M - F^*\|_\infty = O(10^{-1})$ whereas N must exceed $O(10^6)$ for the error to fall below $O(10^{-2})$. These estimates are mean values: the accuracy resulting from fitting one data set to the next will always vary because the noise in each set is different.

4.5 Conclusions

In this chapter, we have developed a pair of algorithms, Algorithms 5 and 6, which can be used to estimate the flip rate function of a 1D, constant-speed Broadwell process from the distribution of exit times out of a finite interval. In particular, the t -method is based on a novel series solution of the backward equation (4.1)-(4.4); see Theorem 1. We also present a set of calculations and asymptotic results that quantify the errors in approximating the exit time distribution with simulated data, and the

corresponding error in the flip rate reconstruction.

We found that polynomial transition rates could be reconstructed if the degree of the polynomial was not too large ($\lesssim 4$) and that fitting to the exit time distribution (t -method) directly versus fitting to the Laplace-transformed distribution (s -method) generally allowed the reconstruction of one extra coefficient in the representation of $F(x)$. Providing our initial guess for the coefficients of $F(x)$ was not too far from the target coefficients, we were able to find $F(x)$ to within $O(10^{-1})$ using $O(10^4)$ exit times. We were also able to find good approximations to non-polynomial flip-rate functions providing they are smooth and slowly varying. Finally, we experimented with reconstructions using different advection speeds. We found that $v = O(1)$ yielded the most accurate reconstructions because very small or large values of v in the Monte-Carlo simulations gave poor representations of the true underlying exit time distribution.

Our results suggest that the t -method is an effective method to infer the spatially-dependent flip rate function of a two-state Broadwell process, if it is known *a-priori* that this function is smooth and structurally simple. The t -method involves explicitly solving for the cumulative density functions (4.1)-(4.4), tracking the discontinuities via (4.8)-(4.9) and minimizing the objective function (4.24). With this method, one can often find $M = 4$ coefficients from about $2N = 20,000$ exit times. The s -method usually reconstructs one less coefficient than the t -method for the same number of exit times, and is more sensitive to the initial guess. However, it is much simpler to implement and only involves solving the ordinary differential equations (4.5)-(4.7) and minimizing (4.25).

Chapter 5

RECONSTRUCTION OF BROADWELL PROCESS USING LAYER STRIPPING METHOD

The layer stripping algorithm (or downward continuation algorithm) [36, 98] was developed by geophysicists to study the one-dimensional inverse scattering (impulse-response) problem in reflection seismology [36]. It has a wide range of applications, such as speech synthesis [37] and transmission-line models [38]. In this chapter, we implement the layer stripping algorithm, which utilizes the finite difference method and the method of characteristics to reconstruct the spatially dependent flip rate function from the exit time distribution layer by layer, where the exit time is defined as the travel time needed for the particle starting from one endpoint of a finite interval to exit from either endpoint. We also study the convergence rate of the algorithm.

In Section 5.1, we describe a two-state Broadwell process and restrict our study to the case with a constant speed and spatially dependent flip rate. We then state both the forward problem and inverse problem. In Section 5.2, we provide details on solving the forward problem. In Sections 5.3 and 5.4, we discuss the numerical scheme implementing the layer stripping algorithm to reconstruct the flip rate functions using the cdf of the exit time data instead of the pdf of exit time data. In Section 5.5, we present our results of reconstruction obtained from simulated exit time data and the convergence rate of the layer stripping algorithm. In Section 5.6, we summarize our findings.

5.1 Two-state Broadwell Model and Statement of Inverse Problem

The two-state Broadwell model can be described as a particle's random walk parameterized by a starting position $x \in [-L/2, L/2]$, a velocity $+v$ (state 1, where

v is a positive constant) or $-v$ (state 2) and, a flip rate $F(y)$, where $y \in [-L/2, L/2]$ represents the current position at time σ . While traveling with speed v , the particle shifts between the two states with probability $F(y)d\sigma$ within the time interval $(\sigma, \sigma + d\sigma)$. When the particle exits from either endpoint, the total travel time is recorded. If the Broadwell process is repeated a large number of times, we obtain the exit time distribution $w_1(x, t)$ for a particle that initially started from x in state 1 and $w_2(x, t)$ for a particle initially starting from x in state 2, where t is the exit time.

In this chapter, we consider the exit time distributions $w_1(-L/2, t)$ and $w_2(L/2, t)$ conditioned on the particle initially being at position $\mp L/2$, having a positive ($+v$) and negative ($-v$) velocity respectively and with a given flip rate function $F(y)$, the exit time distributions also satisfy (2.37) - (2.42). The forward problem is to solve (2.37) - (2.42) for exit time distributions $w_1(x, t)$ and $w_2(x, t)$, $-L/2 < x < L/2$ and $t > 0$, given starting position x , flip rate $F(y)$ and velocity $\pm v$. Therefore, in Figure 5.1, the forward problem is that given Figure (a), we want to generate plots (b) and (c). However, we are more interested in the inverse problem:

Inverse Problem Statement: Consider (2.37) - (2.42). Given velocities $\pm v$ and exit time distributions at the boundaries $x = \pm L/2$: $w_1(-L/2, t)$ and $w_2(L/2, t)$, $t > 0$, reconstruct the flip rate $F(x) \in C[-L/2, L/2]$.

To illustrate the problem, given Figure 5.1(b) and Figure 5.1(c), we want to reconstruct $F(y)$ in Figure 5.1(a). Notice that Figure 5.1(b) and Figure 5.1(c) contain ‘spikes’. The spike is a numerical approximation of a Dirac delta function, which corresponds to an immediate particle exit at time $t = L/v$. For more details see [14].

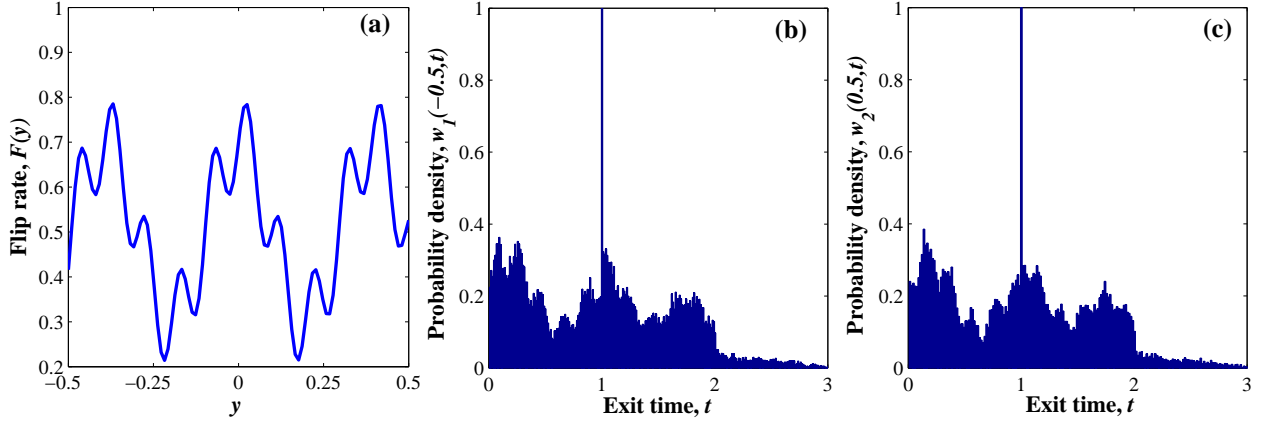


Figure 5.1: Simulated exit time distributions of a Broadwell process with flip rate $F(y) = 0.5 + 0.2 \cos(16y) + 0.1 \sin(64y)$, constant velocity $v = 1$, and $L = 1$. (a) The flip rate function $F(y)$. (b) Exit time distribution w_1 starting from $x = -0.5$ with velocity $+v$, generated by $F(y)$ in (a). (c) Exit time distribution w_2 starting from $x = 0.5$ with velocity $-v$, generated by flip rate $F(y)$ in (a). The number of exit times to generate each distribution is $M = 10^5$.

5.2 Solution to The Forward Problem

5.2.1 Propagation of Singularities

We break up the forward problem (2.37) - (2.42) into two subproblems. First consider

$$\frac{\partial w_1}{\partial t} - v \frac{\partial w_1}{\partial x} = F(x)(w_2 - w_1), \quad (5.1)$$

$$\frac{\partial w_2}{\partial t} + v \frac{\partial w_2}{\partial x} = F(x)(w_1 - w_2), \quad (5.2)$$

$$w_1(L/2, t) = 0, \quad (5.3)$$

$$w_2(-L/2, t) = \delta(t), \quad (5.4)$$

for $t \geq 0$, and

$$w_1(x, t) = 0, \quad w_2(x, t) = 0, \quad \text{for } t < 0.$$

Let H be the Heaviside function, we look for a solution of (5.1) - (5.4) in the form

$$w_1(x, t) = a_0(x, t)\delta(\xi) + a_1(x, t)H(\xi), \quad (5.5)$$

$$w_2(x, t) = b_0(x, t)\delta(\xi) + b_1(x, t)H(\xi), \quad (5.6)$$

where a_0, a_1, b_0, b_1 are differentiable functions and $\xi = t - x/v - L/(2v)$. Substituting (5.5) - (5.6) into boundary conditions (5.3) - (5.4), matching the coefficients of $\delta(\xi)$ and $H(\xi)$, we have

$$\begin{aligned} a_0(L/2, t) &= 0, \\ a_1(L/2, t) &= 0, \\ b_0(-L/2, t) &= 1, \\ b_1(-L/2, t) &= 0. \end{aligned} \tag{5.7}$$

Substituting (5.5) - (5.6) into (5.1) - (5.2), we have

$$\begin{aligned} 2a_0\delta'(\xi) + \left[\frac{\partial a_0}{\partial t} - v\frac{\partial a_0}{\partial x} + 2a_1 - F(b_0 - a_0) \right] \delta(\xi) + \\ \left[\frac{\partial a_1}{\partial t} - v\frac{\partial a_1}{\partial x} - F(b_1 - a_1) \right] H(\xi) &= 0, \\ \left[\frac{\partial b_0}{\partial t} + v\frac{\partial b_0}{\partial x} - F(a_0 - b_0) \right] \delta(\xi) + \left[\frac{\partial b_1}{\partial t} + v\frac{\partial b_1}{\partial x} - F(a_1 - b_1) \right] H(\xi) &= 0, \end{aligned}$$

from which we match the coefficients of $\delta'(\xi)$ and $\delta(\xi)$, and deduce that on $\xi = 0$,

$$a_0\delta'(\xi) = 0, \tag{5.8}$$

$$\begin{aligned} 2a_1 &= F(b_0 - a_0) - \frac{\partial a_0}{\partial t} + v\frac{\partial a_0}{\partial x}, \\ \frac{\partial b_0}{\partial t} + v\frac{\partial b_0}{\partial x} &= F(a_0 - b_0). \end{aligned} \tag{5.9}$$

We shall see in the Appendix A that (5.8) implies

$$a_0 = 0, \quad \text{on } \xi = 0, \tag{5.10}$$

$$\frac{\partial a_0}{\partial t} - v\frac{\partial a_0}{\partial x} = 0, \quad \text{on } \xi = 0. \tag{5.11}$$

Substituting (5.10) - (5.11) into (5.8) - (5.9), we have that when $\xi = 0$, $a_0(x) = 0$, $b_0(x) = \exp \left[- \int_{-L/2}^x \frac{F(x')}{v} dx' \right]$, and

$$a_1(x, t) = a_1(x, x/v + L/(2v)) = \frac{F(x)}{2} \exp \left[- \int_{-L/2}^x \frac{F(x')}{v} dx' \right], \tag{5.12}$$

We also match the coefficients of $H(\xi)$, so that when $\xi > 0$,

$$\frac{\partial a_1}{\partial t} - v \frac{\partial a_1}{\partial x} = F(x)(b_1 - a_1), \quad (5.13)$$

$$\frac{\partial b_1}{\partial t} + v \frac{\partial b_1}{\partial x} = F(x)(a_1 - b_1). \quad (5.14)$$

So, solving (5.1) - (5.4) is equivalent to solving (5.13) - (5.14) in the triangular domain $x > -L/2$, $t - x/v - L/(2v) > 0$, $t < L/(2v)$ with boundary conditions (5.7) and (5.12). Note that, because in the hyperbolic system, the wave moves in a one-dimensional medium with speed v , a disturbance at $x = -L/2$, $t = 0$ can have no ‘effect’ at x until $t > x/v + L/(2v)$, so we have $b_1(x, t) = a_1(x, t) \equiv 0$ in the region $x < L/2$, $t - x/v - L/(2v) < 0$, $t > 0$. See subplot (a) of Figure 5.2.

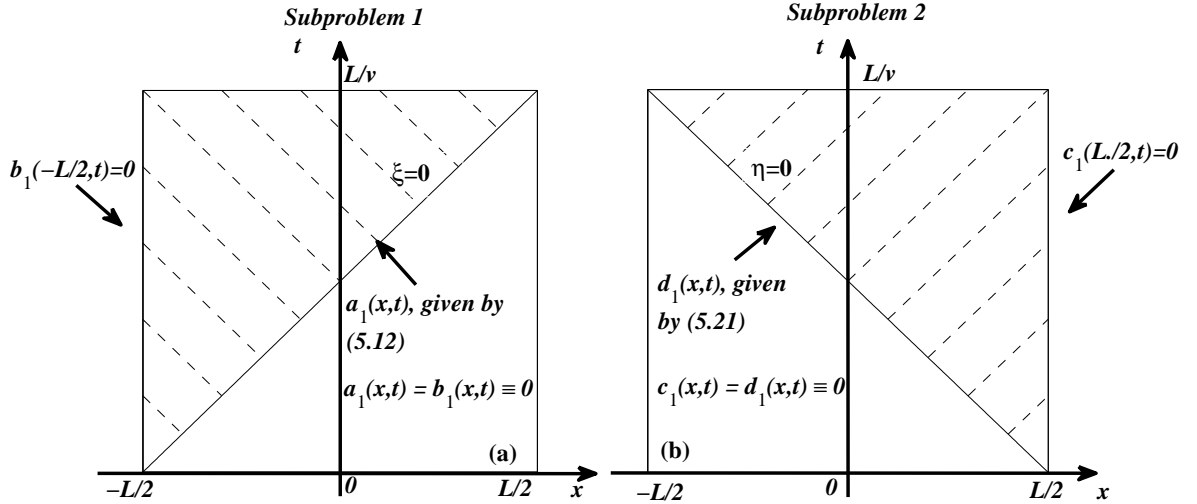


Figure 5.2: (a) Singularity structure of (5.7) and (5.12) - (5.14). (b) Singularity structure of (5.21) - (5.24)

Similarly, we look for a solution to the second subproblem

$$\frac{\partial w_1}{\partial t} - v \frac{\partial w_1}{\partial x} = F(x)(w_2 - w_1), \quad (5.15)$$

$$\frac{\partial w_2}{\partial t} + v \frac{\partial w_2}{\partial x} = F(x)(w_1 - w_2), \quad (5.16)$$

$$w_1(L/2, t) = \delta(t), \quad (5.17)$$

$$w_2(-L/2, t) = 0, \quad (5.18)$$

for $t \geq 0$, and

$$w_1(x, t) = 0, \quad w_2(x, t) = 0, \quad \text{for } t < 0,$$

in the form

$$w_1(x, t) = c_0(x, t)\delta(\eta) + c_1(x, t)H(\eta), \quad (5.19)$$

$$w_2(x, t) = d_0(x, t)\delta(\eta) + d_1(x, t)H(\eta), \quad (5.20)$$

where $\eta = t + x/v - L/(2v)$. After some similar calculations, we have that when $\eta = 0$, $d_0(x, t) = 0$, $c_0(x, t) = \exp\left[-\int_x^{L/2} \frac{F(x')}{v} dx'\right]$ and

$$d_1(x, t) = \frac{F(x)}{2} \exp\left[-\int_x^{L/2} \frac{F(x')}{v} dx'\right]. \quad (5.21)$$

We also have that when $\eta > 0$,

$$\frac{\partial c_1}{\partial t} - v \frac{\partial c_1}{\partial x} = F(x)(d_1 - c_1), \quad (5.22)$$

$$\frac{\partial d_1}{\partial t} + v \frac{\partial d_1}{\partial x} = F(x)(c_1 - d_1). \quad (5.23)$$

So, solving (5.15) - (5.18) is equivalent to solving (5.22) - (5.23) in the triangular domain $x < L/2$, $t + x/v - L/(2v) > 0$, $t < L/(2v)$ with boundary conditions (5.21) and

$$c_1(L/2, t) = 0, \quad (5.24)$$

which comes from setting $x = L/2$ in (5.19) and comparing with (5.17). Note that, because in the hyperbolic system, the wave moves in a one-dimensional medium with speed v , a disturbance at $x = L/2$, $t = 0$ can have no ‘effect’ at x until $t > -x/v + L/(2v)$, so we have $c_1(x, t) = d_1(x, t) \equiv 0$ in the region $x < L/2$, $t + x/v - L/(2v) < 0$, $t > 0$. See subplot (b) of Figure 5.2. In fact, we can solve (5.22) - (5.23) by noting

the following steps: (i) Let $x \rightarrow -x$ in (5.21) - (5.24) (ii) Let $\tilde{c}_1(x, t) = c_1(-x, t)$ and $\tilde{d}_1(x, t) = d_1(-x, t)$. Then equations (5.21) - (5.24) become

$$\frac{\partial \tilde{c}_1}{\partial t} + v \frac{\partial \tilde{c}_1}{\partial x} = F(-x)(\tilde{d}_1 - \tilde{c}_1), \quad (5.25)$$

$$\frac{\partial \tilde{d}_1}{\partial t} - v \frac{\partial \tilde{d}_1}{\partial x} = F(-x)(\tilde{c}_1 - \tilde{d}_1),$$

$$\tilde{c}_1(-L/2, t) = 0,$$

$$\tilde{d}_1(x, t) = \frac{F(-x)}{2} \exp \left[- \int_{-L/2}^x \frac{F(-y)}{v} dy \right], \quad (5.26)$$

$$\text{on } t = x/v + L/(2v),$$

which are exactly the same as (5.12) – (5.7) except $F(x)$ is replaced by $F(-x)$. This symmetry is used to quickly generate solutions to the full problem (2.37) - (2.42), whose solution arises from a superposition of the subproblem solutions and can be represented as

$$w_1(x, t) = a_1(x, t)H(\xi) + c_0(x, t)\delta(\eta) + \tilde{c}_1(-x, t)H(\eta), \quad (5.27)$$

$$w_2(x, t) = b_0(x, t)\delta(\xi) + b_1(x, t)H(\xi) + \tilde{d}_1(-x, t)H(\eta). \quad (5.28)$$

In Section 5.2.2, we give a numerical algorithm to generate the perfect data of the exit time distributions $w_1(-L/2, t)$ and $w_2(L/2, t)$. We could also generate noisy data $w_1(-L/2, t)$ and $w_2(L/2, t)$ by simulating a Broadwell random walk using a Monte-Carlo method which is based on a Rejection-Acceptance algorithm [91]. A full description of our Monte-Carlo simulation is presented in our previous paper [14]. Once $w_1(-L/2, t)$, $w_2(L/2, t)$ are calculated, we are able to find the corresponding cumulative distribution functions:

$$W_1(-L/2, t) = \int_0^t w_1(-L/2, t') dt' \equiv W_{1,\text{data}}(t),$$

$$W_2(L/2, t) = \int_0^t w_2(L/2, t') dt' \equiv W_{2,\text{data}}(t),$$

which will be used for flip rate reconstruction in Section 5.4.

5.2.2 Numerical Method for The Forward Problems

In this section, we numerically solve the forward problem (5.1) - (5.4) to generate the exit time distribution (perfect data) $w_1(-L/2, t)$, $w_2(L/2, t)$. From (5.27) - (5.28), we know that the exit time distributions are then given by

$$w_1(-L/2, t) = c_0(-L/2, t)\delta(t - L/v) + a_1(-L/2, t)H(t) + \tilde{c}_1(L/2, t)H(t - L/v), \quad (5.29)$$

$$w_2(L/2, t) = b_0(L/2, t)\delta(t - L/v) + b_1(L/2, t)H(t - L/v) + \tilde{d}_1(-L/2, t)H(t), \quad (5.30)$$

for $t > 0$. From Figure 5.4, we see that the values of $w_1(-L/2, t)$ at $t = L/(2v)$ and $w_2(L/2, t)$ at $t = L/(2v)$ only affect $F(x)$ at $x = 0$, a set of zero measure. So the delta functions included in (5.29) - (5.30) will only affect $F(x)$ at a single point; hence we ignore the deltas, and only need to solve for a_1 , b_1 , \tilde{c}_1 , and \tilde{d}_1 .

Now we describe the algorithm for solving a_1 , b_1 . Rewrite (5.13) - (5.7) as

$$\frac{da_1(c - vt, t)}{dt} = F(x)(b_1 - a_1), \quad \text{on } t + x/v = c/v, \quad (5.31)$$

$$\frac{db_1(c - vt, t)}{dt} = F(x)(a_1 - b_1), \quad \text{on } t - x/v = c/v, \quad (5.32)$$

$$a_1(x, t) = \frac{F(x)}{2} \exp \left[- \int_{-L/2}^x \frac{F(x')}{v} dx' \right], \quad \text{on } t = x/v + L/(2v), \quad (5.33)$$

$$b_1(-L/2, t) = 0, \quad (5.34)$$

where c is a constant. Let $\Delta x = L/N$, $x_0 = -L/2$, $x_N = L/2$, $t_0 = 0$, $t_N = L/v$, $a_1^{(j,i)} = a_1(x_j, t_i)$, $b_1^{(j,i)} = b_1(x_j, t_i)$, then follow the procedure and Figure 5.3 below to calculate a_1 and b_1 :

1. From (5.33) and (5.34), we know that a_1 (cross) is known on the diagonal $t = x/v + L/(2v)$, b_1 (circle) is known on the left boundary $x = -L/2$. Rewrite (5.31) and (5.32) as

$$b_1^{(j,i)} = \Delta t F_{j-1} \left[a_1^{(j-1,i-1)} - b_1^{(j-1,i-1)} \right] + b_1^{(j-1,i-1)}, \quad (5.35)$$

$$a_1^{(j,i)} = \Delta t F_{j+1} \left[b_1^{(j+1,i-1)} - a_1^{(j+1,i-1)} \right] + a_1^{(j+1,i-1)}, \quad (5.36)$$

from which the value of b_1 along Diag1 $t = x/v + L/(2v)$ is updated.

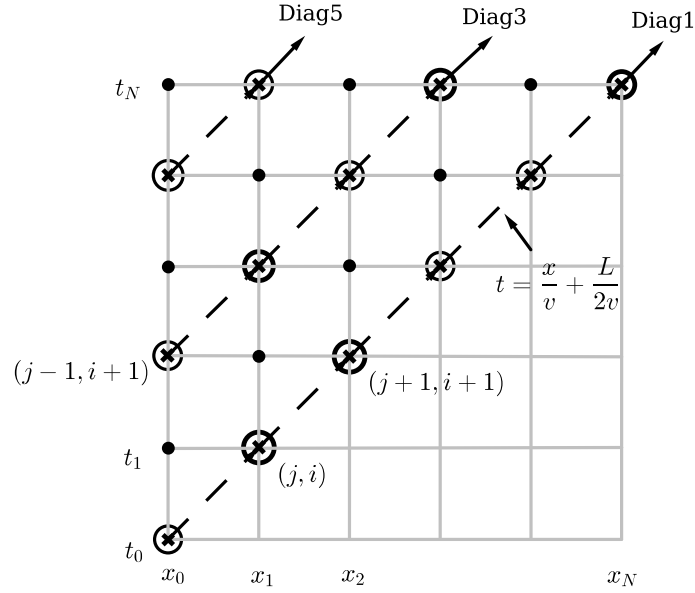


Figure 5.3: Finite difference stencils for forward problem (5.13) – (5.7). a_1 is known on the diagonal $t = x/v + L/(2v)$, b_1 is known on the left boundary $x = -L/2$

2. Use (5.36) and (5.35) to update the values of a_1 and b_1 along Diag 3.
3. Repeat the previous steps to update a_1 and b_1 along every other diagonal.
4. Use linear interpolation to calculate a_1 and b_1 along Diag2, Diag4, \dots , etc.

From Section 5.2.1, we know that \tilde{c}_1 and \tilde{d}_1 can be solved through (5.25) – (5.26) using the same algorithm as (5.13) – (5.7), but using $F(-x)$ instead of $F(x)$. Hence, the solution to the full forward problem (2.37) - (2.42) is constructed by solving (5.31) - (5.32) numerically.

5.3 Relationship between $F(x)$ and w_1, w_2 along $t = \frac{L}{2v} \pm \frac{x}{v}$

In this section, we derive the relationship between $F(x)$ and $w_{1,2}$ along $t = \frac{L}{2v} \pm \frac{x}{v}$ using (5.27) and (5.28).

Assume $-L/2 \leq x \leq 0$. Defining $w_1(x, [\frac{x}{v} + \frac{L}{2v}]^+)$ as $U_1(x)$, we have

$$\begin{aligned}
U_1(x) &\equiv w_1\left(x, \left[\frac{x}{v} + \frac{L}{2v}\right]^+\right) = a_1\left(x, \left[\frac{x}{v} + \frac{L}{2v}\right]^+\right), \\
&= \frac{F(x)}{2} \exp\left[-\int_{-L/2}^x \frac{F(x')}{v} dx'\right], \\
&= -\frac{v}{2} \frac{d}{dx} \exp\left[-\int_{-L/2}^x \frac{F(x')}{v} dx'\right], \\
\Rightarrow F(x) &= \frac{2U_1(x)}{1 - 2 \int_{-L/2}^x \frac{U_1(x')}{v} dx'}, \quad \text{for } -L/2 \leq x \leq 0, \tag{5.37}
\end{aligned}$$

and in particular,

$$F(-L/2) = 2U_1(-L/2). \tag{5.38}$$

For $0 \leq x \leq L/2$, similarly, define $w_2(x, [\frac{L}{2v} - \frac{x}{v}]^+)$ as $U_2(x)$. A similar calculation yields

$$F(x) = \frac{2U_2(x)}{1 - 2 \int_x^{L/2} \frac{U_2(x')}{v} dx'}, \quad \text{for } 0 \leq x \leq L/2, \tag{5.39}$$

and in particular,

$$F(L/2) = 2U_2(L/2). \tag{5.40}$$

Equations (5.37) - (5.40) are the cornerstones of our numerical method for the recovery of $F(x)$.

5.4 Layer Stripping Algorithm to Solve Inverse Problem

We now describe our algorithm for reconstructing the flip rate function $F(x)$ from the exit time distributions $w_1(-L/2, t)$ and $w_2(L/2, t)$. These distributions come from either the solution of the forward problem (perfect data), or directly simulating a Broadwell process (noisy data), details can be found in [14]. However, because the boundary data $w_1(-L/2, t)$ and $w_2(L/2, t)$ are very noisy, we will use $W_1(-L/2, t)$ and $W_2(L/2, t)$ in reconstruction.

Let $W_1(x, t) = \int_0^t w_1(x, t') dt'$, $W_2(x, t) = \int_0^t w_2(x, t') dt'$, then we rewrite (2.37) - (2.40) in terms of cumulative distribution functions $W_1(x, t)$ and $W_2(x, t)$:

$$\frac{\partial W_1}{\partial t} - v \frac{\partial W_1}{\partial x} = F(x)(W_2 - W_1), \quad (5.41)$$

$$\frac{\partial W_2}{\partial t} + v \frac{\partial W_2}{\partial x} = F(x)(W_1 - W_2), \quad (5.42)$$

$$W_1(L/2, t) = H(t),$$

$$W_2(-L/2, t) = H(t).$$

for $t \geq 0$, and

$$W_1 = 0, \quad W_2 = 0, \quad \text{for } t < 0,$$

where $H(t)$ is Heaviside function. Then our inverse problem becomes: given exit time distribution data $W_1(-L/2, t) \equiv W_{1,\text{data}}(t)$, $W_2(L/2, t) \equiv W_{2,\text{data}}(t)$, recover $F(x)$.

To reconstruct $F(x)$, first of all, we use the method of characteristics to rewrite equations (5.41) and (5.42) as

$$\frac{dW_1}{dx} = \frac{F(x)}{v}(W_1 - W_2), \quad \text{along } \frac{x}{v} + t = \text{constant}, \quad (5.43)$$

$$\frac{dW_2}{dx} = \frac{F(x)}{v}(W_1 - W_2), \quad \text{along } \frac{x}{v} - t = \text{constant}. \quad (5.44)$$

Let $W_1^{(j,i)} = W_1(x_j, t_i)$ and $W_2^{(j,i)} = W_2(x_j, t_i)$, $U_{1,j} = U_1(x_j) = w_1(x_j, t_j)$, $U_{2,j} = U_2(x_j) = w_2(x_j, t_j)$ and $F_j = F(x_j)$, where $x_j = j\Delta x$, $t_i = i\Delta t$, $\Delta x = L/(2N)$, $\Delta t = L/(vN)$.

We present both first order and second order numerical methods to reconstruct flip rate function $F(x)$.

5.4.1 First Order Layer Stripping Algorithm

The first order method is realized by using the simple Euler method to solve the ODEs and the rectangle rule to integrate numerically. Firstly, we rewrite (5.43) and (5.44) as

$$W_1^{(j,i)} = W_1^{(j-1,i+1)} + F_{j-1} \left(W_1^{(j-1,i+1)} - W_2^{(j-1,i+1)} \right) \Delta x/v, \quad (5.45)$$

$$W_2^{(j,i)} = W_2^{(j-1,i-1)} + F_{j-1} \left(W_1^{(j-1,i-1)} - W_2^{(j-1,i-1)} \right) \Delta x/v. \quad (5.46)$$

The finite difference stencils for (5.45) and (5.46) are indicated in Figure 5.4.

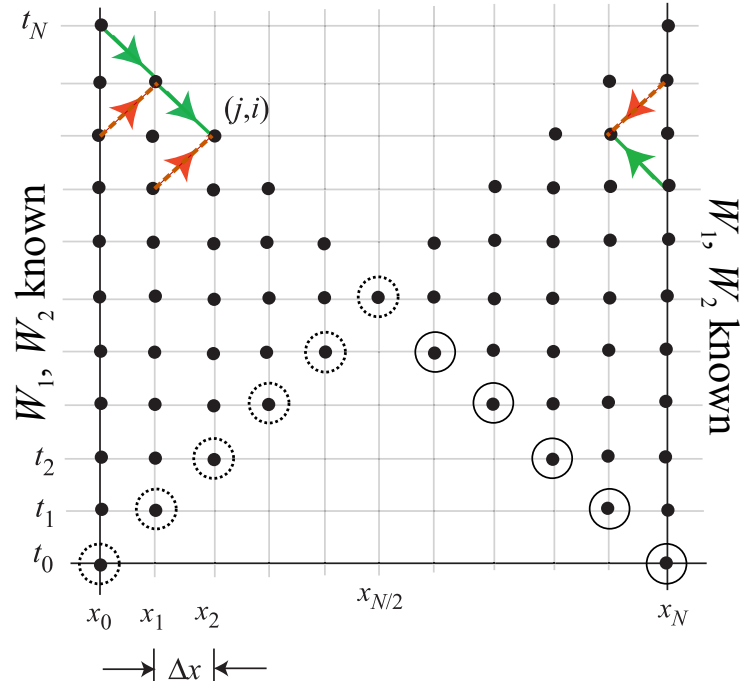


Figure 5.4: Layer stripping algorithm. Dashed circles are values of $W_1(x, [\frac{x}{v} + \frac{L}{2v}]^+) \equiv U_1(x)$. Solid circles are values of $W_2(x, [\frac{L}{2v} - \frac{x}{v}]^+) \equiv U_2(x)$. $W_1^{(j,i)}$ and $W_2^{(j,i)}$ are updated along solid and dashed arrows respectively.

Note that we have the values of $W_1(x_0, t_i) = W_{1,\text{data}}(t_i)$, $W_2(x_0, t_i) = H(t_i)$, $W_1(x_N, t_i) = H(t_i)$ and $W_2(x_N, t_i) = W_{2,\text{data}}(t_i)$ for all $i = 0, 1, 2, \dots, N - 1$, as well as $W_{1,\text{data}}(t_N) = \lim_{t \rightarrow t_N^-} W_1(x_0, t)$ and $W_{2,\text{data}}(t_N) = \lim_{t \rightarrow t_N^-} W_2(x_0, t)$. When $-L/2 \leq x \leq 0$ and N is even, the first order layer stripping algorithm to find $F(x)$ is as follows:

1. Use boundary data $W_{1,\text{data}}(t_i)$ and $H(t_i)$, (5.37) and (5.38) to compute $U_1(x_0)$, $F(x_0)$:

$$\begin{aligned} U_{1,0} &= U_1(x_0) = w_1(x_0, t_0) = w_1^{(0,0)} = \frac{W_1^{(0,1)} - W_1^{(0,0)}}{\Delta t}, \\ F_0 &= F(x_0) = 2U_1(x_0). \end{aligned}$$

2. At each layer $x = x_j$, $j = 1, \dots, \frac{N}{2} - 1$, we use (5.45), (5.46), (5.37) and (5.39) to calculate the values of $W_1(x_j, t_i)$, $W_2(x_j, t_i)$, $U_1(x_j)$ and $F(x_j)$, for $i = j, j + 1, \dots, N - j - 1$, respectively:

$$\begin{aligned} W_1^{(j,i)} &= W_1^{(j-1,i+1)} + F_{j-1} \left(W_1^{(j-1,i+1)} - W_2^{(j-1,i+1)} \right) \frac{\Delta x}{v}, \\ W_2^{(j,i)} &= W_2^{(j-1,i-1)} + F_{j-1} \left(W_1^{(j-1,i-1)} - W_2^{(j-1,i-1)} \right) \frac{\Delta x}{v}, \\ U_{1,j} &= w_1^{(j,j)} = \frac{W_1^{(j,j+1)} - W_1^{(j,j)}}{\Delta t}, \\ F_j &= \frac{2U_{1,j}}{1 - 2(U_{1,0} + \dots + U_{1,j-1})\Delta x/v}. \end{aligned}$$

A similar procedure can be repeated for the right triangle to find $F(x_j)$ when $j = \frac{N}{2} + 1, \frac{N}{2} + 2, \dots, N$, given boundary data $W_{2,\text{data}}(t)$ and $H(t)$. We use linear interpolation to find $F(x_{N/2})$.

5.4.2 Second Order Layer Stripping Algorithm

The second order layer stripping algorithm is developed by replacing the simple Euler method and rectangle rule in Section 5.4.1 by the Predictor-corrector method and trapezoid rule respectively.

When $-L/2 \leq x \leq 0$ and N is even, the second order layer stripping algorithm to find $F(x)$ is as follows:

1. Use first order algorithm, boundary data $W_{1,\text{data}}(t_i)$ and $H(t_i)$, $i = 0, 1, \dots, N$, where $W_{1,\text{data}}(t_N) = \lim_{t \rightarrow t_N^-} W_1(x_0, t)$, as well as (5.37) and (5.38) to predict $U_1(x_0)$, $F(x_0)$, which are written as $\widehat{U}_1(x_0)$, $\widehat{F}(x_0)$:

$$\begin{aligned} \widehat{U}_{1,0} &= \widehat{U}_1(x_0) = \frac{W_1^{(0,1)} - W_1^{(0,0)}}{\Delta t}, \\ \widehat{F}_0 &= \widehat{F}(x_0) = 2\widehat{U}_1(x_0). \end{aligned}$$

Then correct $\widehat{U}_1(x_0)$ by second order differentiation:

$$U_{1,0} = U_1(x_0) = \frac{-W_1^{(0,2)} + 4W_1^{(0,1)} - 3W_1^{(0,0)}}{2\Delta t}, \quad (5.47)$$

$$F_0 = F(x_0) = 2U_1(x_0). \quad (5.48)$$

In practice, because $U_{1,0}$ and F_0 do not depend on $\widehat{U}_{1,0}$ and \widehat{F}_0 , we just use (5.47) and (5.48) immediately.

2. At each layer $x = x_j$, $j = 1, \dots, \frac{N}{2} - 1$, we use the first order algorithms in Section 5.4.1, (5.43), (5.44), (5.37) and (5.39) to predict the values of $W_1(x_j, t_i)$, $W_2(x_j, t_i)$, $U(x_j)$ and $F(x_j)$, for $i = j, j + 1, \dots, N - j$,

$$\left. \begin{aligned} \widehat{W}_1^{(j,i)} &= W_1^{(j-1,i+1)} + F_{j-1} \left(W_1^{(j-1,i+1)} - W_2^{(j-1,i+1)} \right) \frac{\Delta x}{v}, \\ \widehat{W}_2^{(j,i)} &= W_2^{(j-1,i-1)} + F_{j-1} \left(W_1^{(j-1,i-1)} - W_2^{(j-1,i-1)} \right) \frac{\Delta x}{v}, \\ \widehat{U}_{1,j} &= \frac{\widehat{W}_1^{(j,j+1)} - \widehat{W}_1^{(j,j)}}{\Delta t}, \\ \widehat{F}_j &= \frac{2\widehat{U}_{1,j}}{1 - 2(\widehat{U}_{1,0} + \dots + \widehat{U}_{1,j-1})\Delta x/v}. \end{aligned} \right\} \text{Predictor}$$

Then use trapezoid rule to correct them:

$$\left. \begin{aligned} W_1^{(j,i)} &= W_1^{(j-1,i+1)} + \frac{\Delta x}{2v} \left\{ F_{j-1} (W_1^{(j-1,i+1)} - W_2^{(j-1,i+1)}) \right. \\ &\quad \left. + \widehat{F}_j (\widehat{W}_1^{(j,i)} - \widehat{W}_2^{(j,i)}) \right\}, \\ W_2^{(j,i)} &= W_2^{(j-1,i-1)} + \frac{\Delta x}{2v} \left\{ F_{j-1} (W_1^{(j-1,i-1)} - W_2^{(j-1,i-1)}) \right. \\ &\quad \left. + \widehat{F}_j (\widehat{W}_1^{(j,i)} - \widehat{W}_2^{(j,i)}) \right\}, \\ U_{1,j} &= \frac{-W_1^{(j,j+2)} + 4W_1^{(j,j+1)} - 3W_1^{(j,j)}}{2\Delta t}, \\ F_j &= \frac{2U_{1,j}}{1 - 2(U_{1,0}/2 + U_{1,1} + \dots + U_{1,j-1} + U_{1,j}/2)\Delta x/v}. \end{aligned} \right\} \text{Corrector}$$

A similar procedure can be repeated for the right triangle in Figure 5.4 to find $F(x_j)$ when $j = \frac{N}{2} + 1, \frac{N}{2} + 2, \dots, N$, given boundary data $h_2(t)$ and $H(t)$. We use linear interpolation to find $F(x_{N/2})$ from $F(x_{N/2-1})$ and $F(x_{N/2+1})$.

5.5 Results and Discussion

We used the layer stripping algorithm discussed in Section 5.4 to reconstruct flip rate functions from data generated by simulating a Broadwell random walk using a Monte-Carlo method [14]. In the discussion below, the interval length $L = 1$, particle

speed $v = 1$, N is the number of subintervals in $[-L/2, L/2]$, and M is the number of exit times used to generate each exit time distribution $w_1(-L/2, t)$, $w_2(L/2, t)$. Hence, the total number of exit times is always $2M$. Also, notice that the layer stripping algorithm we used does not find the value of $F(x)$ at $x = 0$; so it leaves a ‘‘hole’’ in the $F(x)$, which is filled by interpolation.

In Figure 5.5, we reconstruct four continuous flip rate functions using the first order layer stripping method. The function in 4(a) is a trigonometric function, the function in 4(b) is a combination of trigonometric and exponential functions, the function in 4(c) has discontinuous derivatives within $(-L/2, L/2)$, and the function in 4(d) has many extrema within $(-L/2, L/2)$. Let $F(x)$ be the target flip rate function, $F_p(x)$ be the flip rate function reconstructed from perfect data which is generated by solving the forward problem (2.37) - (2.42) and $F_n(x)$ be the flip rate function reconstructed from noisy data which is generated by simulating the Broadwell process. Define the error for perfect data E_p and the error for noisy data E_n in the L^2 norm as

$$E_p = \left(\sum_{i=0}^N |F(x_i) - F_p(x_i)|^2 \Delta x \right)^{1/2} \approx \left(\int_{-L/2}^{L/2} |F(x) - F_p(x)|^2 dx \right)^{1/2},$$

$$E_n = \left(\sum_{i=0}^N |F(x_i) - F_n(x_i)|^2 \Delta x \right)^{1/2} \approx \left(\int_{-L/2}^{L/2} |F(x) - F_n(x)|^2 dx \right)^{1/2}.$$

In principle, with $N = 100$, we are able to reconstruct any continuous flip rate function with E_p and E_n always within $O(10^{-2})$ given $M = 200,000$. The reconstructed curve becomes less noisy, and the accuracy of the flip rate reconstructions from noisy data improves as M increases. For instance, E_n decreases by 30% - 50% when $M = 1,000,000$, see Figure 5.6. The reconstruction results and errors obtained from first order and second order methods are identical to within three decimal places. Because W_1 and W_2 are noisy, the second order finite difference formula (5.47) is only first order accurate. Hence the accuracy of the Predictor-Corrector method is first order overall. We now validate the correct convergence rate of the layer stripping algorithms used in Section 5.4.1 and 5.4.2, provided that the boundary data for reconstruction is noiseless and corresponds to an actual flip rate function. Assume we are given $0 \leq x \leq L/2$,

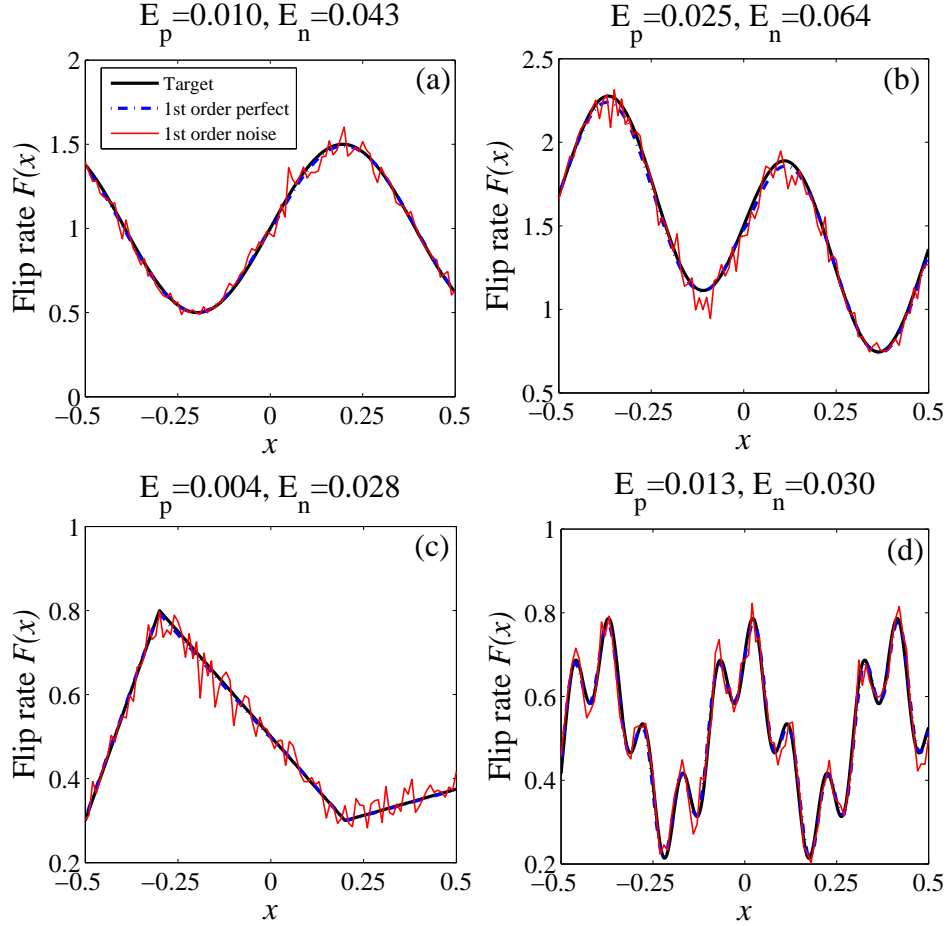


Figure 5.5: Reconstruction of flip rate functions $F(x)$: (a) $F(x) = 0.5 \sin(8x) + 1$, (b) $F(x) = \sin(5x) \cos(8x) + \cos(0.3x) \exp(0.5x) + x^2 \sin(-0.6x^3) + 0.5$, (c) $F(x) = 2.5x + 1.55$ for $-0.5 \leq x \leq -0.3$, $F(x) = -x + 0.5$ for $-0.3 < x < 0.2$, $F(x) = 0.25x + 0.25$ for $0.2 \leq x \leq 0.5$, and (d) $F(x) = 0.5 + 0.2 \cos(16x) + 0.1 \sin(64x)$, $N = 100$, $M = 200,000$.

$W_2(L/2, t) \equiv W_{2,\text{data}}(t)$. Let F_N be the reconstructed flip rate function for an $N + 1$ point discretization (see Figure 5.4). Define the error in terms of L^2 norm:

$$E_N = \left(\sum_{i=0}^N |F_N(x_i) - F_{6000}(x_i)|^2 \Delta x \right)^{1/2} \approx \left(\int_0^{L/2} |F_N(x) - F_{6000}(x)|^2 dx \right)^{1/2},$$

where we use F_{6000} to approximate the true $F(x)$. In Figure 5.7, we plot the error E_N against the number of subintervals in $[-L/2, L/2]$. We find that the reconstruction error scales as $O(N^{-1})$ when using the first order algorithm, which agrees with simple

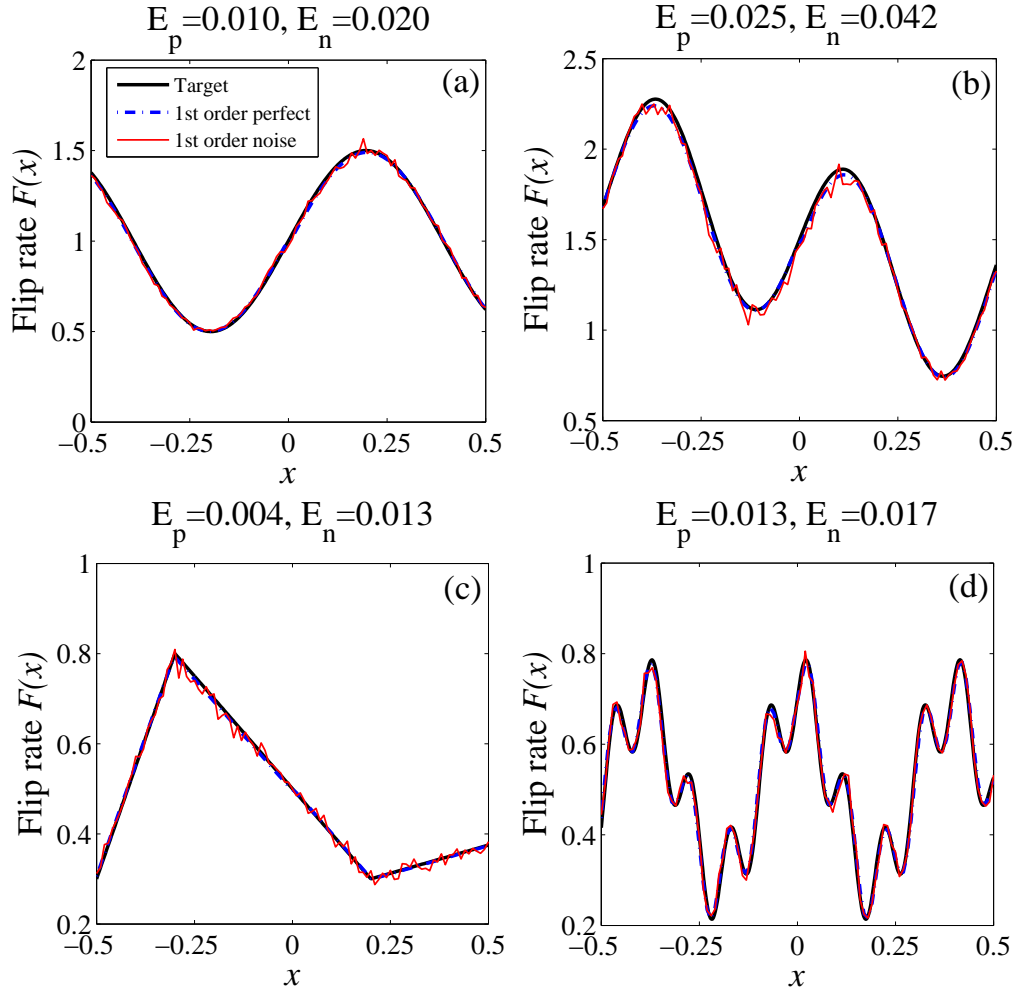


Figure 5.6: Reconstruction of flip rate functions $F(x)$: (a) $F(x) = 0.5 \sin(8x) + 1$, (b) $F(x) = \sin(5x) \cos(8x) + \cos(0.3x) \exp(0.5x) + x^2 \sin(-0.6x^3) + 0.5$, (c) $F(x) = 2.5x + 1.55$ for $-0.5 \leq x \leq -0.3$, $F(x) = -x + 0.5$ for $-0.3 < x < 0.2$, $F(x) = 0.25x + 0.25$ for $0.2 \leq x \leq 0.5$, (d) $F(x) = 0.5 + 0.2 \cos(16x) + 0.1 \sin(64x)$, $N = 100$, $M = 1,000,000$.

Euler and the rectangle rule leading to a first order layer stripping algorithm. The error scales as $O(N^{-2})$ when using second order algorithm, which is consistent with Predictor-Corrector method and the trapezoid rule leading to a second order layer stripping algorithm.

Our original motivation for studying the Broadwell process was to better-understand

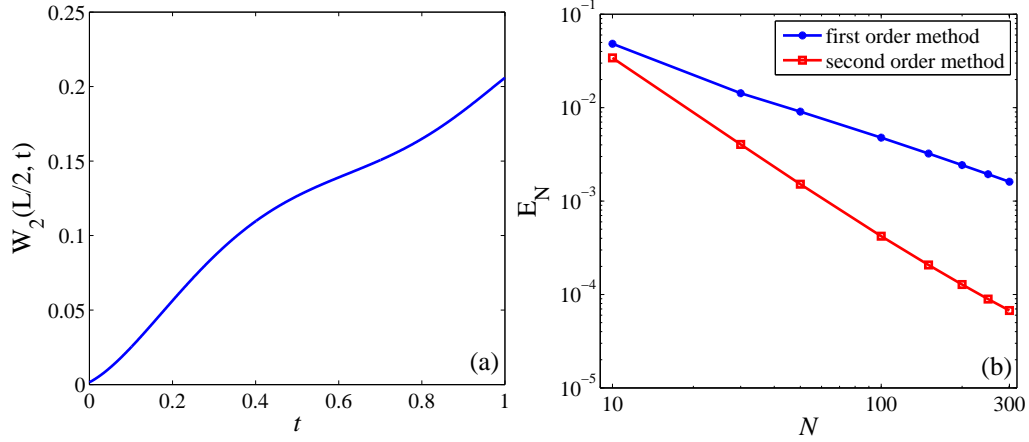


Figure 5.7: Dependence of error in flip rate function $F(x)$ reconstruction on the number of subintervals N . (a) The probability density function $W_2(L/2, t) \equiv W_{2,\text{data}}(t) = -0.1403t^6 - 0.7352t^5 + 2.9494t^4 - 3.1707t^3 + 1.1536t^2 + 0.1476t + 0.0015$ for $t \in [0, L/v]$. (b) Given $W_2(L/2, t)$, we use both first and second order layer stripping methods to reconstruct $F(x)$, $0 \leq x \leq L/2$.

reconstruction from the exit times of a Brownian motion. In the Broadwell process, the transition distance between the two states is shorter if the flip rate is larger, or the velocity is smaller. This property indicates that in the limit of large dimensionless flip rate $\frac{LF(x)}{v}$, the Broadwell process behaves like a diffusive motion. In Figure 5.8, we reconstruct the flip rate $F(x)$ when v is small from two types of noisy data. In Figure 5.8(a) and Figure 5.8(b) the exit time distribution is generated from Monte-Carlo simulation, while in Figure 5.8(c) and Figure 5.8(d), the distribution is generated by adding artificial noise which is uniformly distributed $U[-\varepsilon, \varepsilon]$ to $w_{1p}(-L/2, t)$ and $w_{2p}(L/2, t)$, with $\varepsilon = 10^{-5}$. From Figure 5.8(a) and Figure 5.8(b), we observe that the reconstruction is poor near $x = 0$, because the noise in the pdfs $w_1(-L/2, t)$ and $w_2(L/2, t)$ for $t \in (0, L/v]$ propagates along characteristics $dx/dt = \pm v$. Our algorithm for reconstructing $F(x)$ accumulates the noise because it requires computing the integrals of $w_1(x, [\frac{L}{2v} + \frac{x}{v}]^+)/v$ and $w_2(x, [\frac{L}{2v} - \frac{x}{v}]^+)/v$ through equations (5.37) and (5.39).

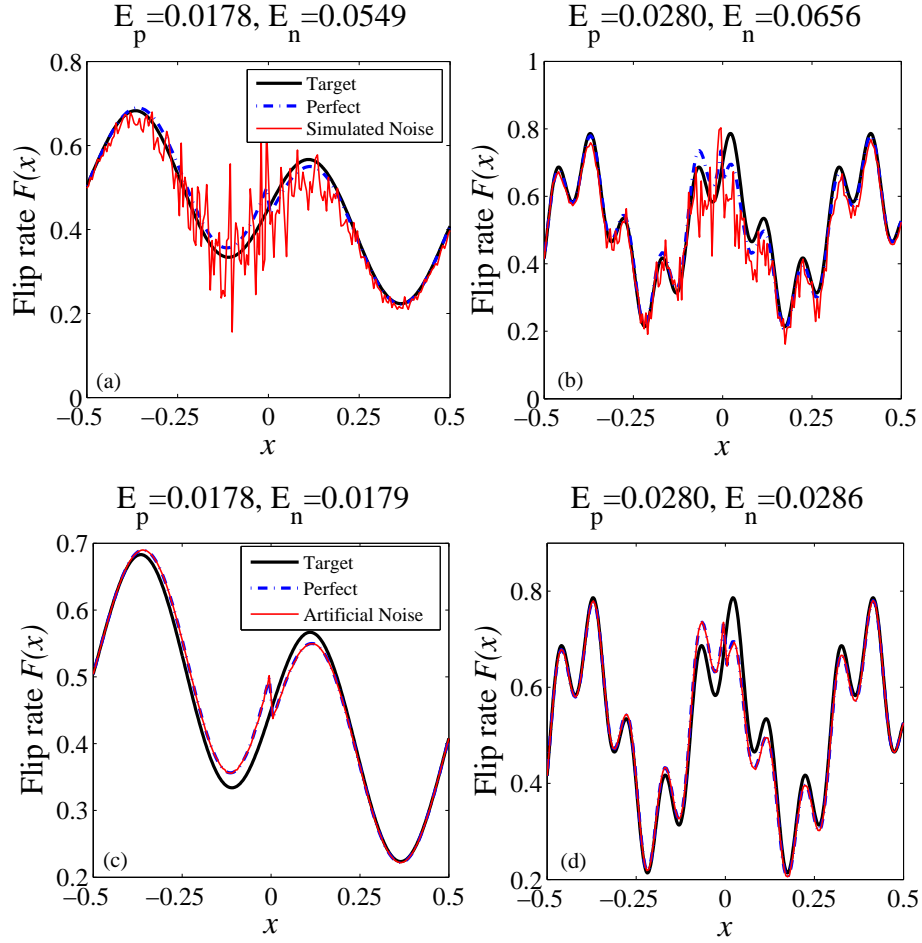


Figure 5.8: Reconstruction of flip rate functions $F(x)$ with small velocity from Monte-Carlo simulation data and artificial noisy data: (a) and (c) $F(x) = 0.3 \sin(5x) \cos(8x) + 0.3 \cos(0.3x) \exp(0.5x) + 0.3x^2 \sin(-0.6x^3) + 0.15$, (b) and (d) $F(x) = 0.5 + 0.2 \cos(16x) + 0.1 \sin(64x)$, $N = 200$, $v = 0.1$. (a) and (b) are reconstructed from simulated noisy data with $M = 1,000,000$. (c) and (d) are reconstructed from artificial noisy data.

We use artificial data to reconstruct flip rate functions in Figure 5.8(c) and Figure 5.8(d) for two main reasons. First of all, in our previous paper [14], we find that all the moments (except for the zeroth moment) of the exit time distribution diverge when $v \ll 1$, so for fixed M , the noisy data generated from simulation becomes less accurate when v gets smaller. Also, given $F(x) = O(1)$, $x \in [-L/2, L/2]$ and $v \ll 1$, it takes a longer time to generate a fixed number of exit times as $v \rightarrow 0$; this

also makes the reconstruction more difficult. Specifically, let $w_{1p}(-L/2, t)$, $w_{2p}(L/2, t)$, and $w_{1n}(-L/2, t)$, $w_{2n}(L/2, t)$ for $t \in (0, L/v]$ be probability density functions obtained from perfect data and from Monte-Carlo simulation respectively. The pdfs $w_{1n}(-L/2, t_j)$ and $w_{2n}(L/2, t_j)$, where $t_j, j = 0, 1, \dots, N$, are defined in Section 5.4, and can be computed as follows. Suppose the two sets of M exit times are $\{\tau_k^{(1)}\}$ and $\{\tau_k^{(2)}\}$, $1 \leq k \leq M$. Then let

$$w_{1n}(-L/2, t) = \frac{m}{M\Delta t}, \quad \text{if } t_{j-1} \leq t < t_j,$$

where $\Delta t = t_j - t_{j-1}$, m is the number of exit times satisfying $t_{j-1} \leq \tau_k^{(1)} < t_j$, for $1 \leq j \leq N$. $w_{2p}(L/2, t_j)$ can be computed similarly. Define the magnitude of noise in $w_{1n}(-L/2, t)$ and $w_{2n}(L/2, t)$ by

$$\varepsilon_1 = \max_{t \in (0, L/v]} |w_{1n}(-L/2, t) - w_{1p}(-L/2, t)|, \quad \varepsilon_2 = \max_{t \in (0, L/v]} |w_{2n}(L/2, t) - w_{2p}(L/2, t)|,$$

respectively. For the data used to generate Figure 5.8(a) and Figure 5.8(b), we find that both ε_1 and ε_2 are $O(10^{-3})$ with $N = 200$ and $2M = 2,000,000$ exit times in total, which takes more than 11 days to generate. To reduce the order of ε_1 and ε_2 to $\varepsilon = 10^{-5}$, the noise level of the data in Figure 5.8(c) and (d), we need to generate more exit times. However, reducing ε_1 and ε_2 to $O(10^{-5})$ would require about $2M = 4,000,000$ exit times, which would take MATLAB 22 days to complete on an AMD Opteron 6174 CPU (Base frequency 2200 MHz).

5.6 Conclusion

In this chapter, we successfully utilize a layer stripping method, which is used by geophysicists in seismology, to study a stochastic inverse problem arising from neuroscience and medical imaging. In principle, we are able to reconstruct a wide range of continuous flip rate functions of a one-dimensional, constant-speed Broadwell process from the exit time distributions, and the error is within $O(10^{-2})$ using $2M = 400,000$ exit times in total. The reconstructed flip rate functions become less noisy, and the

accuracy improves as the number of exit times increases. For instance, the reconstruction error in the L^2 norm decreases by 30% - 50% when using $2M = 2,000,000$ exit times in total.

We develop first order and second order layer stripping methods for flip rate reconstruction, where the second order layer stripping algorithm is developed by replacing the first order simple Euler method and rectangle rule with a Predictor-Corrector method and trapezoid rule. In both of the algorithms, we do not find the value of $F(x)$ at $x = 0$; so it leaves a “hole” in the $F(x)$, which is filled by interpolation. However, the second order finite difference method is second order accurate only when the boundary data is noiseless and corresponds to an actual flip rate function; otherwise, it is only first order accurate.

We are also able to reconstruct the flip rate function $F(x)$ from noisy (artificial and Monte-Carlo simulated) data even when v is small, which is the important limit corresponding to a Brownian random walk. When we reconstruct the flip rate function $F(x)$ from simulated noisy data for small v , we usually have larger deviation near $x = 0$, because the pdfs of the boundary data become less accurate when v gets smaller. To reduce the noise in the pdfs, we can increase the number of exit times, which turns out to be time consuming. The difficulty in data generation and the noise in pdfs explains the difficulties in reconstructing flip rate function for small velocity.

A sequence of studies [22, 13] shows that the inverse problem associated with Brownian motion is ill-posed, and the related existence and uniqueness of the spatially dependent parameters are not well established. However, the reconstruction using Broadwell as the underlying model *is* well-posed and unique [44]. This motivates the use of regularization of the inverse problem by better-modeling of the underlying physics.

The layer stripping algorithm is more powerful than the projection method used in our previous paper [14], where we could reconstruct only fourth order polynomials robustly. However, the layer stripping algorithm can only reconstruct flip rate functions from boundary data generated by starting a Broadwell process from either endpoint

of the interval, while the projection method can reconstruct from data generated by starting a Broadwell process from any position within the interval.

5.7 Future Work

We see three main extensions to this work. The first is to reconstruct spatially dependent advection velocities $v(x)$ as well as transition rates $F(x)$. The second is to develop alternative algorithms for reconstruction. We showed in the last chapter that as the number of coefficients representing the flip rate function increases, our projection method becomes unstable due to the presence of flat minima in the objective functions (see equations (4.24) and (4.25) and Table 4.1. This instability could be alleviated by introducing a small regularization parameter in the objective functions (4.24), (4.25) or developing iterative algorithms based directly on (2.37) - (2.42) and (4.1)-(4.4). The third is to smooth the noisy simulation data by filtering so that we can retain the accuracy of the second order layer stripping method. We will also apply the layer stripping method to a Broadwell process of two advection velocities $v_1(x)$ and $-v_2(x)$, as well as extend our study to higher dimensional Broadwell processes.

Chapter 6

FIRST PASSAGE TIMES IN CLINICAL TRIALS

Clinical trials are an important part of the drug development process and must be performed before pharmaceutical companies can commercialize their new drugs. It takes about 7 years [52] for an oncology drug to complete a trial. This is a significant fraction of the 20 years of patent protection time in the US. Thus, it is very important for pharmaceutical companies to avoid clinical trial delays to guarantee profitability. In this chapter, we are interested in how to accurately estimate the mean recruiting time and efficiently plan drug inventory among multiple testing centers so that the mean recruiting time is minimized. The format of this chapter is as follows. In Section 6.1, we give a detailed description of the clinical trial recruitment process at multiple testing centers, and set up a stochastic model for the recruitment process. In Section 6.2, we derive analytic approximations for the optimal drug distribution and associated (minimal) mean recruiting time for the case of two testing centers. Then we postulate analytic formulas for the general m -site case. In Section 6.3, we show how to implement Laplace's method to approximate the mean recruiting time. In Section 6.4, we show how to generate the mean recruiting times from Monte Carlo simulations. In Section 6.5, we confirm the validity of the analytical solutions by checking against Monte-Carlo simulations. In Section 6.4, we present the conclusions and the future work.

6.1 Stochastic Model of A Clinical Drug Trial

Suppose a pharmaceutical company would like to recruit h patients (h is called the patient horizon), and there are a total of n doses of drugs in the central warehouse to be distributed to $m \geq 1$ testing centers so that each has n_i drugs, $1 \leq i \leq m$, and

$n = \sum_{i=1}^m n_i$. The drugs must be given to patients who arrive at the testing sites. For each center i , assume that patients arrive independently with Poisson rate $\lambda_i > 0$. See Figure 6.1. Assuming patients are instantly recruited into trials as soon as they arrive at a site, we wish to calculate the time for h patients to be recruited.

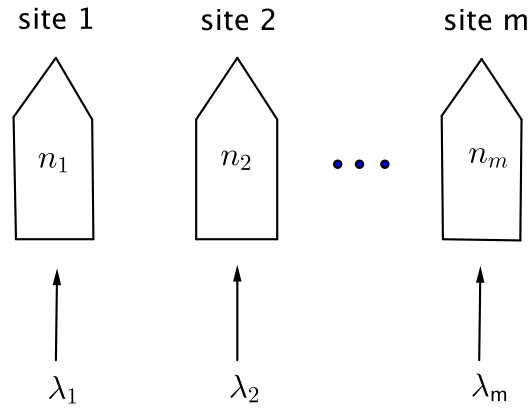


Figure 6.1: Patient recruitment in a drug trial. m sites are allocated n_1, n_2, \dots, n_m drug doses which must be tested. Patients arrive at each site at a rate λ_j , consume the drugs and are recruited into patient horizon is reached.

To gain some insight into the problem, assume that the pharmaceutical company is able to provide a large number of doses to each site so that $n_i = h$ for each i . In that case, none of the centers run out of drugs before the patient horizon is reached and the total patient arrival rate is always $\lambda = \sum_{i=1}^m \lambda_i$ throughout the duration of the trial. For each center, the inter-arrival time between events follows an exponential distribution $\exp(\lambda)$. The recruiting time, which is the sum of all the h inter-arrival times, follows a Gamma distribution $\Gamma(h, 1/\lambda)$. The mean time taken to recruit h patients is therefore h/λ . However, the $n_i = h$ assumption is unreasonable. It is unwise to keep a large supply of drugs in testing centers, because it increases the cost of the trial dramatically. The problem of interest is when $h \leq n < \infty$, $n_i \leq n < \infty$. If one of the sites runs out of drugs and cannot recruit patients anymore, then the

overall recruitment rate is reduced, and makes the overall recruiting time longer than h/λ , which is the theoretical minimum. This scenario is called a stock-out and triggers our interest in exploring how to optimally dispense the drugs to the centers in order to minimize the recruiting time.

In this chapter, we focus on two problems when the total number of doses equals the number of patients needed ($n = h = \sum_{i=1}^m n_i$):

1. Given $\mathbf{n} = [n_1, n_2, \dots, n_m]$, predict the mean recruiting time $t(n_1, n_2, \dots, n_m; h)$ taken to recruit $h = n$ patients.
2. Given the total number of doses n and a patient horizon $h = n$, determine the optimal distribution of drugs $\mathbf{n}^* = [n_1^*, n_2^*, \dots, n_m^*]$ that minimizes the mean recruiting time, and calculate what this time is. In other words, we want to find \mathbf{n}^* such that $t^* = t(n_1^*, n_2^*, \dots, n_m^*; h) = \min_{\substack{n_i \leq n < \infty \\ n_1 + n_2 + \dots + n_m = n}} t(n_1, n_2, \dots, n_m; h)$.

The clinical trial recruitment process can be described as a particle undergoing a random walk on a m -dimensional integer-valued lattice $[0, n_1] \times [0, n_2] \times \dots \times [0, n_m]$, where the particle moves one step in positive direction of i^{th} coordinate with probability p_i if center i recruits one patient, where $\sum_{i=1}^m p_i = 1$. Once the walker moves h steps in total, the travel time is recorded as the exit time. This exit time is actually the desired recruiting time. The mean recruiting time can be obtained by repeating the random walk a large number of times, and taking an average.

Let (k_1, k_2, \dots, k_m) , $0 \leq k_i \leq n_i$, $i = 1, 2, \dots, m$ be the number of patients recruited by each testing center by time t , and $P(k_1, k_2, \dots, k_m, t)dt$ be the probability that the particle is in state (k_1, k_2, \dots, k_m) in the time interval $(t, t + dt)$. Then define $P(k_1, k_2, \dots, k_m, t) = 0$ whenever any one of the $k_j < 0$. We have the master equations

describing the in-flux and out-flux of probability from state (k_1, k_2, \dots, k_m) :

$$\begin{aligned}
\dot{P}(k_1, k_2, \dots, k_m, t) &= \lambda_1 P(k_1 - 1, k_2, k_3, \dots, k_m, t) \\
&+ \lambda_2 P(k_1, k_2 - 1, k_3, \dots, k_m, t) + \dots \\
&+ \lambda_m P(k_1, k_2, k_3, \dots, k_m - 1, t) \\
&- P(k_1, k_2, k_3, \dots, k_m, t) \sum_{j=1}^m \lambda_j (1 - \delta_{k_j, n_j}), \quad (6.1)
\end{aligned}$$

with the absorbing boundary condition

$$P(k_1, k_2, \dots, k_m, t) = 0, \quad \text{if } \sum_{j=1}^m k_j = h,$$

where δ_{k_j, n_j} is the Kronecker delta function. Note that in equations (6.1), $k_j = n_j$ corresponds to a site stocking out of drugs and reduces the out-flux of probability from the state (k_1, k_2, \dots, k_m) . The master equations (6.1) form a set of coupled linear ODEs. The mean exit time is given by

$$t(n_1, n_2, \dots, n_m; h) = \int_0^\infty \sum_{k_m=1}^{n_m} \dots \sum_{k_1=1}^{n_1} P(k_1, \dots, k_m, t) dt. \quad (6.2)$$

For future reference, we define

$$\begin{aligned}
\Lambda &= [\lambda_1, \lambda_2, \dots, \lambda_m], \\
\lambda &= \sum_{i=1}^m \lambda_i, \\
p_i &= \lambda_i / \lambda, \quad i = 1, 2, \dots, m. \quad (6.3)
\end{aligned}$$

6.2 Calculation of Mean Exit Time

6.2.1 The 2-site Case

We first perform the calculation for the $m = 2$ case. We use this case to gain insight into the more general problem and to set up notation.

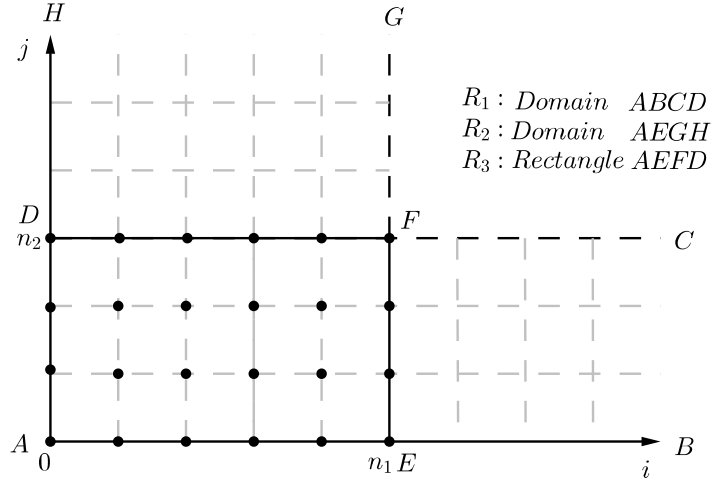


Figure 6.2: Interpretation of $\lambda t(n_1, n_2; h)$ in equation (6.12) by summing terms in the regions R_1, R_2 and R_3 .

Let $P(i, j, t)dt$ be the probability that the particle is in state (i, j) at time $(t, t + dt)$. The master equations are

$$\begin{aligned} \dot{P}(i, j, t) &= \lambda_1 P(i-1, j, t) + \lambda_2 P(i, j-1, t) - \lambda P(i, j, t), & 0 \leq i < n_1, 0 \leq j < n_2, \\ \dot{P}(n_1, j, t) &= \lambda_1 P(n_1-1, j, t) + \lambda_2 P(n_1, j-1, t) - \lambda_2 P(n_1, j, t), & 0 \leq j < n_2, \\ \dot{P}(i, n_2, t) &= \lambda_1 P(i-1, n_2, t) + \lambda_2 P(i, n_2-1, t) - \lambda_1 P(i, n_2, t), & 0 \leq i < n_1, \end{aligned}$$

with the absorbing boundary condition

$$P(n_1, n_2, t) = 0.$$

We can solve these equations analytically following Algorithm 7 below. The exact

Algorithm 7 Solving master equations analytically

- 1: Solve the differential equation for $P(0, 0, t)$ with initial condition $P(0, 0, t = 0) = 1$.
 - 2: **for** $l = 1 : h - 1$ **do**
 - 3: Solve differential equations for $P(i, j, t)$, with initial conditions $P(i, j, t = 0) = 0$, where $i + j = l$, $i \leq n_1$, $j \leq n_2$.
 - 4: **end for**
-

solutions are

$$P(i, j, t) = \frac{(\lambda_1 t)^i (\lambda_2 t)^j}{i! j!} e^{-\lambda t}, \quad 0 \leq i < n_1, 0 \leq j < n_2, \quad (6.4)$$

$$P(i, n_2, t) = \sum_{j=n_2}^{\infty} \frac{(\lambda_1 t)^i (\lambda_2 t)^j}{i! j!} e^{-\lambda t}, \quad 0 \leq i < n_1, \quad (6.5)$$

$$P(n_1, j, t) = \sum_{i=n_1}^{\infty} \frac{(\lambda_1 t)^i (\lambda_2 t)^j}{i! j!} e^{-\lambda t}, \quad 0 \leq j < n_2. \quad (6.6)$$

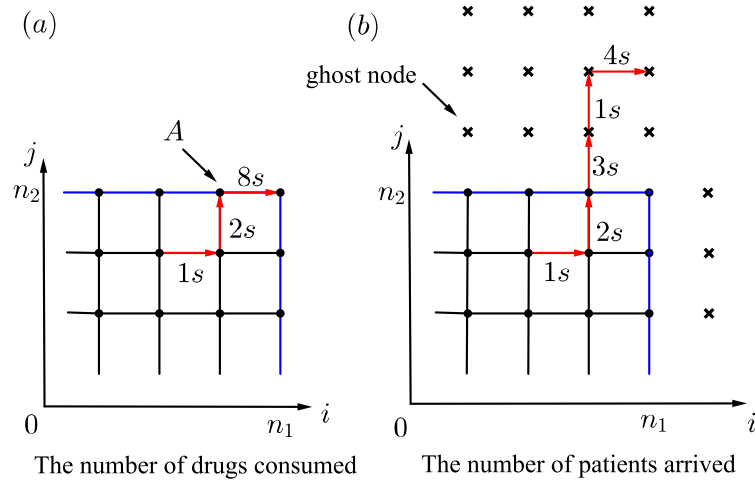


Figure 6.3: Interpretation of equations (6.4) - (6.6). (a) shows the number of drugs consumed. (b) extends the grids to infinity in i and j direction with ghost nodes, and shows the number of patients arrive.

Equation (6.4) is the probability of the particle in the interior of R_3 , where the number of drug consumed equals the number of patients arrived, see Figure 6.3. It can be interpreted as the probability of i patients arrive at center 1 and j patients arrived at center 2. Equations (6.5) and (6.6) are the probabilities that the particle is on the boundary of R_3 , where the number of drugs consumed is less than or equal to the number of patients that arrive. For example, when the particle is at point A in Figure 6.3(a), center 2 runs out of drugs, and only one drug is available at center 1. Then two patients arrive at center 2 afterwards with waiting time three seconds, and one second; but no drugs are available. Then after four seconds, one patient arrives at center 1, and takes the drug. The clinical trial completes. The time taken to recruit

the last patient is eight seconds. So the probabilities of the particle at point A is the sum of all probabilities that patients arrive at center 2 without drugs available. In other words, Equations (6.5) and (6.6) can be interpreted as follows: after site 1 stocks out, the stochastic evolution of the system is equivalent to the particle traversing ghost nodes $i \geq n_1$. Likewise, after site 2 stocks out, the stochastic evolution of the system is equivalent to the particle traversing ghost nodes $j \geq n_2$.

Define

$$\sigma_{ij} = \lambda \int_0^\infty P(i, j, t) dt, \quad (6.7)$$

where (i, j) lies in the bounded region $\Omega = \{(i, j) : 0 \leq i \leq n_1, 0 \leq j \leq n_2\}$. Then, from equation (6.2),

$$\lambda t(n_1, n_2; h) = \sum_{(i,j) \in \Omega} \sigma_{ij} = \sum_{i=0}^{n_1-1} \sum_{j=0}^{n_2-1} \sigma_{ij} + \sum_{i=0}^{n_1-1} \sigma_{i,n_2} + \sum_{j=0}^{n_2-1} \sigma_{n_1,j} + \sigma_{n_1,n_2}, \quad (6.8)$$

where

$$\begin{aligned} \sigma_{ij} &= \frac{(i+j)!}{i!j!} p_1^i p_2^j, & 0 \leq i < n_1, 0 \leq j < n_2, \\ \sigma_{i,n_2} &= \lambda \int_0^\infty P(i, n_2, t) dt = \sum_{j=n_2}^\infty \frac{(i+j)!}{i!j!} p_1^i p_2^j, \\ \sigma_{n_1,j} &= \lambda \int_0^\infty P(n_1, j, t) dt = \sum_{i=n_1}^\infty \frac{(i+j)!}{i!j!} p_1^i p_2^j, \\ \sigma_{n_1,n_2} &= 0. \end{aligned}$$

Equation (6.8) can also be written in the form

$$\lambda t(n_1, n_2; h) = \sum_{(i,j) \in \Omega'} \tilde{\sigma}_{ij}, \quad (6.9)$$

where Ω' and the regions R_1 , R_2 and R_3 (see Figure. 6.2) are defined by

$$\begin{aligned} \Omega' &= (R_1 \cup R_2) \setminus R_3, \\ R_1 &= \{(i, j) : 0 \leq i < \infty, 0 \leq j \leq n_2\}, \\ R_2 &= \{(i, j) : 0 \leq i \leq n_1, 0 \leq j < \infty\}, \\ R_3 &= \{(i, j) : 0 \leq i \leq n_1, 0 \leq j \leq n_2\}, \end{aligned}$$

and

$$\tilde{\sigma}_{ij} = \frac{(i+j)!}{i!j!} p_1^i p_2^j, \quad \text{for all } (i, j) \in \Omega'. \quad (6.10)$$

Then the boundary terms $\sigma_{n_1, j}$ and σ_{i, n_2} are actually

$$\sigma_{n_1, j} = \sum_{i=n_1}^{\infty} \tilde{\sigma}_{i, j}, \quad \sigma_{i, n_2} = \sum_{j=n_2}^{\infty} \tilde{\sigma}_{i, j}. \quad (6.11)$$

In many cases, $\sigma_{n_1, j}$ and σ_{i, n_2} in equation (6.8) are given more weight than interior nodes. This is in line with intuition because hopping rates are reduced on boundary nodes, increasing the dwell time of the particle on the node and the associated probability.

When finding the optimal distribution of drugs $\mathbf{n}^* = [n_1^*, n_2^*]$, where the ‘‘optimal’’ means the minimum recruiting time over all combinations of n_1, n_2 such that $n_1 + n_2 = n$, i.e. $t^* = \min_{n_1+n_2=n} t(n_1, n_2; h)$, the sum (6.8) must be computed many times and this can be quite laborious. Here we seek to approximate the sum with simple elementary functions so that the optimization problem becomes easier.

Let us assume that $n_1 < n_2 < h = n_1 + n_2$. Equation (6.9) involving the mean exit time becomes

$$\begin{aligned} \lambda t(n_1, n_2; h) &= \sum_{i=0}^{n_1-1} \sum_{j=0}^{n_2-1} \tilde{\sigma}_{ij} + \sum_{i=0}^{n_1-1} \left(\sum_{j=0}^{\infty} - \sum_{j=0}^{n_2-1} \right) \tilde{\sigma}_{i, j} + \sum_{j=0}^{n_2-1} \left(\sum_{i=0}^{\infty} - \sum_{i=0}^{n_1-1} \right) \tilde{\sigma}_{i, j}, \\ &= \sum_{i=0}^{n_1-1} \sum_{j=0}^{\infty} \tilde{\sigma}_{ij} + \sum_{j=0}^{n_2-1} \sum_{i=0}^{\infty} \tilde{\sigma}_{ij} - \sum_{i=0}^{n_1-1} \sum_{j=0}^{n_2-1} \tilde{\sigma}_{ij}, \\ &= \sum_{R_2} \tilde{\sigma}_{i, j} + \sum_{R_1} \tilde{\sigma}_{i, j} - \sum_{R_3} \tilde{\sigma}_{i, j}. \end{aligned} \quad (6.12)$$

Now consider each of the sums in (6.12) separately:

$$\begin{aligned}
I_1 &\equiv \sum_{R_2} \tilde{\sigma}_{i,j} = \sum_{i=0}^{n_1-1} \sum_{j=0}^{\infty} \tilde{\sigma}_{i,j}, \\
&= \sum_{i=0}^{n_1-1} \sum_{j=0}^{\infty} \binom{i+j}{i,j} p_1^i p_2^j, \\
&= \sum_{i=0}^{n_1-1} p_1^i \sum_{j=0}^{\infty} \binom{i+j}{i,j} p_2^j, \\
&= \sum_{i=0}^{n_1-1} p_1^i (1-p_2)^{-(i+1)}, \\
&= \frac{n_1}{p_1},
\end{aligned}$$

where we used the fact that

$$\begin{aligned}
(1-x)^{-(m+1)} &= \sum_{r=0}^{\infty} \binom{m+r}{m,r} x^r, \quad 0 < |x| < 1, \\
p_1 + p_2 &= 1.
\end{aligned} \tag{6.13}$$

A similar calculation yields $I_2 \equiv \sum_{R_1} \tilde{\sigma}_{i,j} = \frac{n_2}{p_2}$. The final sum is

$$I_{1,2} \equiv \sum_{R_3} \tilde{\sigma}_{i,j} = \sum_{j=0}^{n_2-1} \sum_{i=0}^{n_1-1} \binom{i+j}{i,j} p_1^i p_2^j. \tag{6.14}$$

In Section 6.3, we demonstrate how to approximate $I_{1,2}$ using elementary functions through Laplace's method. We will show in Section 6.3, Lemma 3, that for $0 < p_1, p_2 < 1, p_1 + p_2 = 1$, when h is large,

- (1) $I_{1,2} \sim \frac{n_1}{p_1}$, as $n_2 \rightarrow \infty$ for n_1 fixed, and $n = n_1 + n_2 \rightarrow \infty$.
- (2) $I_{1,2} \sim \frac{n_2}{p_2}$, as $n_1 \rightarrow \infty$ for n_2 fixed, and $n = n_1 + n_2 \rightarrow \infty$.

Overall, when h is large and $n_2 \gg n_1$ or $n_1 \gg n_2$, we have

$$I_{1,2} = \sum_{j=0}^{n_2-1} \sum_{i=0}^{n_1-1} \binom{i+j}{i,j} p_1^i p_2^j \sim \min \left[\frac{n_1}{p_1}, \frac{n_2}{p_2} \right]. \tag{6.15}$$

Putting all the pieces together,

$$\lambda t(n_1, n_2; h) \sim I_1 + I_2 - I_{1,2} = \frac{n_1}{p_1} + \frac{n_2}{p_2} - \min \left[\frac{n_1}{p_1}, \frac{n_2}{p_2} \right] = \max \left[\frac{n_1}{p_1}, \frac{n_2}{p_2} \right]. \quad (6.16)$$

Equation (6.16) is our main result for the two-site case. The result essentially says that the mean recruiting time is determined by the site that has the longest expected recruiting time. Furthermore, the mean recruiting time cannot fall below h/λ , which is the lower bound for the mean recruiting time (see Figure 6.4), because

$$\begin{aligned} t(n_1, n_2; h) - \frac{h}{\lambda} &= \frac{1}{\lambda} \max \left[\frac{n_1}{p_1}, \frac{n_2}{p_2} \right] - \frac{n_1 + n_2}{\lambda}, \\ &= \begin{cases} \frac{1}{\lambda} \left[\frac{n_1}{p_1} - (n_1 + n_2) \right] = \frac{n_1 p_2 - p_1 n_2}{\lambda p_1}, & \text{if } \frac{n_1}{p_1} \geq \frac{n_2}{p_2}, \\ \frac{1}{\lambda} \left[\frac{n_2}{p_2} - (n_1 + n_2) \right] = \frac{n_2 p_1 - p_2 n_1}{\lambda p_2}, & \text{if } \frac{n_1}{p_1} < \frac{n_2}{p_2}, \end{cases} \\ &\geq 0. \end{aligned}$$

The minimum time h/λ is obtained when taking $n_1^* = p_1 n$, $n_2^* = p_2 n$, i.e. dividing up the total number of drugs according to the arrival probability. And we define $\mathbf{n}^* = [n_1^*, n_2^*]$ be the predicted optimal drug inventory, such that the mean recruiting time is the minimum.

6.2.2 The 3-site Case

Before we postulate our analytical method to a general m -site case, we will illustrate how to implement our analytical solution to a three-site problem.

Consider the case where $h = n_1 + n_2 + n_3$. From equation (6.2), we have

$$\lambda t(n_1, n_2, n_3; h = n_1 + n_2 + n_3) = \sum_{i=0}^{n_1} \sum_{j=0}^{n_2} \sum_{k=0}^{n_3} \sigma_{ijk}, \quad (6.17)$$

where

$$\sigma_{ijk} = \tilde{\sigma}_{ijk} = \frac{(i+j+k)!}{i!j!k!} p_1^i p_2^j p_3^k, \quad \text{if } (i, j, k) \in [0, n_1 - 1] \times [0, n_2 - 1] \times [0, n_3 - 1],$$

$$\begin{aligned} \sigma_{n_1, j, k} &= \sum_{i=n_1}^{\infty} \tilde{\sigma}_{ijk}, & \sigma_{i, n_2, k} &= \sum_{j=n_2}^{\infty} \tilde{\sigma}_{ijk}, & \sigma_{i, j, n_3} &= \sum_{k=n_3}^{\infty} \tilde{\sigma}_{ijk}, \\ \sigma_{n_1, n_2, k} &= \sum_{i=n_1}^{\infty} \sum_{j=n_2}^{\infty} \tilde{\sigma}_{ijk}, & \sigma_{n_1, j, n_3} &= \sum_{i=n_1}^{\infty} \sum_{k=n_3}^{\infty} \tilde{\sigma}_{ijk}, & \sigma_{i, n_2, n_3} &= \sum_{j=n_2}^{\infty} \sum_{k=n_3}^{\infty} \tilde{\sigma}_{ijk}, \end{aligned}$$

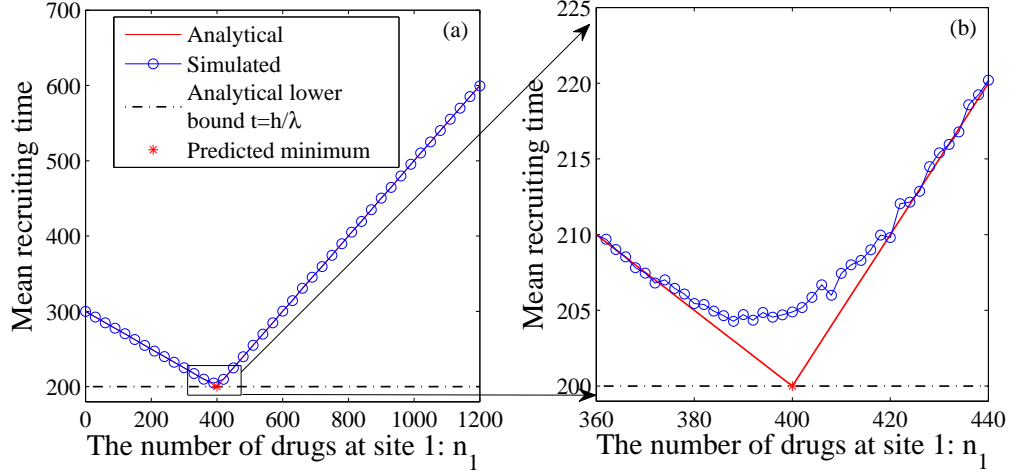


Figure 6.4: Comparison of simulated and analytical mean recruiting time. The total number of drugs $n = 1200$, the number of patients $h = n$, $\Lambda = [2, 4]$, the number of exit times used to generate the mean recruiting time is $K = 10^3$. (a, b) both show simulated and analytical mean recruiting time (equation (6.16)), but (b) zooms in (a), and shows the simulated and analytical mean recruiting time in the neighborhood of the predicted optimal drug inventory $\mathbf{n}^* = [n_1^*, n_2^*]$.

are the three dimensional analogues to equations (6.10) and (6.11). We break equation (6.17) up as follows:

$$\begin{aligned}
\lambda t(n_1, n_2, n_3; h) &= \sum_{i=0}^{n_1-1} \sum_{j=0}^{n_2-1} \sum_{k=0}^{n_3-1} \sigma_{ijk} \\
&+ \underbrace{\sum_{j=0}^{n_2-1} \sum_{k=0}^{n_3-1} \sigma_{n_1, jk} + \sum_{i=0}^{n_1-1} \sum_{k=0}^{n_3-1} \sigma_{i, n_2, k} + \sum_{i=0}^{n_1-1} \sum_{j=0}^{n_2-1} \sigma_{i, j, n_3}}_{\text{symmetric terms I}} \\
&+ \underbrace{\sum_{k=0}^{n_3-1} \sigma_{n_1, n_2, k} + \sum_{j=0}^{n_2-1} \sigma_{n_1, j, n_3} + \sum_{i=0}^{n_1-1} \sigma_{i, n_2, n_3}}_{\text{symmetric terms II}} \\
&+ \underbrace{\sigma_{n_1, n_2, n_3}}_{=0}. \tag{6.18}
\end{aligned}$$

Each of the three terms in “symmetric terms I” and “symmetric terms II” have identical mathematical structure but with indices permuted. We now calculate each of the terms in (6.18) through the following lemma.

Lemma 1. Let $0 < p_1, p_2, p_3 < 1$ be fixed probabilities so that $p_1 + p_2 + p_3 = 1$, $n = n_1 + n_2 + n_3$, define

$$I_{1,2,3} \equiv \sum_{i=0}^{n_1-1} \sum_{j=0}^{n_2-1} \sum_{k=0}^{n_3-1} \frac{(i+j+k)!}{i!j!k!} p_1^i p_2^j p_3^k.$$

Then we can have the asymptotic relations

1. $I_{1,2,3} \sim \frac{n_1}{p_1}$, as $n_2, n_3 \rightarrow \infty$ for n_1 fixed, and $n \rightarrow \infty$.
2. $I_{1,2,3} \sim \frac{n_2}{p_2}$, as $n_1, n_3 \rightarrow \infty$ for n_2 fixed, and $n \rightarrow \infty$.
3. $I_{1,2,3} \sim \frac{n_3}{p_3}$, as $n_1, n_2 \rightarrow \infty$ for n_3 fixed, and $n \rightarrow \infty$.

As a shorthand, we write

$$I_{1,2,3} \sim \min \left[\frac{n_1}{p_1}, \frac{n_2}{p_2}, \frac{n_3}{p_3} \right].$$

when h is large and for l such that $n_l \ll n_i$, $i \neq l$.

Proof. We show the proof by considering three cases: $1 \ll n_1 \ll n_2, n_3$, $1 \ll n_2 \ll n_1, n_3$, and $1 \ll n_3 \ll n_1, n_2$.

1. If $1 \ll n_1 \ll n_2, n_3$,

$$\begin{aligned} & \lim_{\substack{n_2 \rightarrow \infty \\ n_3 \rightarrow \infty}} \sum_{i=0}^{n_1-1} \sum_{j=0}^{n_2-1} \sum_{k=0}^{n_3-1} \frac{(i+j+k)!}{i!j!k!} p_1^i p_2^j p_3^k \\ &= \sum_{i=0}^{n_1-1} \sum_{j=0}^{\infty} \frac{(i+j)!}{i!j!} p_1^i p_2^j \sum_{k=0}^{\infty} \frac{(i+j+k)!}{(i+j)!k!} p_3^k, \end{aligned} \quad (6.19)$$

$$= \sum_{i=0}^{n_1-1} p_1^i (1-p_3)^{-(i+1)} \sum_{j=0}^{\infty} \frac{(i+j)!}{i!j!} p_2^j (1-p_3)^{-j}, \quad (6.20)$$

$$= \sum_{i=0}^{n_1-1} p_1^i (p_1 + p_2)^{-(i+1)} \left(1 - \frac{p_2}{p_1 + p_2} \right)^{-(i+1)},$$

$$= \sum_{i=0}^{n_1-1} p_1^i (p_1 + p_2)^{-(i+1)} \left(\frac{p_1}{p_1 + p_2} \right)^{-(i+1)},$$

$$= \frac{n_1}{p_1},$$

where we used equation (6.13) to simplify equations (6.19) - (6.20).

2. When $1 \ll n_2 \ll n_1, n_3$, and $n_3 \ll n_1, n_2$, using equation (6.13), we can have

$$\lim_{\substack{n_1 \rightarrow \infty \\ n_3 \rightarrow \infty}} \sum_{i=0}^{n_1-1} \sum_{j=0}^{n_2-1} \sum_{k=0}^{n_3-1} \frac{(i+j+k)!}{i!j!k!} p_1^i p_2^j p_3^k = \frac{n_2}{p_2}.$$

3. When $1 \ll n_3 \ll n_1, n_2$, using equation (6.13), we can have

$$\lim_{\substack{n_1 \rightarrow \infty \\ n_2 \rightarrow \infty}} \sum_{i=0}^{n_1-1} \sum_{j=0}^{n_2-1} \sum_{k=0}^{n_3-1} \frac{(i+j+k)!}{i!j!k!} p_1^i p_2^j p_3^k = \frac{n_3}{p_3}.$$

Finally, combining the above results, we have

$$\sum_{i=0}^{n_1-1} \sum_{j=0}^{n_2-1} \sum_{k=0}^{n_3-1} \frac{(i+j+k)!}{i!j!k!} p_1^i p_2^j p_3^k \sim \min \left[\frac{n_1}{p_2}, \frac{n_2}{p_2}, \frac{n_3}{p_3} \right].$$

□

Lemma 2. Let $0 < p_1, p_2, p_3 < 1$ be fixed probabilities so that $p_1 + p_2 + p_3 = 1$,

$n = n_1 + n_2 + n_3$, define

$$\begin{aligned} I_3 &\equiv \sum_{i=0}^{\infty} \sum_{j=0}^{\infty} \sum_{k=0}^{n_3-1} \frac{(i+j+k)!}{i!j!k!} p_1^i p_2^j p_3^k, & I_2 &\equiv \sum_{i=0}^{\infty} \sum_{j=0}^{n_2-1} \sum_{k=0}^{\infty} \frac{(i+j+k)!}{i!j!k!} p_1^i p_2^j p_3^k, \\ I_1 &\equiv \sum_{i=0}^{n_1-1} \sum_{j=0}^{\infty} \sum_{k=0}^{\infty} \frac{(i+j+k)!}{i!j!k!} p_1^i p_2^j p_3^k, & I_{23} &\equiv \sum_{i=0}^{\infty} \sum_{j=0}^{n_2-1} \sum_{k=0}^{n_3-1} \frac{(i+j+k)!}{i!j!k!} p_1^i p_2^j p_3^k, \\ I_{13} &\equiv \sum_{i=0}^{n_1-1} \sum_{j=0}^{\infty} \sum_{k=0}^{n_3-1} \frac{(i+j+k)!}{i!j!k!} p_1^i p_2^j p_3^k, & I_{12} &\equiv \sum_{i=0}^{n_1-1} \sum_{j=0}^{n_2-1} \sum_{k=0}^{\infty} \frac{(i+j+k)!}{i!j!k!} p_1^i p_2^j p_3^k. \end{aligned}$$

Then we can have the following results:

1. $I_3 \sim \frac{n_3}{p_3}$, $I_2 \sim \frac{n_2}{p_2}$, $I_1 \sim \frac{n_1}{p_1}$.
2. $I_{2,3} \sim \min \left[\frac{n_2}{p_2}, \frac{n_3}{p_3} \right]$, $I_{1,3} \sim \min \left[\frac{n_1}{p_1}, \frac{n_3}{p_3} \right]$, $I_{1,2} \sim \min \left[\frac{n_1}{p_1}, \frac{n_2}{p_2} \right]$.

Proof. We only show the proof for I_3 and $I_{2,3}$, other results can be proved similarly.

First of all, we used equation (6.13) twice to simplify I_3 :

$$\begin{aligned}
I_3 &\equiv \sum_{i=0}^{\infty} \sum_{j=0}^{\infty} \sum_{k=0}^{n_3-1} \frac{(i+j+k)!}{i!j!k!} p_1^i p_2^j p_3^k, \\
&= \sum_{k=0}^{n_3-1} \sum_{i=0}^{\infty} \frac{(i+k)!}{i!k!} p_1^i p_3^k \sum_{j=0}^{\infty} \frac{(i+j+k)!}{(i+k)!j!} p_2^j, \\
&= \sum_{k=0}^{n_3-1} p_3^k (1-p_2)^{-(k+1)} \sum_{i=0}^{\infty} \frac{(i+k)!}{i!k!} p_1^i (1-p_2)^{-i}, \\
&= \sum_{k=0}^{n_3-1} p_3^k (p_1+p_3)^{-(k+1)} \left(1 - \frac{p_1}{p_1+p_3}\right)^{-(k+1)}, \\
&= \sum_{k=0}^{n_3-1} p_3^k (p_1+p_3)^{-(k+1)} \left(\frac{p_3}{p_1+p_3}\right)^{-(k+1)}, \\
&= \frac{n_3}{p_3}.
\end{aligned}$$

$$\begin{aligned}
I_{2,3} &\equiv \sum_{i=0}^{\infty} \sum_{j=0}^{n_2-1} \sum_{k=0}^{n_3-1} \frac{(i+j+k)!}{i!j!k!} p_1^i p_2^j p_3^k, \\
&= \sum_{j=0}^{n_2-1} \sum_{k=0}^{n_3-1} p_2^j p_3^k \sum_{i=0}^{\infty} \frac{(i+j+k)!}{i!j!k!} p_1^i, \\
&= \sum_{j=0}^{n_2-1} \sum_{k=0}^{n_3-1} \frac{(j+k)!}{j!k!} \frac{p_2^j p_3^k}{(p_2+p_3)^{-(j+k+1)}}, \\
&\sim \frac{1}{p_2+p_3} \min \left[\frac{n_2}{p_2/(p_2+p_3)}, \frac{n_3}{p_3/(p_2+p_3)} \right], \\
&\sim \min \left[\frac{n_2}{p_2}, \frac{n_3}{p_3} \right].
\end{aligned} \tag{6.21}$$

where we utilize (6.15) to simplify (6.21). We can obtain I_1 , I_2 , $I_{1,2}$, $I_{1,3}$ similarly. \square

Then the first term in ‘‘symmetric terms I’’ and ‘‘symmetric terms II’’ can be rewritten as

$$\sum_{j=0}^{n_2-1} \sum_{k=0}^{n_3-1} \sigma_{n_1,jk} = \sum_{j=0}^{n_2-1} \sum_{k=0}^{n_3-1} \sum_{i=n_1}^{\infty} \tilde{\sigma}_{ijk} = \sum_{j=0}^{n_2-1} \sum_{k=0}^{n_3-1} \left(\sum_{i=0}^{\infty} - \sum_{i=0}^{n_1-1} \right) \tilde{\sigma}_{ijk} = I_{2,3} - I_{1,2,3}.$$

$$\begin{aligned}
\sum_{k=0}^{n_3-1} \sigma_{n_1, n_2, k} &= \sum_{k=0}^{n_3-1} \sum_{i=n_1}^{\infty} \sum_{j=n_2}^{\infty} \tilde{\sigma}_{ijk}, \\
&= \sum_{k=0}^{n_3-1} \left(\sum_{i=0}^{\infty} \sum_{j=0}^{\infty} - \sum_{i=0}^{n_1-1} \sum_{j=0}^{n_2-1} - \sum_{i=n_1}^{\infty} \sum_{j=0}^{n_2-1} - \sum_{i=0}^{n_1-1} \sum_{j=n_2}^{\infty} \right) \tilde{\sigma}_{ijk}, \\
&= \sum_{k=0}^{n_3-1} \left[\sum_{i=0}^{\infty} \sum_{j=0}^{\infty} - \sum_{i=0}^{n_1-1} \sum_{j=0}^{n_2-1} - \sum_{j=0}^{n_2-1} \left(\sum_{i=0}^{\infty} - \sum_{i=0}^{n_1-1} \right) \right. \\
&\quad \left. - \sum_{i=0}^{n_1-1} \left(\sum_{j=0}^{\infty} - \sum_{j=0}^{n_2-1} \right) \right] \frac{(i+j+k)!}{i!j!k!} p_1^i p_2^j p_3^k, \\
&= I_3 - I_{1,2,3} - (I_{2,3} - I_{1,2,3}) - (I_{1,3} - I_{1,2,3}), \\
&= I_3 - I_{1,3} - I_{2,3} + I_{1,2,3}.
\end{aligned}$$

We can obtain the other terms in “symmetric terms I” and “symmetric terms II” in a similar way. Then

$$\begin{aligned}
&\lambda t(n_1, n_2, n_3) \\
&= I_{1,2,3} + \underbrace{(I_{2,3} - I_{1,2,3}) + (I_{1,3} - I_{1,2,3}) + (I_{1,2} - I_{1,2,3})}_{\text{symmetric terms I}} \\
&\quad + \underbrace{(I_3 - I_{1,3} - I_{2,3} + I_{1,2,3}) + (I_2 - I_{1,2} - I_{2,3} + I_{1,2,3}) + (I_1 - I_{12} - I_{1,3} + I_{1,2,3})}_{\text{symmetric terms II}} \\
&= (I_1 + I_2 + I_3) - (I_{1,2} + I_{1,3} + I_{2,3}) + I_{1,2,3}, \\
&= \frac{n_1}{p_1} + \frac{n_2}{p_2} + \frac{n_3}{p_3} - \left(\min \left[\frac{n_1}{p_1}, \frac{n_3}{p_3} \right] + \min \left[\frac{n_2}{p_2}, \frac{n_3}{p_3} \right] + \min \left[\frac{n_1}{p_1}, \frac{n_2}{p_2} \right] \right) \\
&\quad + \min \left[\frac{n_1}{p_1}, \frac{n_2}{p_2}, \frac{n_3}{p_3} \right], \\
&= \max \left[\frac{n_1}{p_1}, \frac{n_2}{p_2}, \frac{n_3}{p_3} \right]. \\
&\Rightarrow t(n_1, n_2, n_3) = \frac{1}{\lambda} \max \left[\frac{n_1}{p_1}, \frac{n_2}{p_2}, \frac{n_3}{p_3} \right]. \tag{6.22}
\end{aligned}$$

6.2.3 The m -site Case

For general m -site case, we solve the master equation (6.1) for the probability flux $P(k_1, k_2, \dots, k_m, t)$, and calculate the mean exit time through (6.2), which involves m sums and is much more complicated than 2-site case. From the results of 2-site case

(see equation (6.16)) and 3-site case (see equation (6.22)), we postulate our results to general m -site case. For m -site problem with $h = n = \sum_{i=1}^m n_i$, $0 < p_i < 1$, $i = 1, 2, \dots, m$, and $\sum_{i=1}^m p_i = 1$, the mean recruiting time can be approximated as

$$\lambda t \left(n_1, n_2, \dots, n_m; h = \sum_{i=1}^m n_i \right) \sim \max_{1 \leq i \leq m} \left[\frac{n_i}{p_i} \right], \quad (6.23)$$

$$t \left(n_1, n_2, \dots, n_m; h = \sum_{i=1}^m n_i \right) \sim \max_{1 \leq i \leq m} \left[\frac{n_i}{\lambda_i} \right]. \quad (6.24)$$

We now provide an alternative interpretation of (6.24). At site i , the time between recruiting the $(q-1)^{st}$ and q^{th} patient follows an exponential distribution: $X_i^{(q)} \sim \exp(\lambda_i)$. The time taken for the i th site to recruit n_i patients therefore satisfies an Erlang distribution, a special case of the Gamma distribution:

$$T_i \equiv \sum_{q=1}^{n_i} X_i^{(q)} \sim \text{Erlang}(n_i, \lambda_i).$$

The mean of the Erlang distribution is $E[T_i] = n_i/\lambda_i$. The time taken to recruit $n = \sum_{i=1}^m n_i$ patients is identical to the time taken for the slowest site to recruit all its patients, i.e.

$$T(n_1, \dots, n_m) = \max(T_1, T_2, \dots, T_m), \quad (6.25)$$

and the mean recruitment time is

$$t = E[T(n_1, \dots, n_m)] = E[\max(T_1, T_2, \dots, T_m)]. \quad (6.26)$$

The order statistics of Erlang random variables has been studied in [99] but the calculations require counting individual trajectories of a random walk which can become extremely laborious in high dimensions. Equation (6.24) essentially interchanges max and expectation operation, replacing equation (6.26) with

$$\begin{aligned} t &\approx \max(E[T_1], E[T_2], \dots, E[T_m]), \\ &= \max \left[\frac{n_1}{\lambda_1}, \frac{n_2}{\lambda_2}, \dots, \frac{n_m}{\lambda_m} \right]. \end{aligned} \quad (6.27)$$

The approximation becomes more accurate whenever $n_j \gg n_1, n_2, \dots, n_{j-1}, n_{j+1}, \dots, n_m$. Equation (6.27) approximates the minimizer of (6.26) as

$$\mathbf{n}^* = [p_1 n, p_2 n, \dots, p_m n]. \quad (6.28)$$

By comparing against Monte-Carlo simulations, we find that the approximation (6.27) typically gives the optimal distribution (minimizer of (6.26)) to within a few percent of n .

6.3 Approximation Using Laplace's Method

Our aim is to approximate the sum $I_{1,2} = \sum_{j=0}^{n_2-1} \sum_{i=0}^{n_1-1} \binom{i+j}{i,j} p_1^i p_2^j$. We show how to calculate $I(n_1, n_2; p_1, p_2)$ in this section. Using the first term in its Euler-Maclaurin series, taking $\Delta X = \Delta Y = 1$, $X = i\Delta X$, $Y = j\Delta Y$, we have

$$\begin{aligned} I_{1,2} &= \Delta X \Delta Y \sum_{j=0}^{n_2-1} \sum_{i=0}^{n_1-1} \binom{i+j}{i,j} p_1^i p_2^j, \\ &\approx \int_0^{n_1} \int_0^{n_2} dX dY \frac{\Gamma(X+Y+1)}{\Gamma(X+1)\Gamma(Y+1)} \exp[X \ln p_1 + Y \ln p_2], \\ &\equiv \tilde{I}. \end{aligned}$$

Let $N_i = n_i/n$, $i = 1, 2$, $N_1 + N_2 = 1$, $X = nrN_1 \cos \theta$, $Y = nrN_2 \sin \theta$, we have

$$\tilde{I} = n^2 N_1 N_2 \int_0^{\pi/2} \int_0^{f(\theta)} e^{G(R,\theta)} r dr d\theta, \quad (6.29)$$

where $R = nr$,

$$\begin{aligned} G(R, \theta) &= R(N_1 \cos \theta \ln p_1 + N_2 \sin \theta \ln p_2) \\ &\quad + \ln \frac{\Gamma(1 + R(N_1 \cos \theta + N_2 \sin \theta))}{\Gamma(1 + RN_1 \cos \theta)\Gamma(1 + RN_2 \sin \theta)}, \end{aligned} \quad (6.30)$$

Typically in drug trials, n is large (typically many hundreds of patients need to be recruited), which motivates the use of Laplace's method. We prove

Lemma 3. *Let $0 < p_1, p_2 < 1$ be fixed probabilities so that $p_1 + p_2 = 1$. Then with \tilde{I} defined in (6.29), we have the asymptotic relations*

1. $I_{1,2} \sim \frac{n_1}{p_1}$, as $n_2 \rightarrow \infty$ for n_1 fixed, and $n = n_1 + n_2 \rightarrow \infty$.
2. $I_{1,2} \sim \frac{n_2}{p_2}$, as $n_1 \rightarrow \infty$ for n_2 fixed, and $n = n_1 + n_2 \rightarrow \infty$.

As a shorthand, we write

$$I_{1,2} \sim \min \left[\frac{n_1}{p_1}, \frac{n_2}{p_2} \right].$$

when h is large and $n_2 \gg n_1$ or $n_1 \gg n_2$.

Proof. First assume that the point near $r = 0$ does *not* give the dominant contribution to I ; we will show this later. So assume $r > 0$ and R is large and positive. Because $h \gg 1$, we can expand (6.30) through the Stirling series $\ln \Gamma(1+z) \sim z \ln z - z + \frac{1}{2} \ln z + \frac{1}{2} \ln 2\pi + O\left(\frac{1}{z}\right)$, when $z \gg 1$ so that

$$G(R, \theta) \sim \begin{cases} RG_0(\theta) + \ln \left[\frac{N_1 \cos \theta + N_2 \sin \theta}{N_1 N_2 \cos \theta \sin \theta} \frac{1}{R} \right]^{1/2} - \frac{1}{2} \ln 2\pi + O(|R|^{-1}), & 0 < \theta < \frac{\pi}{2}, \\ RN_1 \ln p_1, & \theta = 0, \\ RN_2 \ln p_2, & \theta = \pi/2. \end{cases}$$

where

$$\begin{aligned} G_0(\theta) &= N_1 \cos \theta \ln p_1 + N_2 \sin \theta \ln p_2 + (N_1 \cos \theta + N_2 \sin \theta) \ln(N_1 \cos \theta + N_2 \sin \theta) \\ &\quad - N_1 \cos \theta \ln(N_1 \cos \theta) - N_2 \sin \theta \ln(N_2 \sin \theta). \end{aligned}$$

Most of the mass of the integrand lies along a ray $\theta = \bar{\theta}$ such that $G'_0(\bar{\theta}) = 0$:

$$\begin{aligned} G'_0(\bar{\theta}) &= \cos \bar{\theta} \ln p_2 - \rho \sin \bar{\theta} \ln p_1 + (\cos \bar{\theta} - \rho \sin \bar{\theta}) \ln \left(\cos \bar{\theta} + \frac{\sin \bar{\theta}}{\rho} \right) \\ &\quad - \cos \bar{\theta} \ln \left(\frac{\sin \bar{\theta}}{\rho} \right) + \rho \sin \bar{\theta} \ln \cos \bar{\theta} = 0, \end{aligned}$$

and

$$\begin{aligned} G_0(\theta) &\approx \frac{G''_0(\bar{\theta})}{2} (\theta - \bar{\theta})^2 + O(\theta - \bar{\theta})^2, \\ G''_0(\bar{\theta}) &= -G_0(\bar{\theta}) - \left(\frac{N_2 \cos^2 \bar{\theta}}{\sin \bar{\theta}} + \frac{N_1 \sin^2 \bar{\theta}}{\cos \bar{\theta}} \right) + \frac{(N_2 \cos \bar{\theta} - N_1 \sin \bar{\theta})^2}{N_1 \cos \bar{\theta} + N_2 \sin \bar{\theta}}, \\ &= -\frac{N_1 N_2 \csc \bar{\theta} \sec \bar{\theta}}{N_1 \cos \bar{\theta} + N_2 \sin \bar{\theta}} < 0. \end{aligned}$$

Therefore

$$I_{1,2} \sim \frac{h^2 N_1 N_2}{\sqrt{2\pi h}} \int_0^{\pi/2} \int_0^{f(\theta)} \sqrt{r} e^{rhG_0(\theta)} \left(\frac{N_1 \cos \theta + N_2 \sin \theta}{N_1 N_2 \cos \theta \sin \theta} \right)^{1/2} dr d\theta.$$

where

$$f(\theta) = \begin{cases} (\sin \theta)^{-1}, & \pi/4 \leq \theta < \pi/2, \\ (\cos \theta)^{-1}, & 0 < \theta \leq \pi/4. \end{cases}$$

Therefore

$$\begin{aligned} I_{1,2} &\sim N_1 N_2 h^2 \times \frac{1}{\sqrt{2\pi h}} \left(\frac{N_1 \cos \bar{\theta} + N_2 \sin \bar{\theta}}{N_1 N_2 \cos \bar{\theta} \sin \bar{\theta}} \right)^{1/2} \int_0^{f(\bar{\theta})} dr \sqrt{r} \int_{-\infty}^{\infty} d\theta e^{\frac{hrG_0''(\bar{\theta})(\theta-\bar{\theta})^2}{2\delta}}, \\ &= N_1 N_2 h \times \frac{f(\bar{\theta})}{\sqrt{|G_0''(\bar{\theta})|}} \left(\frac{N_1 \cos \bar{\theta} + N_2 \sin \bar{\theta}}{N_1 N_2 \cos \bar{\theta} \sin \bar{\theta}} \right)^{1/2}, \\ &= f(\bar{\theta}) (n_1 \cos \bar{\theta} + n_2 \sin \bar{\theta}), \\ &= \begin{cases} n_1 + n_2 \tan \bar{\theta}, & 0 < \bar{\theta} \leq \pi/4, \\ n_1 \cot \bar{\theta} + n_2, & \pi/4 \leq \bar{\theta} < \pi/2, \end{cases} \end{aligned}$$

where $\bar{\theta} = \bar{\theta}(q)$ satisfies

$$\begin{aligned} &\cos \bar{\theta} \ln p_2 - q \sin \bar{\theta} \ln p_1 + (\cos \bar{\theta} - q \sin \bar{\theta}) \ln \left(\cos \bar{\theta} + \frac{\sin \bar{\theta}}{q} \right) \\ &- \cos \bar{\theta} \ln \left(\frac{\sin \bar{\theta}}{q} \right) + q \sin \bar{\theta} \ln \cos \bar{\theta} = 0, \end{aligned} \quad (6.31)$$

and $q = N_1/N_2 = n_1/n_2 = O(1)$. Substituting $\bar{\theta} = aq$ for some constant a and taking $q \rightarrow 0^+$ in (6.31), we find that $a = p_2/(1 - p_2)$. Note that q (and hence $\bar{\theta}$) is strictly positive because we take $n_1 > 0$ while $n_2 \rightarrow \infty$.

Therefore

$$\bar{\theta} \sim \frac{p_2 q}{1 - p_2} = \frac{p_2 q}{p_1}, \quad q \rightarrow 0^+.$$

Similarly, substituting $\bar{\theta} = \frac{\pi}{2} - \frac{b}{q}$ for some constant b in (6.31) and taking $q \rightarrow \infty$, we find that $b = p_1/(1 - p_1)$ or

$$\bar{\theta} \sim \frac{\pi}{2} - \frac{p_1}{q(1 - p_1)} = \frac{\pi}{2} - \frac{p_1}{qp_2}, \quad q \rightarrow \infty.$$

Note that from (6.3), $\bar{\theta}$ is strictly less than $\pi/2$. Therefore we have

$$I_{1,2} \sim \begin{cases} n_1 + n_2 \bar{\theta}, & \bar{\theta} \rightarrow 0^+, \\ n_1 \left(\frac{\pi}{2} - \bar{\theta} \right) + n_2, & \bar{\theta} \rightarrow \frac{\pi}{2}^-, \end{cases}$$

or

$$I_{1,2} \sim \begin{cases} n_1 + n_2 \left(\frac{p_2 q}{p_1} \right), & q \rightarrow 0^+, \\ n_1 \left(\frac{p_1}{q p_2} \right) + n_2, & q \rightarrow +\infty, \end{cases}$$

or

$$I_{1,2} \sim \begin{cases} \frac{n_1}{p_1}, & n_1 \ll n_2, \\ \frac{n_2}{p_2}, & n_1 \gg n_2. \end{cases} \quad (6.32)$$

Now let's study equation (6.29) near $r = 0$. Expanding equation (6.30) around $R = 0$, we find that

$$G(R, \theta) \sim R(N_1 \cos \theta \ln p_1 + N_2 \sin \theta \ln p_2) + O(R^2),$$

so that

$$I_{1,2} \sim h^2 N_1 N_2 \int_0^{\pi/2} d\theta \int_0^{f(\theta)} r dr \exp [hr(N_1 \cos \theta \ln p_1 + N_2 \sin \theta \ln p_2)].$$

Taking $\eta = hr$, we have

$$I_{1,2} \sim \int_0^{\pi/2} d\theta \int_0^\infty \eta d\eta \exp [\eta(N_1 \cos \theta \ln p_1 + N_2 \sin \theta \ln p_2)] = O(1),$$

whereas the contribution from $r > 0$ is $O(n_1, n_2)$ in equation (6.32). Therefore $r = 0$ does not contribute significantly to I . \square

Thus, when h is large, and $n_2 \gg n_1$ or $n_1 \gg n_2$,

$$I_{1,2} = \sum_{j=0}^{n_2} \sum_{i=0}^{n_1} \binom{i+j}{i, j} p_1^i p_2^j \sim \min \left[\frac{n_1}{p_1}, \frac{n_2}{p_2} \right].$$

6.4 Monte-Carlo Simulation

Suppose there are a total of N doses of drugs in the warehouse to be distributed to $m \geq 1$ testing centers, each with a supply of $n_i, 1 \leq i \leq m$ drugs. Let the total number of patients to be recruited be h . We develop simulation algorithm for general

case $1 \leq h \leq n$, but we will test analytical solutions for $h = n$. For each center i , the patients arrive with independent Poisson arrival rate $\lambda_i > 0$. The time between each pair of consecutive patients at center i has an exponential distribution with parameter λ_i and each of these inter-arrival times is assumed to be independent of the other inter-arrival times. We are interested in finding the mean time taken to recruit h patients $t(n_1, n_2, \dots, n_m; h)$.

We now show details of the Monte-Carlo method (Algorithm 8) used to simulate the process of recruiting h patients from m testing centers. This method is based on the inverse transform method [91, 100, 101], a widely used method for generating random variables from a cdf whose functional form is known. In the context of our problem, the cdf for generating inter-arrival times is

$$F(\theta) = \begin{cases} 1 - \exp(-\lambda\theta), & \text{if } \theta \geq 0, \\ 0, & \text{if } \theta < 0. \end{cases}$$

We notice that when the number of drugs in total equals the number of patients recruited, i.e. $h = n = \sum_{i=1}^m n_i$, the time taken to recruit n_i patients at the i^{th} testing center is just $T_i = \sum_{j=1}^{n_i} \theta_j^{(i)}$, $i = 1, 2, \dots, m$ (see equation (6.34)). Therefore, the time taken to recruit h patients is identical to the time taken for the site with the slowest rate to recruit all its patients, i.e. equation (6.25), and the mean recruiting time is obtained from equation (6.26).

6.5 Results and Discussion

In this section, we want to test our analytic approximation, equation (6.24), and the optimal drug distribution, equation (6.28) by comparing the results with those obtained from Monte-Carlo simulation. Now let

- $\Lambda = [\lambda_1, \lambda_2, \dots, \lambda_m]$ be patient arrival rates for m testing centers,
- $\mathbf{n} = [n_1, n_2, \dots, n_m] \in \Omega_0$, where $\Omega_0 = \{[n_1, n_2, \dots, n_m] : \sum_{i=1}^m n_i = n, 0 \leq n_i \leq n\}$,
- $t(\mathbf{n}; h)$ be the predicted mean recruiting time calculated from (6.24), given drug distribution \mathbf{n} ,

Algorithm 8 Generating mean recruiting times

- 1: Require: the number of testing centers m , parameters λ_i , the number of drugs in each center n_i , where $i = 1, 2, \dots, m$, the number of realizations K .
- 2: **for** $j = 1 : K$ **do**
- 3: **for** $i = 1 : m$ **do**
- 4: **for** $k = 1 : n_i$ **do**
- 5: Generate inter-arrival time $\theta_k^{(i)} \sim \exp(\lambda_i)$, which is the time between k^{th} and $(k - 1)^{th}$ patient arrivals at center i , :

$$\begin{aligned} u_k^{(i)} &= U(0, 1), \\ \theta_k^{(i)} &= -\ln(u_k^{(i)})/\lambda_i, \end{aligned} \tag{6.33}$$

where equation (6.33) generates a uniformly distributed random number.

- 6: Calculate the k^{th} patient's arrival time $t_k^{(i)}$ at center i :

$$t_k^{(i)} = \sum_{j=1}^k \theta_j^{(i)}. \tag{6.34}$$

- 7: **end for**
 - 8: **end for**
 - 9: Sort all the n arrival times $t_k^{(i)}$ from m centers in ascending order, the h^{th} one is the time taken to recruit h patients from m testing centers, denoted as τ_j .
 - 10: **end for**
 - 11: The mean recruiting time $t = \frac{1}{K} \sum_{i=1}^K \tau_i$.
-

- $t_{sim}(\mathbf{n}; h)$ be the simulated mean recruiting time obtained from Monte-Carlo simulation (Algorithm 8), given drug distribution \mathbf{n} ,
- K be the number of simulations run to calculate $t_{sim}(\mathbf{n}; h)$,
- $\mathbf{n}^* = [n_1^*, n_2^*, \dots, n_m^*]$, where $n_i^* = p_i n$, be the the predicted optimal drug distribution and let $t^* \equiv t(\mathbf{n}^*; h)$,
- $\mathbf{n}_{sim}^* = [N_1^*, N_2^*, \dots, N_m^*]$ be the simulated optimal drug distribution, such that $t_{sim}^* \equiv t_{sim}(\mathbf{n}_{sim}^*; h) = \min_{\mathbf{n} \in \Omega_g \text{ or } \Omega_l} t_{sim}(\mathbf{n}; h)$, where $\Omega_g, \Omega_l \in \Omega_0$, are domains for Global Search and Local Search which are defined in Algorithm 9 and Algorithm 10.

To test the analytical approximation, equation (6.24), we can compare $t(\mathbf{n}; h)$ with $t_{sim}(\mathbf{n}; h)$, for any $\mathbf{n} \in \Omega_g$ or Ω_l . Here, we choose the pair: $t(\mathbf{n}^*; h)$ and $t_{sim}(\mathbf{n}^*; h)$. We define the relative percentage error ε_t for predicted recruiting time

$$\varepsilon_t = \frac{|t(\mathbf{n}^*; h) - t_{sim}(\mathbf{n}^*; h)|}{t_{sim}(\mathbf{n}^*; h)} \times 100.$$

Notice that because of the randomness in stochastic simulation, the accuracy of $t_{sim}(\mathbf{n}; h)$ depends on the number of simulations K . To estimate the accuracy of $t_{sim}(\mathbf{n}; h)$, we generate K simulated recruiting times $\tau_1, \tau_2, \dots, \tau_K$, and calculate the variance σ^2 . From the Central Limit Theorem, we know that the mean recruiting time is normal distributed with standard deviation $\tilde{\sigma} = \sigma/\sqrt{K}$, which roughly gives the accuracy of $t_{sim}(\mathbf{n}; h)$. When $K \leq 5,000$, $\tilde{\sigma} = O(10^{-1})$; when $5,000 < K < 10^6$, $\tilde{\sigma} = O(10^{-2})$; when $K \geq 10^6$, $\tilde{\sigma} = O(10^{-3})$.

Table 6.1, where we take $K = 1000$ to obtain simulation results, show the comparison results of $t_{sim}(\mathbf{n}^*; h)$ and $t(\mathbf{n}^*; h)$ for $m = 3, 4, 5$. $t_{sim}(\mathbf{n}^*; h)$ is correct to $O(1)$ and the relative errors are always within 10%.

To test the optimal drug distribution, equation (6.28), we compare \mathbf{n}^* with \mathbf{n}_{sim}^* , and define the relative percentage error ε_n for optimal drug distribution prediction in the Euclidean norm

$$\varepsilon_n = \frac{\|\mathbf{n}^* - \mathbf{n}_{sim}^*\|_2}{\|\mathbf{n}_{sim}^*\|_2} \times 100.$$

Table 6.1: Compare $t(\mathbf{n}^*; h)$ and $t_{sim}(\mathbf{n}^*; h)$ for different number of sites

	Λ	n	\mathbf{n}^*	$t(\mathbf{n}^*; h)$	$t_{sim}(\mathbf{n}^*; h)$	$\varepsilon_t(\%)$
3-site	[3, 4, 7]	800	[172, 229, 399]	57.25	60	4.6
	[8, 6, 4]	900	[400, 300, 200]	50.00	52	3.9
	[4, 4.1, 4.2]	1100	[358, 367, 375]	89.51	94	4.8
4-site	[10, 8, 6, 3]	1000	[371, 297, 223, 109]	37.17	40	7.1
	[15, 5, 3, 2]	1200	[720, 240, 144, 96]	48.00	52	7.7
	[6, 5, 3, 3]	1000	[353, 295, 177, 175]	59.00	63	6.8
5-site	[1, 2, 3, 4, 5]	800	[54, 107, 160, 214, 265]	54.00	59	8.5
	[2, 4, 6, 8, 10]	1200	[80, 160, 240, 320, 400]	40.00	43	7.0
	[1, 3, 5, 7, 9]	800	[32, 96, 160, 225, 287]	32.14	35	8.2

We develop two algorithms: Global Search (Algorithm 9) and Local Search (Algorithm 10), to calculate \mathbf{n}_{sim}^* .

In Table 6.2, we show the Global Search and Local Search results \mathbf{n}_{sim}^* for $m = 3, 4, 5$, when $n = h$. For Global Search, we take the number of points M in Ω_g be equal to 50,000. For Local Search, we take the number of simulation repeated for recruiting time calculation $K = 1000$, the $m - 1$ dimensional ball $\mathcal{B}(\mathbf{n}^*, R)$ centered at $\mathbf{n}^* = [n_1^*, n_2^*, \dots, n_{m-1}^*]$ with radius $R = 25$. We also see that the relative error of \mathbf{n}^* through Global Search and Local Search are all within 6%. Notice that when $m > 5$, $\mathcal{B}(\mathbf{n}^*, R)$ contains $(2R + 1)^{m-1}$ ($\geq 51^5$) grid points. It takes a tremendous amount of time to complete the simulation using Local Search. As m increases, the dimension of \mathbf{n} increases, the sample size $M = 50,000$ for \mathbf{n} is not large enough to search globally, or provide a reliable result. The simulation time rapidly increases if M increases. Hence, we only give results for $m \leq 5$.

For the Local Search of the three-site problem, we are able to display the results of Table 6.1 and Table 6.2 in Figure 6.5, where we extend the search radius R to 100. In (a, d, g), we show the contour plot for t_{sim} in the region of $\mathcal{B}(\mathbf{n}^*, R)$. In (b, e, h), we show the contour plot for t in the region of $\mathcal{B}(\mathbf{n}^*, R)$. The contours in (a, d, g) and (b, e, h) are almost the same, except that (a, d, g) have smooth corners, while (b, e,

Algorithm 9 Global Search for optimal drug distribution

- 1: Require: m , the number of testing centers; λ_i , $i = 1, 2, \dots, m$, patient arrival rates; K , the number of realizations; $\Omega_0 = \{[n_1, n_2, \dots, n_m] : \sum_{i=1}^m n_i = n, 0 \leq n_i \leq n\}$, M , the number of points randomly drawn from Ω_0 .
- 2: Randomly draw M points: $\mathbf{n}^{(j)} = [n_1^{(j)}, n_2^{(j)}, \dots, n_m^{(j)}]$, $j = 1, 2, \dots, M$, from Ω_0 . These M points form the Global Search Region Ω_g :

$$\Omega_g = \left\{ [n_1^{(j)}, n_2^{(j)}, \dots, n_m^{(j)}] : \sum_{i=1}^m n_i^{(j)} = n, 0 \leq n_i^{(j)} \leq n, j = 1, 2, \dots, M \right\},$$

- and are randomly and uniformly generated using the MATLAB code *randfixedsum.m* written by Roger Stanford [102].
- 3: Calculate the simulated recruiting time $t_{sim}(\mathbf{n}^{(j)}; h)$, for $j = 1, 2, \dots, M$. See Algorithm 8.
 - 4: Take the minimum of the M simulated recruiting times calculated in step 3, the corresponding $\mathbf{n}^{(j)}$ is the optimal drug distribution $\mathbf{n}_{sim}^* = [N_1^*, N_2^*, \dots, N_m^*]$. In other words, \mathbf{n}_{sim}^* satisfies

$$t_{sim}(\mathbf{n}_{sim}^*; h) = \min_{\mathbf{n} \in \Omega_g} t_{sim}(\mathbf{n}; h).$$

Algorithm 10 Local Search

- 1: Require: m , the number of testing center; λ_i , $i = 1, 2, \dots, m$, patient arrival rates; K , the number of realizations;
- 2: Let $\mathcal{B}(\mathbf{n}^*, R) = \{[n_1, n_2, \dots, n_{m-1}] : [n_1^* - R, n_1^* + R] \times [n_2^* - R, n_2^* + R] \times \dots \times [n_{m-1}^* - R, n_{m-1}^*]\}$ be a $m - 1$ dimensional ball centered at $\mathbf{n}^* = [n_1^*, n_2^*, \dots, n_{m-1}^*]$ with radius R , the Local Search region:

$$\Omega_l = \left\{ [n_1, n_2, \dots, n_m] : [n_1, n_2, \dots, n_{m-1}] \in \mathcal{B}(\mathbf{n}^*, R), \text{ and } n_m = n - \sum_{j=1}^{m-1} n_j \right\}.$$

- 3: Calculate the simulated recruiting time $t_{sim}(\mathbf{n})$, for any $\mathbf{n} \in \Omega_l$. See Algorithm 8.
- 4: Take the minimum of all the simulated recruiting times calculated in step 3, the corresponded \mathbf{n} is the optimal drug distribution $\mathbf{n}_{sim}^* = [N_1^*, N_2^*, \dots, N_m^*]$. In other words,

$$t_{sim}^* = t_{sim}(\mathbf{n}_{sim}^*; h) = \min_{\mathbf{n} \in \Omega_l} t_{sim}(\mathbf{n}; h).$$

Table 6.2: Global and local search results for different number of sites.

	Λ	n	\mathbf{n}^*	$\mathbf{n}_{\text{sim}}^*$	$\varepsilon_n(\%)$
3-site					
Global	[3, 4, 7]	800	[172, 229, 399]	[166, 228, 406]	2.16
	[8, 6, 4]	900	[400, 300, 200]	[408, 299, 193]	1.97
	[4, 4.1, 4.2]	1100	[358, 367, 375]	[356, 364, 380]	0.97
Local	[3, 4, 7]	800	[172, 229, 399]	[161, 229, 410]	3.13
	[8, 6, 4]	900	[400, 300, 200]	[403, 301, 196]	0.94
	[4, 4.1, 4.2]	1100	[358, 367, 375]	[359, 364, 377]	0.59
4-site					
Global	[10, 8, 6, 3]	1000	[371, 297, 223, 109]	[385, 290, 220, 105]	3.04
	[15, 5, 3, 2]	1200	[720, 240, 144, 96]	[748, 224, 138, 90]	4.18
	[6, 5, 3, 3]	1000	[353, 295, 177, 175]	[362, 291, 173, 174]	2.03
Local	[10, 8, 6, 3]	1000	[371, 297, 223, 109]	[382, 297, 219, 102]	2.52
	[15, 5, 3, 2]	1200	[720, 240, 144, 96]	[740, 238, 136, 86]	3.00
	[6, 5, 3, 3]	1000	[353, 295, 177, 175]	[361, 297, 170, 172]	2.13
5-site					
Global	[1, 2, 3, 4, 5]	800	[54, 107, 160, 214, 265]	[51, 106, 164, 222, 257]	3.14
	[2, 4, 6, 8, 10]	1200	[80, 160, 240, 320, 400]	[76, 159, 246, 332, 387]	3.23
	[1, 3, 5, 7, 9]	800	[32, 96, 160, 225, 287]	[30, 86, 148, 240, 296]	5.62
Local	[1, 2, 3, 4, 5]	800	[54, 107, 160, 214, 265]	[48, 101, 162, 216, 273]	3.00
	[2, 4, 6, 8, 10]	1200	[80, 160, 240, 320, 400]	[92, 156, 227, 323, 402]	3.12
	[1, 3, 5, 7, 9]	800	[32, 96, 160, 225, 287]	[25, 91, 160, 229, 295]	2.98

h) have sharp corners. They are the 3-dimensional generalizations of Figure 6.4. In (c, f, i), we can see that the largest difference between the predicted and simulated mean recruiting time occurs at \mathbf{n}^* . In 3-dimensional space, $t(n_1, n_2, n - n_1 - n_2; h)$ is a paraboloid near \mathbf{n}^* ; (a, d, g) show the level of the curves. We can also see that the predicted and simulated optimal drug distributions \mathbf{n}^* and $\mathbf{n}_{\text{sim}}^*$ are very close to each other.

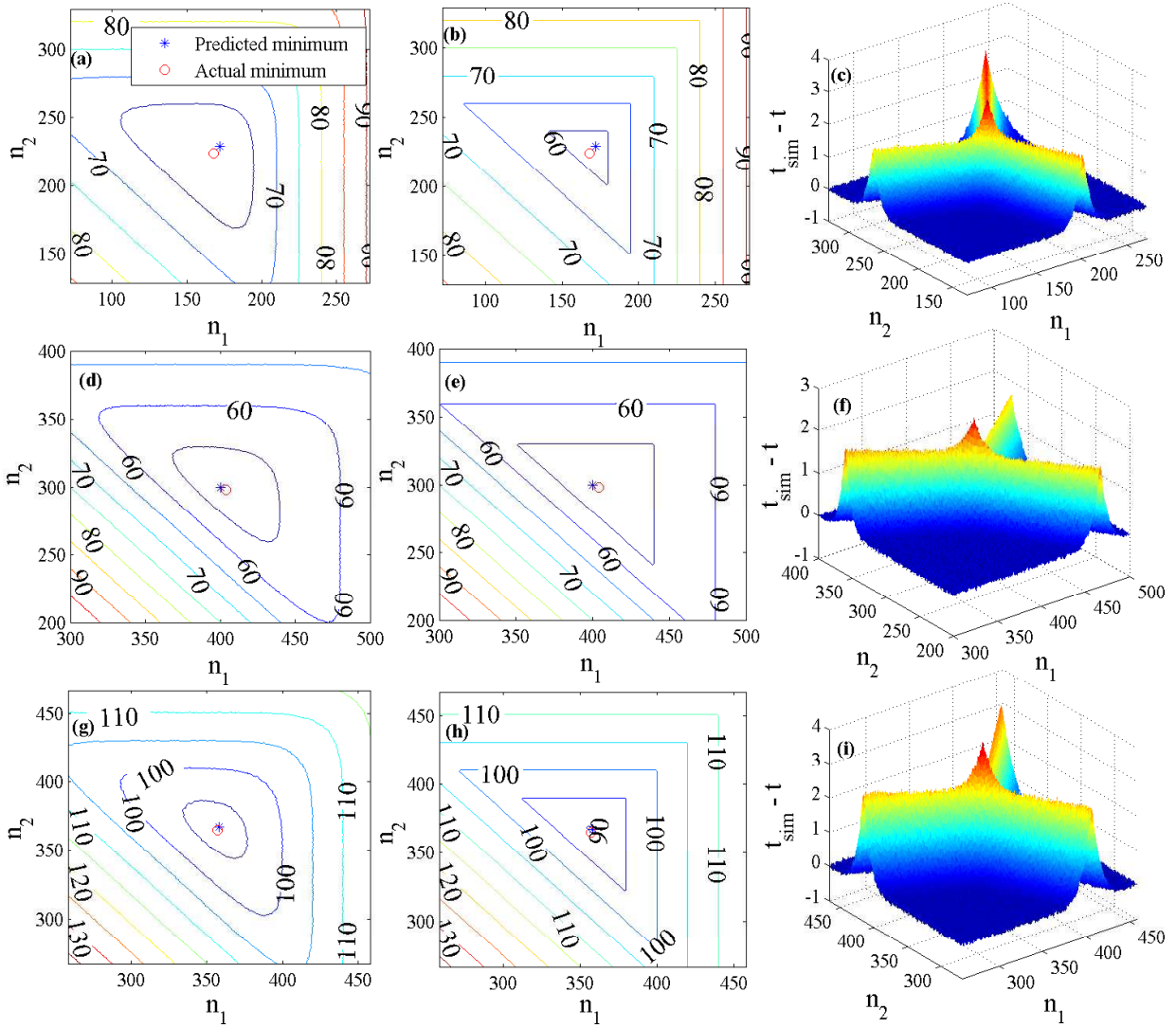


Figure 6.5: Contour plots for t_{sim} , t and surface plot for $t_{sim} - t$. (a, b, c) $n = 800$, $\Lambda = [3, 4, 7]$, $R = 100$, $\mathbf{n}^* = [172, 229, 399]$, $\mathbf{n}_{sim}^* = [168, 224, 408]$. (d, e, f) $n = 900$, $\Lambda = [8, 6, 4]$, $R = 100$, $\mathbf{n}^* = [400, 300, 200]$, $\mathbf{n}_{sim}^* = [404, 298, 198]$. (g, h, i) $n = 1100$, $\Lambda = [4, 4.1, 4.2]$, $R = 100$, $\mathbf{n}^* = [358, 367, 375]$, $\mathbf{n}_{sim}^* = [356, 364, 380]$.

6.6 Conclusions and Future Work

In this chapter, we make two contributions. First, we model clinical trial recruitment as a random walk and use the theory of exit times of a random walk to

describe the clinical trial recruitment process and its completion time when the number of drugs available in total is equal to the number of patients needed. Secondly, we utilize Laplace’s method to approximate the clinical trial’s mean recruiting time, and use two algorithms (Global Search Algorithm 9 and Local Search Algorithm 10) to find the optimal drug distribution such that the mean recruiting time is minimized. By comparing analytical and Monte-Carlo simulations, which calculate the mean recruiting time from $K = 1000$ realizations, we find that when the number of testing centers $m \leq 5$, equation (6.24) typically gives a good estimate, with relative error less than 10%, and equation (6.28) typically gives the optimal distribution (minimizer of (6.26)) to within 6% of relative error. We are also able to display the analytical solution (equation (6.24)) and simulated solution for the 3-site problem through contour plots. The contour plots for both solutions are similar except that the contours in the analytical solution have sharp corners, while the contours in the simulated solution are smooth. We also find that the maximum deviation between the analytical and simulated solutions occurs at the predicted optimal drug distribution \mathbf{n}^* , see Figure 6.5 (c, f, i). Our analytical solution also has an intuitive explanation in reality. The mean recruiting time is actually equal to the time taken for the test center with slowest rate to complete recruitment. The shortest mean recruiting time occurs when the drugs are distributed according to patient arrival probability, so that the centers are able to complete at the same time.

Our study has a couple of limitations. First of all, the approximated solution of mean recruiting time is valid only when h is large and there exists an n_k such that $n_k \ll n_j$, for all $j \neq k$. Secondly, because it takes a long time to find the optimal drug distribution through simulation and local search, we are only able to verify our analytical solution for up to five test centers. Thirdly, we only consider the case when the number of drugs is equal to the number of patients. But in practice, supply managers keep a number of drugs larger than h at testing centers to shorten the recruiting time.

In the future, we would consider iteratively conducting Local Search (Algorithm 10) by reducing the radius R and increasing the number of realizations K in simulation for each iteration. We will also extend our work to the case when the total number of drugs provided by the pharmaceutical company is strictly larger than the target number of patients, which is more practical in clinical trials.

BIBLIOGRAPHY

- [1] S. D. Servetto and G. Barrenechea. Constrained random walks on random graphs: routing algorithms for large scale wireless sensor networks, 2002.
- [2] R. C. Shah, S. Roy, S. Jain, and W. Brunette. Data mules: Modeling and analysis of a three-tier architecture for sparse sensor networks. *Ad Hoc Networks*, 1(2):215–233, 2003.
- [3] E. F. Fama. The behavior of stock-market prices. *The journal of Business*, 38(1):34–105, 1965.
- [4] E. F. Fama. Random walks in stock market prices. *Financial Analysts Journal*, 51(1):75–80, 1995.
- [5] F. Bartumeus, M. G. E. Da Luz, G. M. Viswanathan, and J. Catalan. Animal search strategies: A quantitative random-walk analysis. *Ecology*, 86(11):3078–3087, 2005.
- [6] P. Bovet and S. Benhamou. Spatial analysis of animals’ movements using a correlated random walk model. *Journal of theoretical biology*, 131(4):419–433, 1988.
- [7] S. Redner. *A Guide to First-Passage Processes*. Cambridge University Press, 2001.
- [8] A. N. Burkitt. A review of the integrate-and-fire neuron model: I. homogeneous synaptic input. *Biological Cybernetics*, 95(1):1–19, 2006.
- [9] W. Gerstner and W. M. Kistler. *Spiking neuron models: Single neurons, populations, plasticity*. Cambridge University Press, 2002.
- [10] H. C. Tuckwell. *Stochastic processes in the neurosciences*. SIAM, 1989.
- [11] H. C. Tuckwell, R. Rodriguez, and F. Y. M. Wan. Determination of firing times for the stochastic fitzhugh-nagumo neuronal model. *Neural Computation*, 15(1):143–159, 2003.
- [12] J. Dshalalow. On exit times of multivariate random walk with some applications to finance. *Nonlinear Analysis: Theory, Methods and Applications*, 63(5):e569–e577, 2005.

- [13] P.-W. Fok and T. Chou. Reconstruction of potential energy profiles from multiple rupture time distributions. *Proceedings of the Royal Society A: Mathematical, Physical and Engineering Sciences*, 466(2124):3479–3499, 2010.
- [14] P.-W. Fok, Q. Han, and T. Chou. Reconstruction of a persistent random walk from exit time distributions. *IMA Journal of Applied Mathematics*, 2013.
- [15] V. Rajani, G. Carrero, D. E. Golan, G. De Vries, and C. W. Cairo. Analysis of molecular diffusion by first-passage time variance identifies the size of confinement zones. *Biophysical journal*, 100(6):1463–1472, 2011.
- [16] O. K. Dudko. Single-molecule mechanics: New insights from the escape-over-a-barrier problem. *Proceedings of the National Academy of Sciences of the United States of America*, 106(22):8795–6, 2009.
- [17] L. B. Freund. Characterizing the resistance generated by a molecular bond as it is forcibly separated. *Proceedings of the National Academy of Sciences of the United States of America*, 106(22):8818–23, 2009.
- [18] G. Hummer and A. Szabo. Kinetics from nonequilibrium single-molecule pulling experiments. *Biophysical journal*, 85(1):5–15, 2003.
- [19] M. Schlierf and M. Rief. Single-molecule unfolding force distributions reveal a funnel-shaped energy landscape. *Biophysical journal*, 90(4):L33–L35, 2006.
- [20] S. R. Arridge. Optical tomography in medical imaging. *Inverse Problems*, 41:41–93, 1999.
- [21] S. R. Arridge and J. C. Hebden. Optical imaging in medicine: Ii. modelling and reconstruction. *Physics in medicine and biology*, 42(5):841–53, 1997.
- [22] G. Bal and T. Chou. On the reconstruction of diffusions from first-exit time distributions. *Inverse Problems*, 20:1053–1065, 2003.
- [23] J. E. Broadwell. Shock structure in a simple discrete velocity gas. *Physics of Fluids*, 7:1243, 1964.
- [24] J. E. Broadwell. Study of rarefied shear flow by the discrete velocity method. *Journal of Fluid Mechanics*, 19(03):401–414, 1964.
- [25] A. J. Christlieb, J. A. Rossmanith, and P. Smereka. The broadwell model in a thin channel. *Communications in Mathematical Sciences*, 2(3):443–476, 2004.
- [26] T. Nishida and M. Mimura. On the broadwell’s model for a simple discrete velocity gas. *Proceedings of the Japan Academy, Series A, Mathematical Sciences*, 50(10):812–817, 1974.

- [27] C. Xue and H. G. Othmer. Multiscale models of taxis-driven patterning in bacterial populations. *SIAM Journal on Applied Mathematics*, 70(1):133–167, 2009.
- [28] D. J. Bicout. Green’s functions and first passage time distributions for dynamic instability of microtubules. *Physical Review E*, 56, 1997.
- [29] P.-W. Fok, C.-L. Guo, and T. Chou. Charge-transport mediated recruitment of dna repair enzymes. *Journal of Chemical Physics*, 129:235101, 2008.
- [30] P. Degond and S. Motsch. Continuum limit of self-driven particles with orientation interaction. *Mathematical Models and Methods in Applied Sciences*, 18(supp01):1193–1215, 2008.
- [31] S. Goldstein. On diffusion by discontinuous movements and on the telegraph equation. *Quarterly journal of mechanics and applied mathematics*, 4:129–156, 1951.
- [32] J. Masoliver and G. H. Weiss. Telegrapher’s equations with variable propagation speeds. *Physical Review E*, 49:3852–3854, 1994.
- [33] J. F. Claerbout. Fundamentals of geophysical data processing. *Geophysical Journal of the Royal Astronomical Society*, 86(1), 1986.
- [34] R. W. Clayton. Common midpoint migration. In *SEP-14: Stanford Exploration Project*, pages 21–36, 1978.
- [35] C. C. Stolk and M. V. De Hoop. Modeling of seismic data in the downward continuation approach. *SIAM journal on applied mathematics*, 65(4), 2005.
- [36] K. P. Bube and R. Burridge. The one-dimensional inverse problem of reflection seismology. *SIAM Review*, 25(4):497–559, 1983.
- [37] M. M. Sondhi and J. R. Resnick. The inverse problem for the vocal tract: numerical methods, acoustical experiments, and speech synthesis. *The Journal of the Acoustical Society of America*, 73(3):985–1002, 1983.
- [38] A. M. Bruckstein and T. Kailath. Inverse scattering for discrete transmission-line models. *SIAM Review*, 29(3), 1987.
- [39] F. Santosa and H. Schwetlick. The inversion of acoustical impedance profile by methods of characteristics. *Wave Motion*, 4(1):99–110, 1982.
- [40] M. G. Krein. On a method for the effective solution of the inverse boundary value problem. *Doklady Akademii Nauk Sssr*, 94(6):987–990, 1954.
- [41] B. Gopinath and M. M. Sondhi. Determination of the shape of the human vocal tract from acoustical measurements. *Bell System Technical Journal*, 49:1195–1214, 1970.

- [42] B. Gopinath and M. M. Sondhi. Inversion of the telegraph equation and the synthesis of nonuniform lines. *Proceedings of the IEEE*, 59(3):383–392, 1971.
- [43] R. Burridge. The gelfand-levitan, the marchenko, and the gopinath-sondhi integral equations of inverse scattering theory, regarded in the context of inverse impulse-response problems. *Wave Motion*, 2(4):305–323, 1980.
- [44] I. M. Gelfand and B. M. Levitan. *On the Determination of a Differential Equation from Its Spectral Function*. American Mathematical Society, 1955.
- [45] Z. S. Agranovich, V. A. Marchenko, and B. D. Seckler. *The inverse problem of scattering theory*. Gordon and Breach, New York, 1964.
- [46] T. Kailath, B. Levy, L. Ljung, and M. Morf. The factorization and representation of operators in the algebra generated by toeplitz operators. *SIAM Journal on Applied Mathematics*, pages 467–484, 1979.
- [47] J. Rissanen. Algorithms for triangular decomposition of block hankel and toeplitz matrices with application to factoring positive matrix polynomials. *Mathematics of computation*, 27(121):147–154, 1973.
- [48] M. T. Giraud and L. Sacerdote. An improved technique for the simulation of first passage times for diffusion processes. *Communications in Statistics - Simulation and Computation*, 28:1135–1163, 1999.
- [49] M. T. Giraud, L. Sacerdote, and C. Zucca. A monte carlo method for the simulation of first passage times of diffusion processes. *Methodology and computing in applied probability*, 3:215–231, 2001.
- [50] R. Mannella and V. Palleschi. Fast and precise algorithm for computer simulation of stochastic differential equations. *Physical Review A*, 40, 1989.
- [51] T. Taillefumier and M. O. Magnasco. A fast algorithm for the first-passage times of gauss-markov processes with holder continuous boundaries. *Journal Statistical Physics*, 140:1–27, 2010.
- [52] M. L. Lanthier, R. Sridhara, J. R. Johnson, A. Farrell, P. Keegan, R. Justice, and R. Pazdur. Accelerated approval and oncology drug development timelines. *Journal of Clinical Oncology*, 28(14):e226–e227, 2010.
- [53] F. A. Thiers, A. J. Sinskey, and E. R. Berndt. Trends in the globalization of clinical trials. *Nature Reviews Drug Discovery*, 7(1):13–14, 2008.
- [54] S. W. Glickman, J. G. Mchutchison, E. D. Peterson, C. B. Cairns, R. A. Harrington, R. M. Califf, and K. A. Schulman. Ethical and scientific implications of the globalization of clinical research. *New England Journal of Medicine*, 360(8):816–823, 2009.

- [55] M. Powell. Bristol-myers squibb's evolution from a big pharma company to a mid size biopharma company, 2010.
- [56] P. Vallance. Bristol-myers squibb's evolution from a big pharma company to a mid size biopharma company, 2011.
- [57] M. K. Campbell, C. Snowdon, D. Francis, D. Elbourne, A. M. Mcdonald, R. Knight, V. Entwistle, J. Garcia, I. Roberts, A. Grant, A. Grant, and Steps Group. Recruitment to randomised trials: strategies for trial enrollment and participation study. the steps study. *Health technology assessment*, 11(48), 2007.
- [58] K. A. Getz and A. De Bruin. Breaking the development speed barrier: Assessing successful practices of the fastest drug development companies. *Drug information journal*, 34(3):725–736, 2000.
- [59] R. E. Carter, S. C. Sonne, and K. T. Brady. Practical considerations for estimating clinical trial accrual periods: application to a multi-center effectiveness study. *BMC medical research methodology*, 5:11, 2005.
- [60] M. A. Moussa. Planning a clinical trial with allowance for cost and patient recruitment rate. *Computer programs in biomedicine*, 18(3):173–179, 1984.
- [61] V. V. Anisimov. Using mixed poisson models in patient recruitment in multicentre clinical trials, 2008.
- [62] V. V. Anisimov and V. V. Fedorov. Modelling, prediction and adaptive adjustment of recruitment in multicentre trials. *Statistics in medicine*, 26(27):4958–4975, 2007.
- [63] R. E. Carter. Application of stochastic processes to participant recruitment in clinical trials. *Controlled Clinical Trials Controlled Clinical Trials*, 25(5):429–436, 2004.
- [64] W. O. Williford, S. F. Bingham, D. G. Weiss, J. F. Collins, K. T. Rains, and W. F. Krol. The "constant intake rate" assumption in interim recruitment goal methodology for multicenter clinical trials. *Journal of chronic diseases*, 40(4):297–307, 1987.
- [65] B. J. Gajewski, S. D. Simon, and S. E. Carlson. Predicting accrual in clinical trials with bayesian posterior predictive distributions. *Statistics in medicine*, 27(13):2328–2340, 2008.
- [66] I. Abbas, J. Rovira, and J. Casanovas. Clinical trial optimization: Monte carlo simulation markov model for planning clinical trials recruitment. *Contemporary clinical trials*, 28(3):220–231, 2007.

- [67] C. Abdelkafi, B. H. L. Beck, B. David, C. Druck, and M. Horoho. Balancing risk and costs to optimize the clinical supply chain - a step beyond simulation. *Journal of Pharmaceutical Innovation*, 4(3):96–106, 2009.
- [68] Y. Chen, L. Mockus, S. Orcun, and G. V. Reklaitis. Simulation-optimization approach to clinical trial supply chain management with demand scenario forecast. *Computers and Chemical Engineering*, 40:82–96, 2012.
- [69] Y. Chen, L. Mockus, S. Orcun, and G. V. Reklaitis. Simulation-based optimization approach to clinical trial supply chain management. *Computer Aided Chemical Engineering*, 28:145–150, 2010.
- [70] Y. Chen, J. F. Pekny, and G. V. Reklaitis. Integrated planning and optimization of clinical trial supply chain system with risk pooling. *Industrial and Engineering Chemistry Research*, 52(1):152–165, 2013.
- [71] M. Peterson, B. Byrom, N. Dowlman, and D. Mcentegart. Optimizing clinical trial supply requirements: simulation of computer-controlled supply chain management. *Clinical Trials*, 1(4):399–412, 2004.
- [72] N. Shah. Pharmaceutical supply chains: key issues and strategies for optimisation. *Computers and Chemical Engineering*, 28(6-7), 2004.
- [73] W. D. Dupont and W. D. Plummer Jr. Power and sample size calculations: A review and computer program. *Controlled Clinical Trials*, 11(2):116–128, 1990.
- [74] J. M. Lachin. Introduction to sample size determination and power analysis for clinical trials. *Controlled clinical trials*, 2(2):93–113, 1981.
- [75] D. Machin, M. J. Campbell, S.-B. Tan, and S.-H. Tan. *Sample Size Tables for Clinical Studies*. John Wiley and Sons, 2011.
- [76] T. V. Sakpal. Sample size estimation in clinical trial. *Perspectives in Clinical Research*, 1(2):67–69, 2010.
- [77] J. R. Beeler Jr. Distribution functions for the number of distinct sites visited in a random walk on cubic lattices: Relation to defect annealing. *Physical Review*, 134(5A):A1396–A1401, 1964.
- [78] E. Montroll. Random walks on lattices. In *Proceedings of the Symposium on Applied Mathematics*, volume 16, pages 193–230, Providence, RI, 1964. American Mathematical Society.
- [79] E. W. Montroll and G. H. Weiss. Random walks on lattices. ii. *Journal of Mathematical Physics*, 6(2):167–181, 1965.
- [80] G. Polya. ber eine aufgabe der wahrscheinlichkeitsrechnung betreffend die irrfahrt im straennetz. *Mathematische Annalen*, 84(1-2):149–160, 1921.

- [81] H. B. Rosenstock. Random walks on lattices with traps. *Journal of Mathematical Physics*, 11(2):487–490, 1970.
- [82] G. H. Weiss. Asymptotic form for random walk survival probabilities on three-dimensional lattices with traps. *Proceedings of the National Academy of Sciences*, 77(8):4391–4392, 1980.
- [83] G. Zumofen and A. Blumen. Random-walk studies of excitation trapping in crystals. *Chemical Physics Letters*, 88(1):63–67, 1982.
- [84] D. G. Cahill and R. O. Pohl. Heat flow and lattice vibrations in glasses. *Solid State Communications*, 70(10):927–930, 1989.
- [85] A. C. Damask and G. J. Dienes. *Point defects in metals*. Gordon and Breach, 1963.
- [86] R. H. J. Fastenau, C. M. Van Baal, P. Penning, and A. Van Veen. On the sink concentration dependence of reaction constants for point defect trapping. *Physica Status Solidi (A)*, 52(2):577–586, 1979.
- [87] H. B. Rosenstock. Luminescent emission from an organic solid with traps. *Physical Review*, 187(3):1166–1168, 1969.
- [88] H. Scher and M. Lax. Continuous time random walk model of hopping transport: Application to impurity conduction. *Journal of Non-Crystalline Solids*, 8-10:497–504, 1972.
- [89] H. Scher and M. Lax. Stochastic transport in a disordered solid. i. theory. *Physical Review B*, 7(10):4491–4502, 1973.
- [90] L. J. S. Allen. *An introduction to stochastic processes with applications to biology*. Pearson/Prentice Hall, 2003.
- [91] S. Asmussen and P. W. Glynn. *Stochastic Simulation: Algorithms and Analysis*. Springer, 2010.
- [92] R. G. Novikov. The inverse scattering problem at fixed energy for the three-dimensional schrödinger equation with an exponentially decreasing potential. *Communications in Mathematical Physics*, 161:569–595, 1994.
- [93] M. V. De Hoop, H. Smith, G. Uhlmann, and R. D. Van Der Hilst. Seismic imaging with the generalized radon transform: a curvelet transform perspective. *Inverse Problems*, 25, 2009.
- [94] L. N. Trefethen. *Spectral Methods in Matlab*. SIAM, 2000.
- [95] P. Sacks and W. Symes. Recovery of the elastic parameters of a layered half-space. *Geophysical Journal of the Royal Astronomical Society*, 88:593–620, 1987.

- [96] W. W. Symes. A differential semblance algorithm for the inverse problem of reflection seismology. *Computers and Mathematics with Applications*, 22:147–178, 1991.
- [97] R. Kress. *Linear Integral Equations*. Springer-Verlag, 1989.
- [98] G. M. L. Gladwell. *Inverse Problems in Scattering: An Introduction*. Springer, 1993.
- [99] M. Hlynka, P. H. Brill, and W. Horn. A method for obtaining laplace transforms of order statistics of erlang random variables. *Statistics and Probability Letters*, 80:9–18, 2010.
- [100] G. Fishman. *Monte Carlo: Concepts, Algorithms, and Applications*. Springer, 1996.
- [101] J. E. Gentle. *Random Number Generation and Monte Carlo Methods*. Springer, 2003.
- [102] R. Stafford. Random vectors with fixed sum (from matlab central online), January 2006.

Appendix
DERIVATION OF EQUATIONS

We now show that from

$$a_0 \delta'(\xi) = 0, \tag{A.1}$$

we can derive (5.10) – (5.11) (recall that a_0 is continuous and differentiable). We first represent a_0 in terms of characteristic variables $\xi = t - x/v - L/2/v$ and $\eta = t + x/v - L/2/v$ so that $a_0(x, t) = f(\xi, \eta)$ for some function f . Define the inner product $\langle \alpha, \beta \rangle = \int \alpha(\xi)\beta(\xi) d\xi$. Then eq. (A.1) implies that for all test functions $\phi(\xi)$,

$$\langle a_0(x, t)\delta'(\xi), \phi(\xi) \rangle = 0, \tag{A.2}$$

$$\Rightarrow \langle \delta'(\xi), f(\xi, \eta)\phi(\xi) \rangle = 0, \tag{A.3}$$

$$\Rightarrow -\langle \delta(\xi), \partial_\xi[f(\xi, \eta)\phi(\xi)] \rangle = 0, \tag{A.4}$$

$$\Rightarrow -\left(f_\xi(\xi, \eta)\phi(\xi) \Big|_{\xi=0} + f(\xi, \eta)\phi'(\xi) \Big|_{\xi=0} \right) = 0. \tag{A.5}$$

Taking $\phi(\xi) \equiv 1$, we find $f_\xi(0, \eta) = 0$. Taking $\phi(\xi) = \xi\psi(\xi)$ with $\psi(0) \neq 0$, we have $f(0, \eta) = 0$. Since $\partial_\xi = \partial_t - v\partial_x$, we find that

$$a_0(x, t) = 0, \tag{A.6}$$

$$\frac{\partial a_0}{\partial t} - v \frac{\partial a_0}{\partial x} = 0, \tag{A.7}$$

on $\xi = t - x/v - L/2/v = 0$.